A mechanistic understanding of bacterial chromosome organisation

Dissertation

zur Erlangung des Grades eines

Doktor der Naturwissenschaften

(Dr. rer.nat.)

des Fachbereichs Biologie der Philipps-Universität Marburg

Vorgelegt von

Ismath Sadhir

aus Mudappallur, Indien

Marburg, im Juli 2023

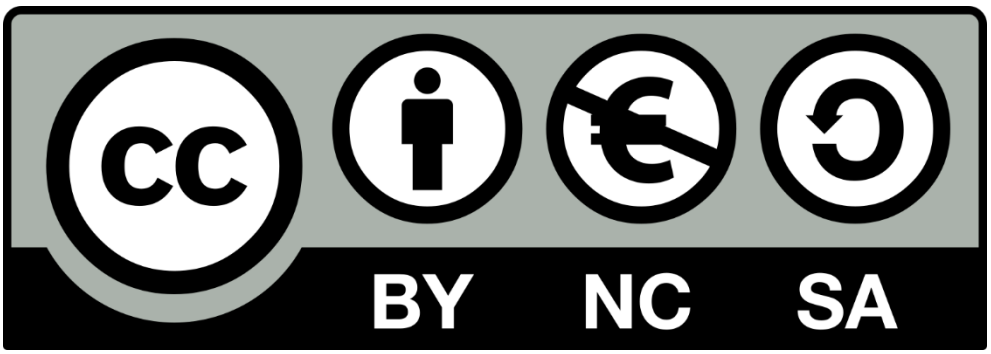

Die vorliegende Dissertation wurde von September 2019 bis Juli 2023 am Max-Planck-Institut für Terrestrische Mikrobiologie unter Leitung von Dr. Seán Murray angefertigt.

Vom Fachbereich Biologie der Philipps-Universität Marburg (Hochschulkennziffer 1180) als Dissertation angenommen am _____

Erstgutachter(in): Dr. Seán Murray

Zweitgutachter(in): Prof. Dr. Martin Thanbichler

Weitere Mitglieder der Prüfungskommission:

Prof. Dr. Peter Graumann

Prof. Dr. Lennart Randau

Tag der Disputation: _____

Erklärung

Ich versichere, dass ich meine Dissertation mit dem Titel „A mechanistic understanding of bacterial chromosome organisation“ selbstständig ohne unerlaubte Hilfe angefertigt und mich dabei keiner anderen als der von mir ausdrücklich bezeichneten Quellen und Hilfsmittel bedient habe.

Diese Dissertation wurde in der jetzigen oder einer ähnlichen Form noch bei keiner anderen Hochschule eingereicht und hat noch keinen sonstigen Prüfungszwecken gedient.

Marburg, den 21.07.2023

Ismath Sadhir

Die während der Promotion erzielten Ergebnisse wurden in folgender Originalpublikationen veröffentlicht:

Sadhir, I. and Murray, S.M., 2023. Mid-cell migration of the chromosomal terminus is coupled to origin segregation in *Escherichia coli*. *bioRxiv,* pp.2023-03.

Köhler R, **Sadhir I**, Murray SM. ★Track: Inferred counting and tracking of replicating DNA loci. Biophys J. 2023;122(9):1577-1585.

Table of contents

List of abbreviations

AMP	- Adenosine Monophosphate
ATP	- Adenosine Triphosphate
CFP	- Cyan Fluorescent Protein
CFU	- Colony Forming Units
ChIP	- Chromatin Immunoprecipitation
CID	- Collision-Induced Dissociation
CRP	- C-reactive Protein
CTP	- Cytidine Triphosphate
Dps	- DNA protection during starvation
DUE	- DNA Unwinding Element
Fis	- Factor for Inversion Stimulation
FISH	- Fluorescence In Situ Hybridization
FOV	- Field of View
FROS	- Fluorescent Repressor Operator System
GFP	- Green Fluorescent Protein
HU	- HupA/HupB heterodimer
IHF	- Integration Host Factor
LB	- Lysogeny Broth
Lrp	- Leucine-responsive Regulatory Protein
MatP	- Macrodomain Ter Protein
matS	- Macrodomain Ter sequences
NAP	- Nucleoid-Associated Protein
ori	- Origin region of chromosome
oriC	- Origin of Chromosome Replication
(p)ppGpp	- Guanosine pentaphosphate or Guanosine tetraphosphate
SMC	- Structural Maintenance of Chromosomes
TAD	- Topologically Associating Domains
ter	- Terminus region of chromosome
WT	- Wild-type strain
ZapA	- Z-ring Associated Protein A
ZapB	- Z-ring Associated Protein B

Zusammenfassung

Chromosomen dienen als Speicher für genetische Informationen, die für das Überleben aller lebenden Organismen entscheidend sind. Bakterien, in ihrer Einfachheit, bieten ein ideales Modell zur Untersuchung der Komplexität der Chromosomendynamik. Trotz ihres Mangels an Kompartimentierung zeigen bakterielle Chromosomen eine räumlich-zeitliche Organisation, ähnlich wie eukaryotische Zellen. Allerdings ist das Verständnis der Mechanismen der bakteriellen Chromosomenorganisation und -segregation, insbesondere bei dem ausgiebig erforschten Modellorganismus *Escherichia coli*, noch unvollständig.

Bei *E. coli*, wie bei den meisten Bakterien, ist der Origin of replication der erste Teil des Chromosoms, der repliziert und segregiert wird. Während bei anderen Bakterien zentromerähnliche Sequenzen zur Segregation des Chromosoms identifiziert wurden, wurden bei *E. coli* noch keine entdeckt. Der SMC-Komplex, der DNA bindet, zu dem Origin hingezogen wird und mit dem Origin während des gesamten Zellzyklus kolokalisiert, wurde als wichtiger Bestandteil für Positionierung und Segregation identifiziert. Allerdings wurde bisher noch keine DNA-Sequenzen bestimmt, welche diese Interaktionen begünstigen.

Unsere Studie begann mit einem umfassenden genomischen Screening, um zentromerähnliche DNA-Sequenzen zu identifizieren, die die Origin Positionierung in *E. coli* begünstigen könnten. Unsere Hypothese wurde durch die Beobachtung motiviert, dass spezifische Chromosomenregionen, wenn sie in instabilen Plasmiden mit geringer Kopienzahl vorhanden sind, zu deren aktiver Positionierung und Aufrechterhaltung führen. Wir fanden heraus, dass zwei Loci im *E. coli*-Genom, in der Nähe der *spoT*- und *seqA*-Gene, einem instabilen Plasmid ein moderates Maß an Stabilität verleihen. Der Stabilitätseffekt des *spoT*-Locus ist stammspezifisch, während der *seqA*-Locus eine Stabilität aufweist, die über verschiedene Stämme hinweg konsistent ist. Aufgrund von Zeitbeschränkungen bleibt der genaue Mechanismus für letzteres unidentifiziert. Unsere Ergebnisse in diesem Stadium stützen die etablierte Ansicht der Nichtexistenz einer zentromerähnlichen DNA-Sequenz für die Origin Positionierung im *E. coli*-Genom.

Obwohl Origin oft im Fokus vieler Studien ist, spielt auch die Terminus region - das letzte Chromosomensegment, das eine Replikation und Segregation durchläuft - eine entscheidende Rolle bei der Zellteilung, indem sie die gleichmäßige Verteilung des genetischen Materials zwischen Tochterzellen gewährleistet. In langsam wachsenden *E. coli*-Zellen wandert Terminsregion während des Zellzyklus vom neuen Pol zur Mitte der Zelle. Im Gegensatz zu anderen Chromosomensegmenten ist Terminus region für den größten Teil des Zellzyklus in der Zellmitte positioniert, selbst nach ihrer Verdoppelung. Das Verständnis des

Verhaltens von Ter bietet umfassende Einblicke in verschiedenste Aspekte der bakteriellen Chromosomenorganisation und -segregation.
Mit einem Hochdurchsatz-Ansatz auf Einzelzellenebene verfolgten wir Zehntausende von Zellzyklen, um den Übergang der Terminsregion vom neuen Pol zur Zellmitte quantitativ zu analysieren und ihre Beziehung zu verschiedenen Zellzyklusereignissen zu untersuchen. Wir fanden heraus, dass die Zentralisierung des Termins, ein schnelles diskretes Ereignis, eng mit dem Abschluss der Ori-Segregation verbunden ist, selbst in Abwesenheit seiner Verknüpfung mit dem Divisom. Dies enthüllte eine zuvor unerforschte Beziehung zwischen Origin und Terminus regionen des Chromsoms. Darüber hinaus entdeckten wir, dass *E. coli* unter Bedingungen langsamen Wachstums eine längsorientierte Chromosomenorganisation aufweist.

Zusammenfassend hat unsere Forschung unser Verständnis der Chromosomen organisation in *E. coli* erheblich erweitert und den Weg für die Anwendung unserer Methoden auf die Untersuchung der Chromosomenorganisation in anderen Bakterienarten geebnet.

Summary

Chromosomes serve as repositories of genetic information, crucial to the functionality of all living organisms. Bacteria, in their simplicity, offer an ideal model to investigate the intricacies of chromosomal dynamics. Despite their lack of compartmentalisation, bacterial chromosomes display spatiotemporal organization like eukaryotic cells. However, understanding the mechanisms of bacterial chromosome organization and segregation, particularly in the extensively studied model organism, *Escherichia coli*, remains incomplete.

In *E. coli*, like most bacteria, the origin of replication is the first part of the chromosome to be replicated and segregated. While centromere-like sequences aiding origin segregation have been identified in other bacteria, none have been discovered in *E. coli*. The SMC complex, which the origin is attracted to and co-localizes with throughout the cell cycle, has been identified as important for positioning and segregation. However, a sequence identity facilitating this interaction has yet to be determined.

Our study began with comprehensive genomic screening to identify sequences that might aid origin positioning in *E. coli*. Our hypothesis was motivated by the observation that specific chromosomal regions, when present within unstable low-copy plasmids, lead to their active positioning and maintenance within the population. We found that two loci in the *E. coli* genome, near the *spoT* and *seqA* genes, confer a moderate degree of stability to an unstable plasmid. The stability effect of the *spoT* locus is strain-specific, while the *seqA* locus demonstrates stability that is consistent across different strains. Due to time constraints, the precise mechanism for the latter remains unidentified. Our findings at this stage support the established view of the absence of a centromere-like sequence for origin positioning in the *E. coli* genome.

While the origin of replication has been the focus of many studies, the terminus region—the last chromosomal segment to undergo replication and segregation—also plays a vital role in successful completion of cell cycle, ensuring the equal distribution of genetic material between daughter cells. In slow-growing *E. coli* cells, the terminus region transitions from the new pole at birth to the midcell during the cell cycle. Unlike other chromosomal regions, it maintains the midcell positioning for the majority of the cell cycle, even after its duplication. Understanding the behavior of the terminus region can provide insights into the broader aspects of bacterial chromosome organization and segregation.

Using a high-throughput single-cell approach, we tracked tens of thousands of cell cycles to quantitatively analyse the transition of the terminus region from the new pole to midcell and investigated its relationship to various cell cycle events. We found that terminus centralisation, a rapid discrete event, is closely associated with the completion of origin segregation, even in

the absence of its linkage to the divisome. This revealed a previously unexplored relationship between origin and terminus. Additionally, we found that *E. coli* exhibits a longitudinal-like chromosome organization even under slow growth conditions.

In conclusion, our research significantly advances our understanding of chromosome organization in *E. coli* and paves the way for the application of our methodologies to studying chromosomal organization in other bacterial species.

I. Introduction

Bacterial chromosomes are folded three orders of magnitude to fit within the dimensions of the cells. Initially, it was believed that the bacterial genomes were randomly arranged since bacteria lack a compartmentalised structure. However, in 1976, Kavenoff and Ryder obtained vitreous sections of gently lysed *Escherichia coli* cells in electron micrographs which revealed that the bacterial genome exists as a collection of plectonemic loops emanating from a dense core (Kavenoff and Ryder, 1976) (**Figure 1)**. This finding challenged the previous assumption of random arrangement. Years later, advancements in fluorescence microscopy and the development of chromosomal loci labelling systems, such as Fluorescence *In Situ* Hybridization (FISH), Fluorescence repressor-operator system (FROS) and ParB/*parS* labelling, enabled researchers to observe recurring localisation patterns of chromosomal regions within bacterial cells. This indicated that bacterial chromosomes are spatially and temporally organised. Subsequent studies probing chromosomal contacts have identified the existence of large domain boundaries such as Macrodomains and Chromosome Interacting Domains (CIDs), which are defined by frequency of interactions within a limited region of the genome. These domain boundaries isolate and structure different parts of bacterial genomes and are reminiscent of the Topologically Associated Domains (TAD) in eukaryotes (Le et al., 2013; Niki et al., 2000; Valens et al., 2004).

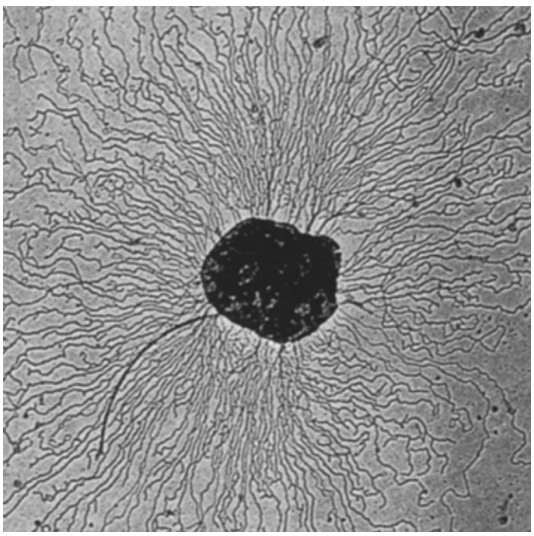

Figure 1: Electron micrograph of gently lysed *E. coli* cells (Kavenoff and Ryder, 1976)

1.1 Chromosome organisation in bacteria

In contrast to eukaryotes, bacteria coordinate the replication and segregation of their chromosomes simultaneously, even amidst the ceaseless activity of other ongoing cellular processes. This simultaneous orchestration of processes within a single compartment underscores the necessity of precise spatiotemporal organisation. This organisation is critical, given the short generation time and multifork replication in bacteria, to ensure symmetric

segregation of replicating genetic material between two daughter cells in coordination with cell division. Consequently, any perturbations to this organisation can lead to chromosome segregation defects, potentially causing the formation of anucleate cells and cell death.

The spatiotemporal organisation of chromosomes varies widely among bacterial species. Bacteria that are closely related and share the same nucleoid-associated proteins, especially the Structural Maintenance of Chromosome (SMC) complexes (discussed later), exhibit similar organisational patterns. Generally, bacterial chromosomes are seen as either longitudinally or transversely organised (**Figure 2**). In a (true) longitudinal or *ori-ter* organisation, the chromosomes stretch from pole to pole, with origin (*ori*) and terminus (*ter*) regions residing at opposite poles and the chromosomal arms aligned parallel to each other between them. On the other hand, in a transverse organisation, the *ori* resides near the midcell, generating a 'left-*ori*-right' pattern with the left and right chromosomal arms situated in in opposite cell halves. In some bacteria it has also been observed that the chromosome organisation alternates between longitudinal and transverse patterns (Badrinarayanan et al., 2015; Surovtsev and Jacobs-Wagner, 2018; Wang et al., 2013).

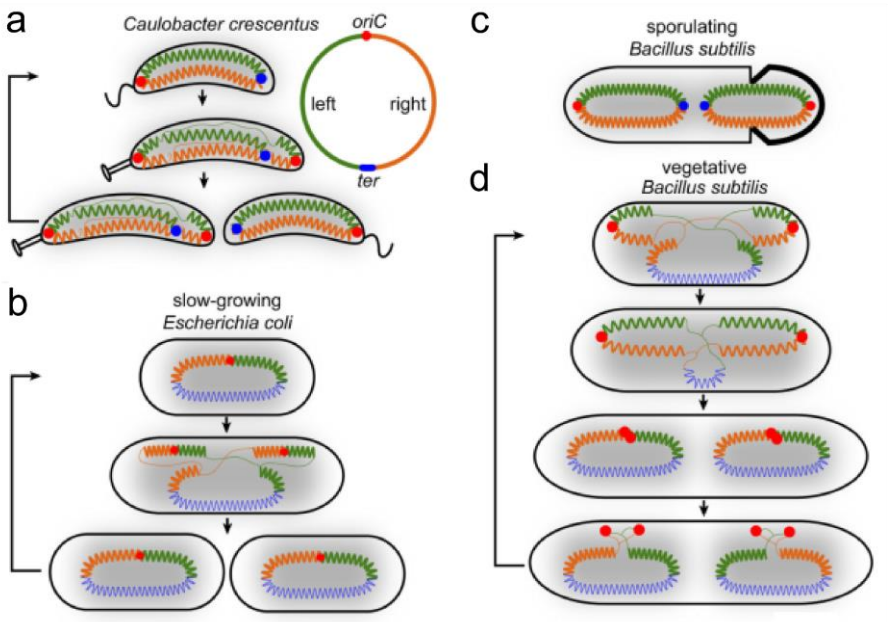

Figure 2: Chromosome organisation in different bacteria
a. Longitudinal organisation chromosome in *C. crescentus* **b**. Transverse organisation of chromosome suggested for *E. coli* **c**. Longitudinal chromosome organisation in sporulating *B. subtilis* **d.** Alternating chromosome organisation in vegetative *B. subtilis* (adapted from Badrinarayanan et al., 2015)

Among bacterial species, different organisational patterns predominate. For example, the *ori-ter* organisation is predominant in bacteria such as *Caulobacter crescentus, Myxococcus xanthus* and sporulating *Bacillus subtilis*. In *E. coli* and some other enterobacteria a left-*ori*-

right configuration is proposed to predominate during slow-growth conditions, while fast growth conditions favour an *ori-ter* organisation. Some other bacteria such as vegetative *Bacillus subtilis* and *Pseudomonas aeruginosa*, the organisation alternates between left-*ori*-right and *ori-ter* configurations throughout the cell cycle (Badrinarayanan et al., 2015; Vallet-Gely and Boccard, 2013; Wang and Rudner, 2014).

1.2 Nucleoid associated proteins

The spatiotemporal organisation of the bacterial chromosome is profoundly influenced by the actions of DNA-binding proteins, particularly a heterogeneous class of abundant proteins known as Nucleoid-Associated Proteins (NAPs). Typically, small (~20 kDa), NAPs bind non-specifically across bacterial genomes, enacting functions such as wrapping, bending, or bridging DNA. These local actions of NAPs significantly influence global chromosome organisation and often alter transcriptional patterns. The most crucial among these are HU, IHF, H-NS, and Fis (Badrinarayanan et al., 2015; Dillon and Dorman, 2010).

HU is a small (18 kDa), histone-like protein found in *E. coli* and many other bacteria (Drlica and Rouviere-Yaniv, 1987; Rouvière-Yaniv and Gros, 1975). It is composed of two subunits - alpha (HupA) and beta (HupB) which can form both homo- and heterodimers depending on the growth phase (Claret and Rouviere-Yaniv, 1997). HU binds to DNA in a relatively non-specific manner, as shown by its ChIP-Seq profile (Prieto et al., 2012), and it does so by inserting itself into the minor groove of DNA (Swinger and Rice, 2007).

Integration Host Factor (IHF), on the other hand, binds to DNA with greater specificity and can induce bends of over 160 degrees (Rice et al., 1996). The activity of IHF is notably important for transcription regulation, where it can either activate or inhibit RNA polymerase by bringing its distant regulatory elements closer together (Santero et al., 1992). Both HU and IHF share the ability to form heterodimers.

Two additional NAPs, H-NS and the Factor for Inversion Stimulation (Fis), are known to regulate gene expression and chromosome compaction. H-NS prefers to bind to AT-rich or curved DNA, bridges them, and silences promoters, especially those of horizontally acquired DNA (Grainger et al., 2006; Kahramanoglou et al., 2011; Lucchini et al., 2006). On the other hand, Fis can bend DNA similarly to IHF but to a lesser extent (Finkel and Johnson, 1992). Fis promotes DNA compaction and gene expression regulation by forming topological barriers that block supercoiling diffusion (Dages et al., 2020).

Some NAPs, such as Fis and Dps, exhibit expression levels that depend on the growth phase. Under optimal growth conditions, Fis is highly expressed, with up to 60,000 copies per cell. However, its expression decreases to around 100 molecules per cell during the stationary

phase (Ali Azam et al., 1999). In contrast, Dps is repressed during exponential growth and increases in number as cells enter the stationary phase (Grainger et al., 2008). Dps serves to protect DNA from oxidative damage by sequestering iron (Nair and Finkel, 2004; Orban and Finkel, 2022).

Furthermore, certain transcription factors also exhibit NAP-like properties. The Leucine-responsive regulatory protein (Lrp) is one such factor, regulating the expression of approximately 10% of *E. coli* genes (Tani et al., 2002). Another is the cyclic AMP regulatory protein (CRP), which binds to hundreds of sites in the *E. coli* genome and induces bending (Grainger et al., 2005).

1.3 SMC complexes

While NAPs are generally small proteins, some large proteins also stably associate with and influence the structure of chromosomes. Most prominent in this category is the widely conserved protein SMC complex, homologous to eukaryotic condensin. They usually function as dimers, forming a ring-like structure that can encircle DNA (Gligoris and Löwe, 2016; Haering et al., 2002; Melby et al., 1998). Recently, SMCs have been shown to condense DNA by loop extrusion in eukaryotes (Ganji et al., 2018).

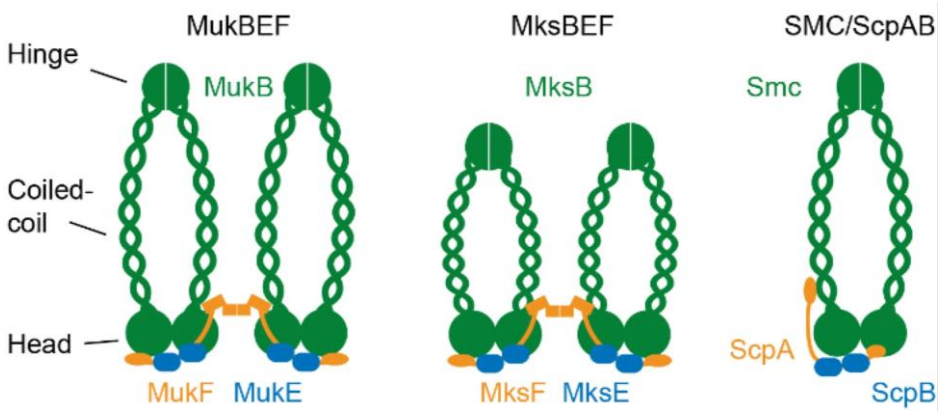

Figure 3: SMC complexes found in bacteria (Mäkelä and Sherratt, 2020a)

In bacteria, three classes of SMCs have been identified (**Figure 3**). Common to all SMC complexes is the SMC monomer, which self-assembles into a rod-shaped structure through anti-parallel coiled-coil interactions. This assembly results in an ATP-binding "head" domain, composed of N- and C-terminal regions, positioned at one end, and a "hinge" domain at the opposite end (Nolivos and Sherratt, 2014). The SMC subunit subsequently homodimerizes via the hinge domain, forming a characteristic V-shaped structure (Melby et al., 1998). Each class is distinguished by its unique set of associated proteins and specialised functions in

chromosome organisation and dynamics. Both the SMC subunit and the accessory proteins are required for the generation of a functional SMC complex.

1.3.1 The Smc-ScpAB complex

In most bacteria, Smc-ScpAB is the predominant SMC complex. Its Smc subunit is closely related to eukaryotic and archaeal SMC proteins (Zhao et al., 2020). It forms a homodimer and interacts with two accessory proteins - ScpA and ScpB (Hirano and Hirano, 2002; Mascarenhas et al., 2002). ScpA belongs to the kleisin family of the proteins, and its C-terminal interacts with the lower 'cap' region of one of the subunits of Smc homodimer while its N-terminal interacts with the neck region of the other subunit. ScpB on the other hand belongs to the kite family of proteins. It forms a dimer and attaches to the central region of ScpA (Bürmann et al., 2013; Kamada et al., 2017). Together in its entirety, Smc-ScpAB form a pentameric complex and exhibits a highly elongated form, possessing a central channel encircled by a closed tripartite ring created by the Smc dimer and the $ScpAB_2$ sub-complex. Additionally, the Smc head domains of the homodimer can directly interact with each other through a shared interface that comprises two ATP molecules. The biochemical activity of the Smc–ScpAB complex is likely regulated and propelled by ATP binding, head engagement, and ATP hydrolysis (Soh et al., 2015; Wilhelm et al., 2015).

1.3.2 The MukBEF complex

E. coli and many other *gammaproteobacteria* do not encode Smc-ScpAB. Instead, they possess an analogous complex known as MukBEF with MukB being the analog to Smc (Badrinarayanan et al., 2015; Nolivos and Sherratt, 2014; Petrushenko et al., 2011). In fact, MukB was the first condensin to be discovered following the isolation of an *E. coli* mutant that produced anucleate cells (Hiraga et al., 1989). The term 'Muk' was thus derived from 'Mukaku', a Japanese word meaning 'anucleate'. It was later found that in *E. coli*, the *mukB* gene resides in an operon that include three additional genes, *smtA, mukE* and *mukF*. The *mukE* and *mukF* encode accessory proteins which are indispensable for the functionality of MukB (Yamanaka et al., 1996, 1995). The first gene in the operon encodes a methyltransferase SmtA/CmoM, which has an unrelated function to that of MukBEF (Sakai et al., 2016; Yamanaka et al., 1995). Moreover, it was found that the *mukFEB* operon often co-occurs with genes such as *dam, seqA, matP*, which are mostly exclusive to *gammaproteobacteria* (Badrinarayanan et al., 2015; Brézellec et al., 2006; Mercier et al., 2008; Waldminghaus and Skarstad, 2009).

Like other Smc proteins, MukB has an ATPase head region, a hinge region and an antiparallel coiled-coil region between the head and the hinge (Bürmann et al., 2021, 2019; Rybenkov et al., 2015). It forms a homodimer using the hinge region and associates with the subcomplex

formed by MukE and MukF (Niki et al., 1992; Woo et al., 2009). MukF, analogous to ScpA, is the kleisin while MukE, analogous to ScpB, is the kleisin accessory protein (kite). Both MukF and MukE have the ability to form dimers. MukE dimers can associate with the central region of MukF monomers and interact with MukB. MukF, through its N-terminal, forms a homodimer and its C-terminal can interact with the ATPase head region of MukB. Upon ATP binding, the MukB heads close upon each other, forming a MukB homodimer ring similar to Smc-ScpAB, with the MukF C-terminal interacting with the ATPase heads (Bahng et al., 2022; Gloyd et al., 2007; Zawadzka et al., 2018). While MukB can bind the DNA on its own, formation of MukBEF complex and subsequent ATP binding and hydrolysis activity of the complex has been implicated to carry out the function of DNA condensation (Badrinarayanan et al., 2012b; Woo et al., 2009).

1.3.3 The MksBEF complex

Recently a new class of bacterial SMC complex known as MksBEF was identified. Found across a range of bacteria, MksBEF often accompanies another condensin complex. These proteins display a distant relation to MukBEF and share a similar operon organisation and predicted secondary structures, though they have significantly shorter coiled coils between the head and the hinge regions (Petrushenko et al., 2011). Their discovery challenges the long-standing assumption that bacterial genomes encode only one bacterial condensin involved in chromosome organisation, either MukBEF or Smc-ScpAB. MksBEF has been shown to partially complement anucleate cell formation in SMC deficient cells as well as increase the range of *cis* contacts along the chromosomal arms (Lioy et al., 2020; Petrushenko et al., 2011). Furthermore, MksB loading onto DNA is not regulated by ATP hydrolysis (Pradhan et al., 2020). More recently it was identified that a complex formed by a nuclease MksG with MksBEF (MksBEFG) has been shown to function as a plasmid defense system in *Corynebacterium glutamicum* (Weiß et al., 2023).

1.4 Role of SMC complexes in chromosome organisation

One of the main factors influencing chromosome organisation in bacteria are the SMC complexes. Typically, bacteria have either one of the two, Smc-ScpAB or MukBEF, as the predominant SMC complex (Nolivos and Sherratt, 2014; Petrushenko et al., 2011; Yatskevich et al., 2019). These complexes have a significant role in bacterial chromosome organisation, such that any deviation from their normal function or their complete absence can lead to pleiotropic effects including decondensed chromosomes, temperature sensitivity, and anucleate cell formation (Britton et al., 1998; Hiraga et al., 1989; Jensen and Shapiro, 1999).

High-throughput Chromosome Conformation Capture (Hi-C) studies have demonstrated a specific activity for Smc-ScpAB. It has been shown that the activity of Smc-ScpAB dimers, which load at the ParB-bound *parS* sites near the *ori* and traverse in a 'zip-up' fashion towards the *ter*, increase the contact frequency between the left and right chromosomal arms (Le et al., 2013; Wang et al., 2017). This activity has been suggested to contribute to *ori-ter* organisation.

On the other hand, in bacteria such as *E. coli*, where MukBEF is the predominant SMC complex, its role does not involve aligning the chromosomal arms. Instead, it promotes long-range contacts wherever it is present (Lioy et al., 2018). As a result, *E. coli* exhibits a chromosomal contact map and a chromosome organisation pattern that differs from bacteria in which Smc-ScpAB is the predominant SMC complex.

B. subtilis SMC and *E. coli* MukBEF have been shown to associate with the origin-proximal region (Danilova et al., 2007; Wang et al., 2014). While the origin-proximal association of Smc-ScpAB can be explained by the fact that SMC loads at ParB-bound *parS* sites situated near the origin (Bock et al., 2022; Sullivan et al., 2009), the mechanism by which MukBEF loads onto chromosomes has not been characterised yet. Current evidence suggests that MukBEF loads onto chromosomes non-specifically and becomes enriched near the origin due to its exclusion from the terminus by the presence of a terminus-specific protein, MatP (Mäkelä and Sherratt, 2020b; Nolivos et al., 2016)

1.5 Chromosome segregation in bacteria

Bacteria employ intricate mechanisms to ensure accurate chromosome segregation, guaranteeing that each daughter cell inherits a complete and faithful copy of the genome. These mechanisms ensure that replicated DNA is distributed equally between each cell half so that upon division, each daughter cell receives an identical share of genetic material. This is true even for small, mobile DNA elements such as plasmids.

The *par* locus, first identified in the P1 plasmid, and later in *B. subtilis* and many other bacteria, provided an initial insight into how bacterial chromosomes are segregated equally between daughter cells (Austin and Abeles, 1983; Ireton et al., 1994; Mohl and Gober, 1997). However, the absence of a *par* locus in *E. coli* and many other *gammaproteobacteria*, as well as the dispensability of the *parABS* system in some of the bacteria, suggests the existence of alternative mechanisms of chromosome segregation (Gogou et al., 2021).

1.5.1 The ParABS system

The identification of the *par* locus in bacteria hinted at a process equivalent to chromosome segregation in eukaryotes. The *par* locus consists of three elements - *parS*, *parB*, and *parA*. The *parS* is a centromere-like sequence to which ParB binds and nucleates. There are usually multiple *parS* sites on chromosomes, and ParB can spread from these sites to cover a larger region of the DNA (Livny et al., 2007). ParB is a CTPase that can dimerize and form a clamp-like structure which allows it to spread around the *parS* sites. Additionally, it stimulates the ATPase activity of ParA upon interaction as well as act as an anchor point for SMC complexes to load onto the chromosome. (Gruber and Errington, 2009; Jalal et al., 2021, 2020; Osorio-Valeriano et al., 2019; Soh et al., 2019). The third element ParA is an ATPase that dimerizes and binds non-specifically to DNA upon ATP binding (Davis et al., 1996). The interaction of DNA bound ParA with the *parS*-ParB complex stimulates ATP hydrolysis, thus releasing it from the nucleoid (**Figure 4**).

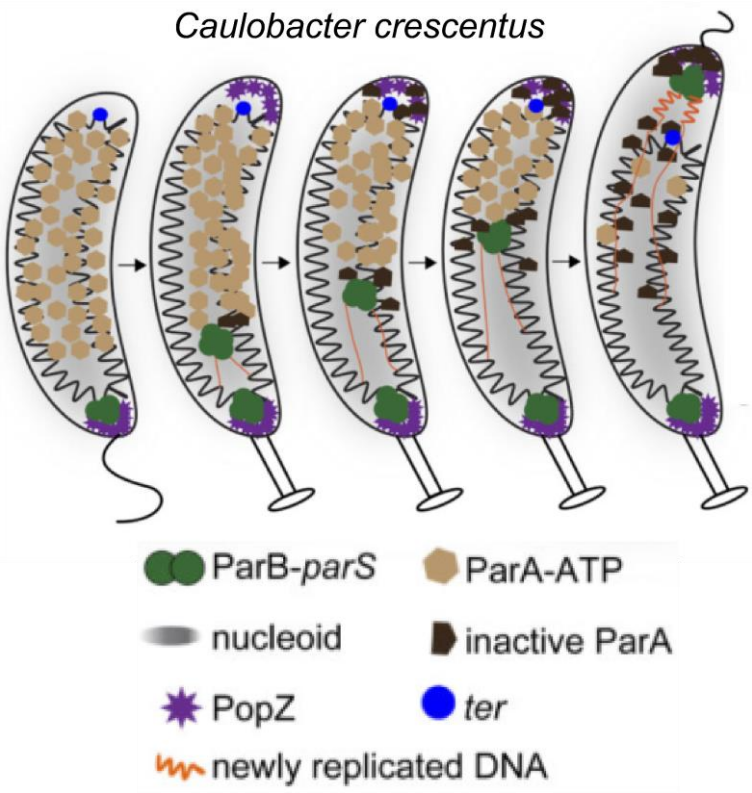

Figure 4: The ParABS system for chromosome segregation
(adapted from Badrinarayanan et al., 2015)

The positioning of DNA cargo by ParABS is well studied in plasmids. Two models - the DNA relay model and the Brownian Ratchet model (Hu et al., 2017; Surovtsev et al., 2016), have been proposed to explain the mechanism by which the ParABS system positions low-copy

plasmids inside the cell. In the DNA Relay model, elastic fluctuations of DNA and protein bonds drive the movement of plasmids across the nucleoid, reversing their direction upon reaching either a cell pole or another plasmid. Over time, this results in a positioning effect that, on average, appears regular. However, this model does not achieve 'true' regular positioning, in which plasmids are consistently located at fixed locations within the cell. The Brownian Ratchet model, on the other hand, proposes that plasmids undertake local movements around a 'home' position, which is influenced by the distance they segregate post-replication and other local conditions. This model results in a consistent inter-plasmid spacing along the long axis of the nucleoid but does not achieve regular positioning within the cell.

These models are not mutually exclusive, and both contribute to our understanding of plasmid positioning by the ParABS system. In both models, the segregation force for the *parS*-ParB complex is provided by chromosomal fluctuations and transmitted through the ParB-ParA tethers. The ATP hydrolysis stimulated by interaction with the *parS*-ParB complex generates a gradient of ParA along the long axis, which the *parS*-ParB complex follows, thereby ensuring segregation. This mechanism is applicable to chromosomal *parS*-ParB complexes as well.

Approximately 70% of the 400 prokaryotic species studied possess chromosomal *parS* sites, with 75% of them located within 5% of the genomic distance from *ori*. This indicates the importance of the ParABS system in *ori* segregation during the cell cycle (Livny et al., 2007). However, *E. coli* and many other *gammaproteobacteria* do not encode a *parABS* homolog responsible for *ori* segregation.

1.5.2 Entropy driven chromosome segregation

While active DNA transport mechanisms are recognized in bacteria for the segregation of origin, their role is distinct from the bulk segregation of replicating chromosomes. For instance, though ParABS system is critical for processes like the segregation of low-copy-number plasmids and the positioning of *ori* sites, it is dispensable for survival in many bacteria that possess it (Lee and Grossman, 2006; Wang et al., 2014), suggesting that it cannot completely account for bulk chromosome segregation. Moreover, given its absence in many bacteria, including *E. coli,* and its limited role in bulk chromosome segregation, further investigation into alternative mechanisms that might underlie bacterial chromosome segregation is warranted.

Recently, a new perspective on how chromosomes separate has been gaining attention. This perspective, based entirely on physical principles, involves the spontaneous demixing of interwoven DNA polymers when they are in a confined space (**Figure 5**). This separation process increases disorder or 'entropy' because the mixed state of the polymers limits their possible arrangements (Jun and Mulder, 2006). This kind of separation occurs under certain conditions, like when there are long polymers (such as chromosomal DNA) in a small area,

and the confinement is cylindrical in shape. Simulations have shown that this entropy-driven push-away effect can assist chromosomes in separating within the boundaries of a cell (Gogou et al., 2021; Jun and Wright, 2010).

This process seems to cause the newly replicated chromosome mass to move outward towards the free space at the cell poles. Consequently, any unreplicated DNA is kept between the newly replicated mass, that is, at the middle of the cell (Youngren et al., 2014). This is reminiscent of sequential segregation of newly replicated chromosomal regions in *E. coli*. However, the segregation is also influenced by the size of the polymers relative to the confined space, meaning it applies to larger structures, like chromosomes, but not to smaller ones, like plasmids.

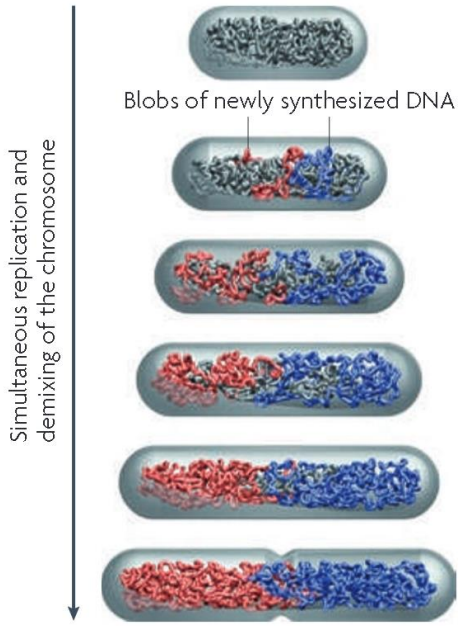

Figure 5: Spontaneous demixing of newly replicated chromosomes (adapted from Jun and Wright, 2010)

The theory of entropy-driven chromosome segregation is relatively new, and hence there have been few experiments to validate the hypothesis. Recently, Japaridze et al. showed that timely segregation of chromosomes was compromised due to the loss of cell wall confinement caused by drug-induced expansion. Additionally, in expanded cells, the initial segregation of *ori* occurred randomly until the replication of the chromosomal mass reached a certain level of confinement, which then directed the *ori* towards the cell poles (Japaridze et al., 2020). Similarly, in cells lacking a cell wall (L-form cells), which results in loss of cylindrical confinement, the nucleoid was observed to orient randomly. However, when cell-wall size confinement was imposed using microfluidic channels, successful segregation was achieved

(Wu et al., 2020). These results indicate that physical forces operate in concert with biological processes to influence the timely segregation of chromosomes.

1.6 Chromosome organisation in *E. coli*

E. coli has a 4.6 Mb genome. It can be subdivided into Mb-sized domains called Macrodomains based on the observation that certain regions share the same restricted cytoplasmic space when observed using FISH (Niki et al., 2000). Later, the genome was classified into four macrodomains and two unstructured regions based on frequency of recombination. The genetic loci within the same macrodomain demonstrate higher interaction and recombination frequency than those located in different macrodomains (Valens et al., 2004). The macrodomains are named Ori, Right, Left, and Ter. The Ori macrodomain contains the origin of replication (*oriC*), while the Ter macrodomain contains the terminus region (*ter*). The Right and Left macrodomains are named for their positions relative to Ori. However, more recently, based on Hi-C analyses, it has been found that chromosomal contacts between different parts of chromosome classify the *E. coli* genome into two regions - *ter* and the rest of the chromosome (Lioy et al., 2018). This classification is primarily based on the range of chromosomal contacts introduced by the action of NAPs, particularly the SMC complex, MukBEF. It is found to introduce long-range contacts between regions that are >280 kb apart. However, these interactions are absent in *ter* as a consequence of exclusion of MukBEF from *ter* by the terminus specific protein MatP (discussed below).

1.6.1 The *ori* region

The *ori* region, which contains *oriC*, is the first region of the chromosome to be duplicated following the initiation of DNA replication. The *oriC* contains specific sequences, including DnaA-boxes and an AT-rich DNA unwinding element (DUE), that serve as recognition sites for the DNA replication machinery, such as the initiation protein DnaA. DnaA binds to these sequences, triggering the unwinding of the DNA double helix and facilitating the access of the replication machinery to the DNA template. Moreover, DnaA helps load the bacterial replicative helicase onto the single-stranded DNA, enabling the replisome complexes to move bidirectionally towards the terminus, thereby completing the replication process (Costa et al., 2013; Zawilak-Pawlik et al., 2017).

In *E. coli*, several factors control the initiation of *ori* replication, including growth rate, cell volume, and media composition. Once replication begins, the *ori* region— the first part of the chromosome to be segregated— lays the groundwork for evenly distributing the replicating genetic material between the cell halves during replication.

Under fast-growing conditions (with a generation time of less than 60 minutes), the *E. coli* chromosome undergoes multifork replication (Youngren et al., 2014). This process involves the initiation of a new round of replication before the ongoing one has concluded. As a result, under these conditions, daughter cells invariably receive a complete, albeit partially replicated chromosome, meaning that chromosome replication and division occur simultaneously. On the other hand, in slow-growing conditions (where the generation time exceeds approximately 100 minutes), the chromosome initiates replication only once in each cell cycle. This results in the daughter cells receiving a fully replicated chromosome (Kleckner et al., 2018). Notably, these varying growth conditions also correspond to distinct spatial organisations within the cells.

In fast growth conditions, *E. coli* adopts an *ori-ter* configuration where the *ori* and *ter* are situated near opposite poles, with the chromosome arms aligning between them. However, in slow-growing conditions, the organisation shifts to a left-*ori*-right configuration, in which the left and right chromosomal arms occupy opposite cell halves with the *ori* situated between them. Upon duplication, the *ori* moves to quarter positions, which subsequently become the new mid-cell of the daughter cells (Li et al., 2002; Niki et al., 2000; Niki and Hiraga, 1998; Wang et al., 2006).

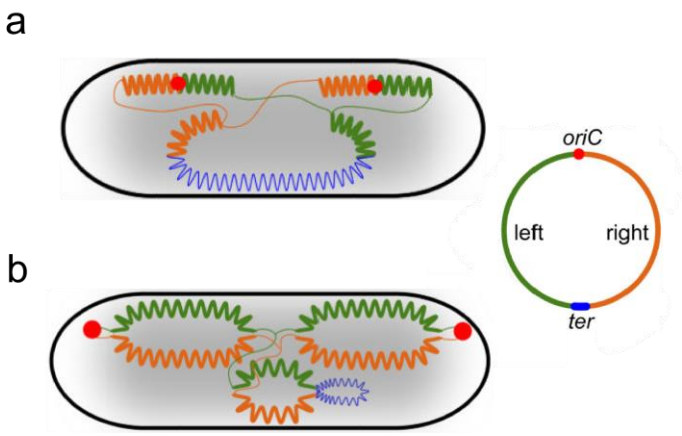

Figure 6: Illustration of *ori* positioning during *E. coli* cell cycle
a. *ori* positioning in *E. coli* during slow growth conditions **b.** *ori* positioning in *E. coli* during fast growth conditions (adapted and modified from Badrinarayanan et al., 2015)

The SMC complex MukBEF has been identified as a crucial factor in maintaining the left-*ori*-right configuration. Absence of MukBEF results in abnormal chromosome positioning within the cells, with the *ori* region tending to localise near the poles rather than near the mid-cell (Badrinarayanan et al., 2012a, 2012b; Danilova et al., 2007). Additionally, Δ*mukB* cells exhibit a temperature-sensitive phenotype and result in a significant number of anucleate cells (Mäkelä et al., 2021).

Following the identification of *parS* sequences in *B. subtilis*, Yamaichi and Niki reported a sequence in the *E. coli* genome, which they proposed might possess centromere-like properties (Yamaichi and Niki, 2004). This sequence, annotated as *migS*, appeared to contribute to the polar positioning of the *ori* region. However, its absence did not appear to disrupt chromosome segregation. Furthermore, when *migS* was introduced into an otherwise unstable plasmid, it did not result in plasmid stabilisation. This contrasts with the behaviour of the *parS* sequence which, when incorporated into an unstable plasmid, brought about its stability (Lin and Grossman, 1998). Based on these observations, *migS,* unlike *parS*, may not play a direct role in chromosome segregation.

More recently, Valens et al. identified a region within the Ori macrodomain that impacted the mobility of the region (Valens et al., 2016). This sequence, annotated as *maoS*, is a *cis*-acting sequence that operates in conjunction with its cognate partner protein, MaoP. It has been observed that the MaoP/*maoS* system restricts the mobility of the Ori macrodomain, and its inactivation leads to increased interaction between the Ori macrodomain and other regions. However, this system appears to have no influence on the positioning of the nucleoid or the *ori* region within the cell following replication. The authors, therefore, concluded that the positioning of the *E. coli* chromosome follows a yet unidentified mechanism.

Studies indicate that MukBEF co-localizes with *ori* during the cell cycle. Unlike Smc-ScpAB, which loads at ParB-bound *parS* sites, no preferred loading site for MukBEF has yet been identified. Furthermore, ChIP-seq data implies that MukBEF is not particularly enriched near the *ori*. Therefore, it has been suggested that MukBEF's colocalization with the *ori* might be due to its exclusion from the *ter* region by the protein MatP (Mäkelä and Sherratt, 2020b; Nolivos et al., 2016).

Recent studies have proposed that the positioning of MukBEF clusters near the mid-cell or quarter positions could be explained by the Turing patterning mechanism (Murray and Sourjik, 2017). Furthermore, it has been observed that the *ori* tends to move towards MukBEF, rather than MukBEF moving towards the *ori* (Hofmann et al., 2019). However, despite this intriguing relationship, a centromere-like site that could explain the directed motion of *ori* towards MukBEF has yet to be identified.

1.6.2 The *ter* region

The terminus region is the last part of the chromosome to be replicated and segregated following the initiation of replication (Li et al., 2003). This is the region where the replisome dissociates upon encountering the Tus-Ter complex, which effectively halts the progression of DNA polymerase, marking the end of replication (Mulcair et al., 2006). The *ter* region is also where two crucial complexes, XerCD and FtsK, exert their functions. XerCD is responsible for

resolving chromosome dimers into monomers at the *dif* site (Castillo et al., 2017). FtsK, on the other hand, is an ATP-dependent DNA translocase that transports DNA across the site of cell division and activates recombination through XerCD (Aussel et al., 2002; Grainge et al., 2011; Stouf et al., 2013).

The *E. coli* terminus region is characterised by the presence of 23 *matS* (macrodomain ter sequence) sites spread over an 800 kb region. The 'Macrodomain Ter Protein', MatP binds specifically to these *matS* sites and excludes the SMC complex MukBEF from the terminus region (Lioy et al., 2018; Mercier et al., 2008; Nolivos et al., 2016). MatP is a 17 kDa protein found exclusively in *gammaproteobacteia*. It comprises three contiguous domains: a large N-terminal four-helix bundle domain required for specific *matS* binding, a central RHH domain required for MatP dimerization which in turn is a prerequisite for binding to *matS*, and a C-terminal coiled-coil domain involved in tetramerization and interaction with the divisome protein ZapB (Dupaigne et al., 2012; Espéli et al., 2012; Monterroso et al., 2019). Deletion of *matP* causes cell filamentation and leads to the formation of anucleate cells in rich media conditions (Mercier et al., 2008).

MatP foci have been found to co-localize well with chromosomal loci from the *ter* region and its presence has been shown to reduce the interfoci distance between *ter* loci. This observation, along with the ability of MatP to form tetramers upon binding to *matS*-containing DNA, led to the proposal that MatP could compact and bridge DNA in the *ter* region (Dupaigne et al., 2012; Mercier et al., 2008). However, chromosomal contact maps of the terminus region did not show any increase in contact frequency between the *matS* sites. In fact, the terminus region was found to have decreased long-range contacts compared to the rest of the chromosome (Lioy et al., 2018). Additionally, it has been shown that *matS* bridging by MatP is outcompeted by non-specific DNA binding (Crozat et al., 2020). Taking into account the latter two observations, it appears that the bridging activity of MatP may not have significant relevance *in vivo.*

MatP plays a crucial role in the formation of a structure known as the *ter*-linkage, which connects the *ter* region to the divisome complex through two other proteins, ZapB and ZapA. ZapB and ZapA are divisome proteins associated with FtsZ. It has been suggested that the interaction between the C-terminal of MatP and the N-terminal of ZapB is likely important for the formation of the *ter*-linkage (Bailey et al., 2014; Espéli et al., 2012). Furthermore, recent studies have shown that MatP is capable of interacting with lipids *in vitro* hinting at additional regulatory mechanisms involving MatP (Monterroso et al., 2019).

In slow-growing *E. coli* cells, the MatP-bound *ter* region is initially localised near the new pole at the birth of a cell. This localisation subsequently shifts towards the mid-cell during the cell cycle, where it remains for the majority of cell cycle (Espéli et al., 2012; Männik et al., 2016).

Shortly before division, the *ter* foci separate near the division septum, and the aforementioned localisation pattern repeats (**Figure 7**). Unlike other chromosomal regions, the loci within the *ter* region display unique dynamics. Whereas the rest of the chromosome undergoes progressive segregation from the mid-cell following replication, the *ter* region remains at mid-cell until division (Mäkelä et al., 2021; Nielsen et al., 2006a). This mid-cell localisation of the *ter* region is thought to result from the *ter*-linkage, which connects MatP to the divisome protein FtsZ (Espéli et al., 2012; Männik and Bailey, 2015). Furthermore, the mid-cell localisation may enable the *ter* region to serve as a positive regulator of divisome positioning (Bailey et al., 2014). Despite existing studies, the factors contributing to mid-cell localisation of *ter* and its role in the chromosome segregation process remain unclear.

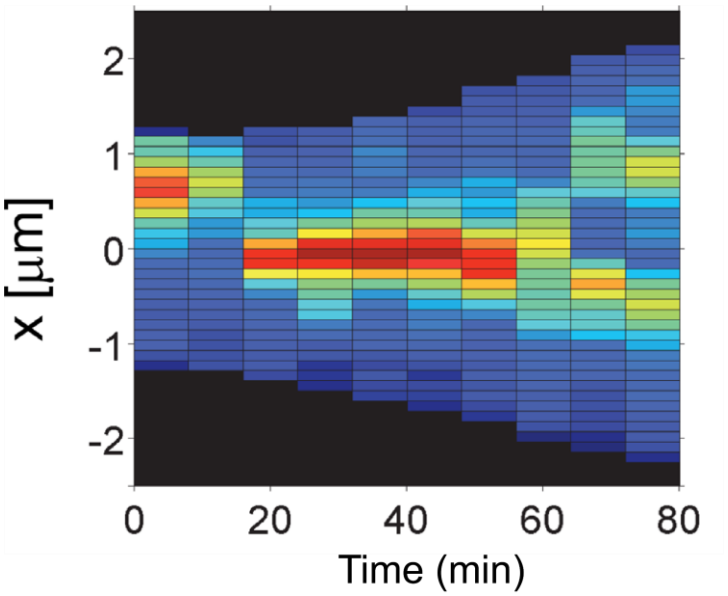

Figure 7: Kymograph of *ter* dynamics during a cell cycle (adapted and modified from Männik et al., 2016)

1.7 Aims of the study

In the first project, our aim was to determine the centromere-like sequence responsible for origin positioning in *E. coli*. Based on existing studies in *B. subtilis* (Lin and Grossman, 1998), we hypothesised that, if such a region exists in the *E. coli* genome, its presence on an unstable low-copy plasmid would be able to stabilise the plasmid. To facilitate our study, we planned to create an *E. coli* genomic DNA library in a low-copy unstable plasmid for our selection experiment. Subsequently, we aimed to use Next-Generation Sequencing to identify the regions in the *E. coli* genome that could confer stability to the otherwise unstable plasmid.

In the second project, we intended to study the localisation of *ori* and *ter* during the cell cycle, with an emphasis on *ter* dynamics. The *ter* is initially found near the new pole at birth, but relocalises to the mid-cell during the cell cycle, where it remains for the majority of the cell cycle. This distinct dynamic differs from other chromosomal regions, which are brought to the approximate midcell to be replicated, but then sequentially segregated away from the midcell following replication. The factors leading to, and the consequences of this unique dynamics of *ter* remain unclear. We aimed to use high-throughput single-cell imaging and analysis to quantitatively establish the choreography and timing of various events involving *ter* in slow-growing *E. coli* cells. By observing thousands of cell cycles, we aimed to identify the factors involved in the relocalisation of *ter* from the new pole to the mid-cell. Concurrently, we sought to quantitatively describe the temporal sequence of events contributing to chromosome segregation. Overall, the work presented in my thesis aims to enhance our understanding of bacterial chromosome organisation during the cell cycle.

II. Results

Part I

2. A whole genome screen to identify potential centromere-like sequences in *Escherichia coli*

In our aim to identify the sequence(s) responsible for origin positioning in *E. coli*, we used a forward genetics approach based on plasmid stability. It is well-established that an active partitioning system is crucial for maintaining the stability of low-copy plasmids in bacteria. Conversely, a low-copy plasmid devoid of an active partitioning system (also known as unstable plasmids) may not always be evenly distributed among the daughter cells through diffusion, leading to its rapid loss in the population.

A previous study had shown that the presence of a chromosomal *parS* sequence from B. *subtilis* genome in an otherwise unstable plasmid could stabilise the plasmid in *B. subtilis* (Lin and Grossman, 1998). This stability arises from the ability of partition complexes formed at the chromosomal *parS* sites to also recognize the plasmid due to the presence of the *parS* site, thus facilitating its partitioning alongside the chromosomal *parS*. Additionally, it has been shown in *E. coli* that the presence of *matS* sequences in plasmids positions them near the mid-cell due to the formation of *ter-linkage* by MatP-bound *matS* interacting with divisome proteins (Espéli et al., 2012). Collectively, these findings suggest that the introduction of specific chromosomal sequences into plasmids can affect their spatial distribution within the cell, which may contribute to the stabilisation of an otherwise unstable plasmid. This concept forms the basis of our hypothesis for identifying sequences with potential centromere-like properties within the *E. coli* genome.

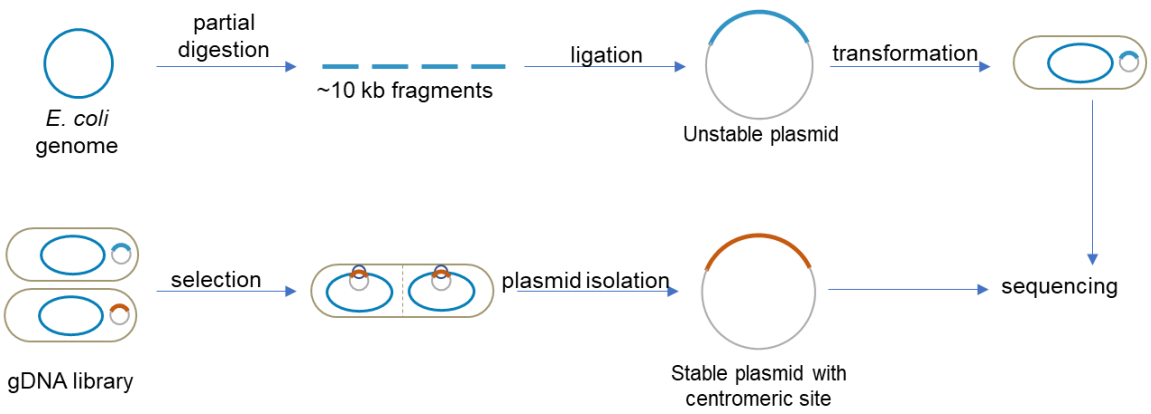

Figure 8: Experimental design for identifying centromere-like sequences

According to our hypothesis, unstable plasmids carrying a centromere-like fragment, if present in the *E. coli* genome, would be enriched in the population after several hours of growth in a non-selective media (**Figure 8**). This is due to the stability imparted by the action of the chromosomal partitioning complex on the plasmid, mirroring what was observed in *B. subtilis*. As a result, any unstable plasmid lacking a centromere-like sequence would be rapidly lost in the population, allowing the stable ones to persist after several generations of growth. Subsequently, the isolation and sequencing of these enriched plasmids would reveal the sequences responsible for their stability in the population.

2.1 Construction of *E. coli* genome library

For the creation of the genome library, we needed to first engineer a low-copy unstable plasmid. We accomplished this by modifying a stable mini-F plasmid. The modified plasmid retains genes for copy number control and initiation of replication, but lacks partitioning genes (*sopABC*), which makes it unstable. Additionally, a *sacB* gene having a BamHI restriction site was also present for cloning and counter selection of plasmids containing genomic DNA (gDNA) fragments (**Figure 9**). The BamHI site is compatible with ligation to the gDNA fragments having the GATC ends generated by partial digestion with Sau3AI, which is a 4 base-pair (bp) cutter and recognizes the sequence -GATC- and cuts at G, leaving a GATC overhang which is compatible with ligation to a plasmid digested with BamHI (G↓GATCC). The partial digestion using Sau3AI would result in the generation of gDNA fragments with each region covered in multiple different ways since the GATC sites are present on average every 243 bases in the *E. coli* genome. We aimed to create a library with an average gDNA fragment size of 10kb and a coverage of 10X, thus yielding a resolution of 1 kb, theoretically. The choice of fragment size and the coverage was chosen to find a balance between the number of colonies needed to cover the entire genome (4.6 Mb) in at least 10 different ways.

Our original plan was to create the library in a MG1655 Δ*recA* strain, but since the transformation efficiency of the library with this strain was very low, we proceeded with the experiment using the libraries made in the cloning strain (a derivative of DH10β), which also has a non-functional *recA*. The absence of a functional copy of *recA* in the strain is critical to the experimental plan in order to avoid the selection due to recombination events that would result in the integration of gDNA fragment along with the plasmid backbone into chromosome, leading to 'perpetual stability'. In fact, in our first attempt to create the genome library using gDNA from wild-type MG1655, we found that the population became enriched with strains carrying fragments belonging to *recA* locus. This serendipitous observation serves as a proof of concept which suggests that presence of a sequence that would stabilise the plasmid would

be enriched in the library population after several hours of growth in a non-selective media such as LB.

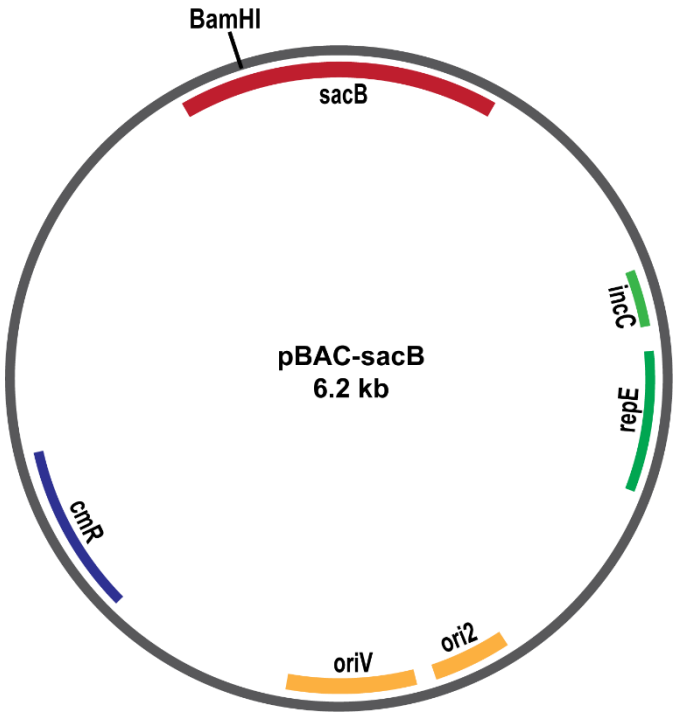

Figure 9: The low-copy unstable plasmid used for creation of gDNA library

Our initial attempts to construct the intended library failed due to contamination of small gDNA fragments. Presence of small fragments gave rise to a subpopulation which had a plasmid size similar to that of an empty plasmid. Such a subpopulation would lead to underestimation of library coverage and hence should be avoided. This problem was overcome by subjecting the partially digested gel purified DNA to another round of gel purification. With this strategy, we initially constructed a pilot library with more than 2X coverage using DNA from MG1655 Δ*recA* cells to establish and test the experiment protocol.

Once the experiment protocols were standardised, we created a library with over 10x coverage to cover all the regions in multiple different ways. We pooled more than 5000 colonies, each harbouring an average of 10kb fragments from the *E. coli* genome (**Figure 10**). Subsequently, the experiment was run according to the standardised protocols (see Materials and Methods).

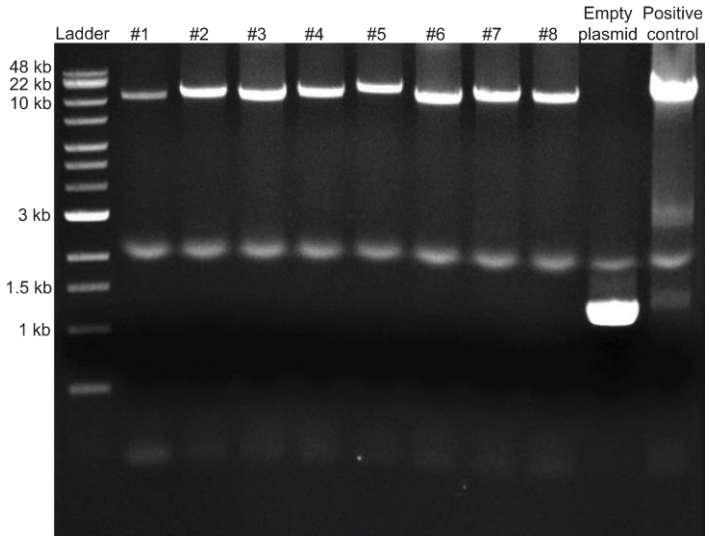

Figure 10: Fragment sizes of random colonies in the 10X library

2.2 Enriched genomic regions vary between growth conditions

To identify the enriched regions from the sequencing data, we began by aligning the sequencing reads to the *E. coli* genome, calculated the read depths, and normalised them with total reads. We then grouped the read depths into 1000 base pair bins, taking into account that a 10X coverage library represents each region of the genome in at least 10 different ways, thereby delivering a 1 kb resolution. We observed that the Day 0 reads near the *oriC* (~3900kb) were relatively higher and decreased as the distance from the *oriC* increased (**Figure 11**). This observation can be attributed to *E. coli* undergoing overlapping rounds of replication, as a result of which more copies of regions close to the origin are present in the cell at any given time. To account for differences in coverage of various regions, we normalized the read depths obtained for days 2, 3, and 4 with Day 0.

In our first experiment, the cultures were diluted twice every 24 hours, involving 16 hours in non-selective media and 8 hours in selective media. Considering the conditions, the cells would transition through lag, exponential, and stationary growth phases. This led us to the suspicion that certain regions might become enriched due to these varied growth conditions and not necessarily due to the presence of centromere-like sequences. This is because the presence of supplementary or functional copies of some of the *E. coli* genes in the plasmid could offer a selection advantage during a specific growth phase. We were concerned that this might obscure the selection process for enriching centromere-like sequences, which should be able to provide stability to the plasmids, independent of growth conditions.

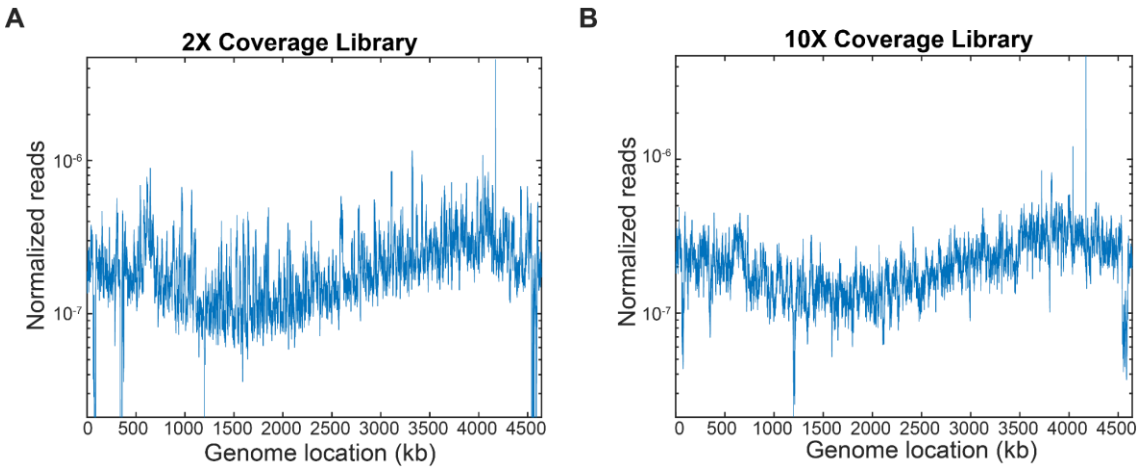

Figure 11: Read coverage of genomic libraries on Day 0

A. Profile of sequencing reads obtained from the genomic library with 2X coverage. **B.** Profile of sequencing reads obtained from the genomic library with 10X coverage. Read depths for each nucleotide were binned into 1000 bp bins based on their genome location and normalised by the total number of reads.

To address this issue, we conducted a second experiment in which cells were constantly maintained in the exponential phase by continuous dilution (every 8 hours). We found that the enriched regions varied between experiments, indicating that the selection is affected by growth conditions. Unfortunately, we could not sequence the plasmids from Day 3 of 10X coverage library due to the emergence of an unexpected population that produced a plasmid lacking the cloning site (and therefore the gDNA fragment) after Day 2. Despite this, as we cannot rule out the possibility of the presence of a centromere-like sequence in the unique peaks between experiments that we were able to sequence, we decided to screen regions that appear to have prominent peaks in each experiment for centromere-like properties. Furthermore, we sorted the enriched regions that are consistent across Day 2 and Day 4 on the basis of modified Z-score, as shown in **Table 1**.

	2X Library Experiment 1	10X Library Experiment 1	2X Library Experiment 2	10X Library Experiment 2 (Day 2 only)
0 – 1000 kb (*seqA*)	287	235, 578, 584…586, **704…712***	80, 623…629, **705…716***	122..124, 154..156, 171…180, 201, 223, 234..236, 397…408, 452..454, 582…587, 611…619, 639…645, 678..680, **702…718*,** 955, 958, 961
1001 – 2000 kb			997…1005, 1076…1075, 1088…1092,1200,1201, 1205,1206, 1829…1838	1003, 1189,1190, 1215…1218, 1245
2001 – 3000 kb	2793	2108, 2111, 2992, 2994, 2995	2359…2367, 2436…2444, 2800…2811	2107…2115, 2189…2190, 2267, 2485…2494, 2987…2996
3001 – 4000 kb (*oriC* (3.92 Mb), *maoS* (3.94 Mb), *migS* (4.13 Mb))	**3814, 3818…3832***	3331, 3429, 3447, 3455, 3456, 3473, 3801…3804, **3813…3832***	3318…3328, 3642..3644, **3822…3831***	3429..3431, 3440…3456, 3470…3478, 3630..3632, 3801…3807, 3921, 3942
4001 – 4652 kb			4102…4111, 4261…4265, 4548	4165..4167, 4173…4180, 4211

Table 1. Enriched regions with modified Z-score greater than 2
***Peaks corresponding to *seqA* (~700 kb) and *spoT* (~3800 kb) loci were the most consistent among the prominent peaks

2.3 Significant enrichment found near *spoT* locus in Experiment 1

The results from both the 2X and 10X coverage libraries in Experiment 1 (dilution twice a day) showed that the region near *spoT* (~3800 kb) became enriched starting from Day 2 and appeared to be the most prominent among all enriched regions (**Figure 12, 14B**). This locus was of particular interest due to its location within the Ori macrodomain and its proximity to *oriC*, which is located at ~3.92 Mb. However, this region was not among the most prominent peaks detected in Experiment 2 (**Figure 13**), suggesting that its selection might have been on the basis of growth condition and not due to the presence of centromere-like sequences. Despite this, we performed plasmid stability and localization assays to investigate the potential centromere-like properties of the region (discussed below).

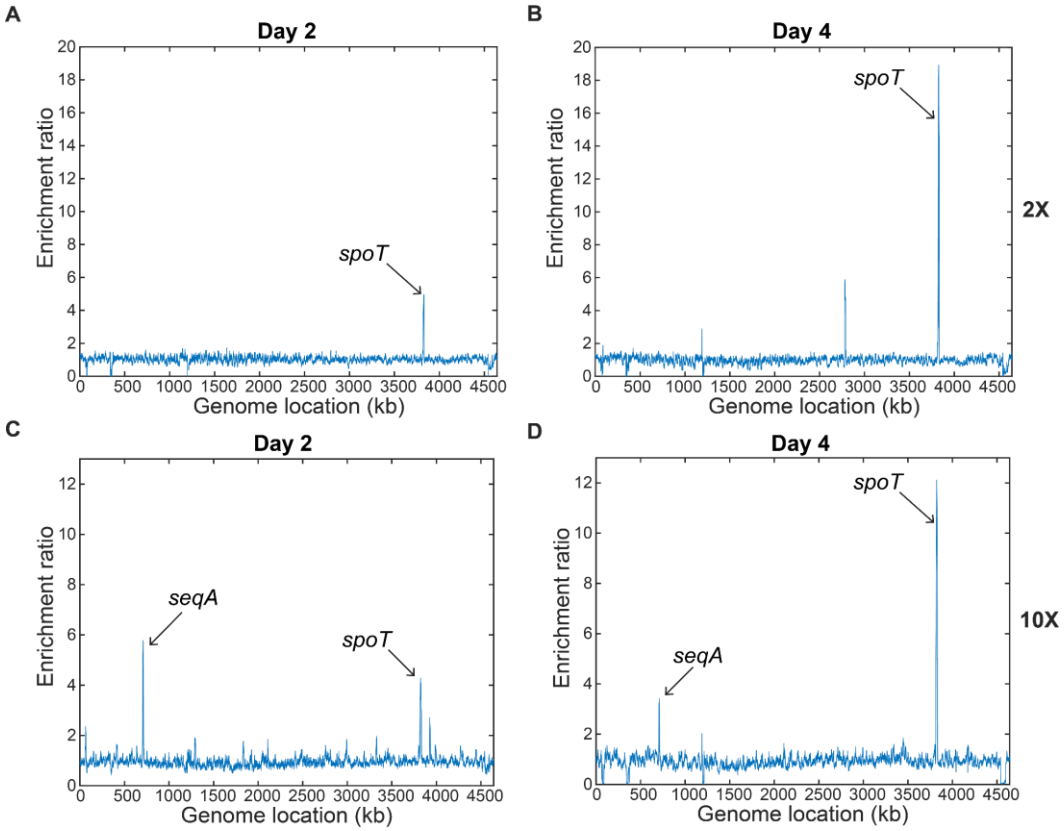

Figure 12: Enriched regions in *E. coli* genome from Experiment 1

Ratio of read depths relative to Day 0 mapped to genome location. **A, B.** Ratio for Day 2 and Day 4 from 2X coverage library. **C, D.** Ratio for Day 2 and Day 4 from 10X coverage library

2.4 Significant enrichment found near *seqA* locus in Experiment 1 and 2

The next prominent peak associated with enriched regions was identified near the *seqA* locus (~700 kb). This region appeared as the second most prominent peak on Experiment 1 (**Figure 12**) and the most prominent peak on Experiment 2 (**Figure 13, 14A)**. The *seqA* gene is part of a group of genes that have co-evolved with several other genes, such as *mukFEB*, *matP* and *damA*, which are exclusive to *gammaproteobacteria* and are known to be involved in chromosome organisation. Specifically, the *seqA* gene plays a role in negatively regulating replication initiation by binding to hemimethylated GATC sequences, sequestering newly replicated origins. This process allows time for chromosome segregation and cell division to take place.

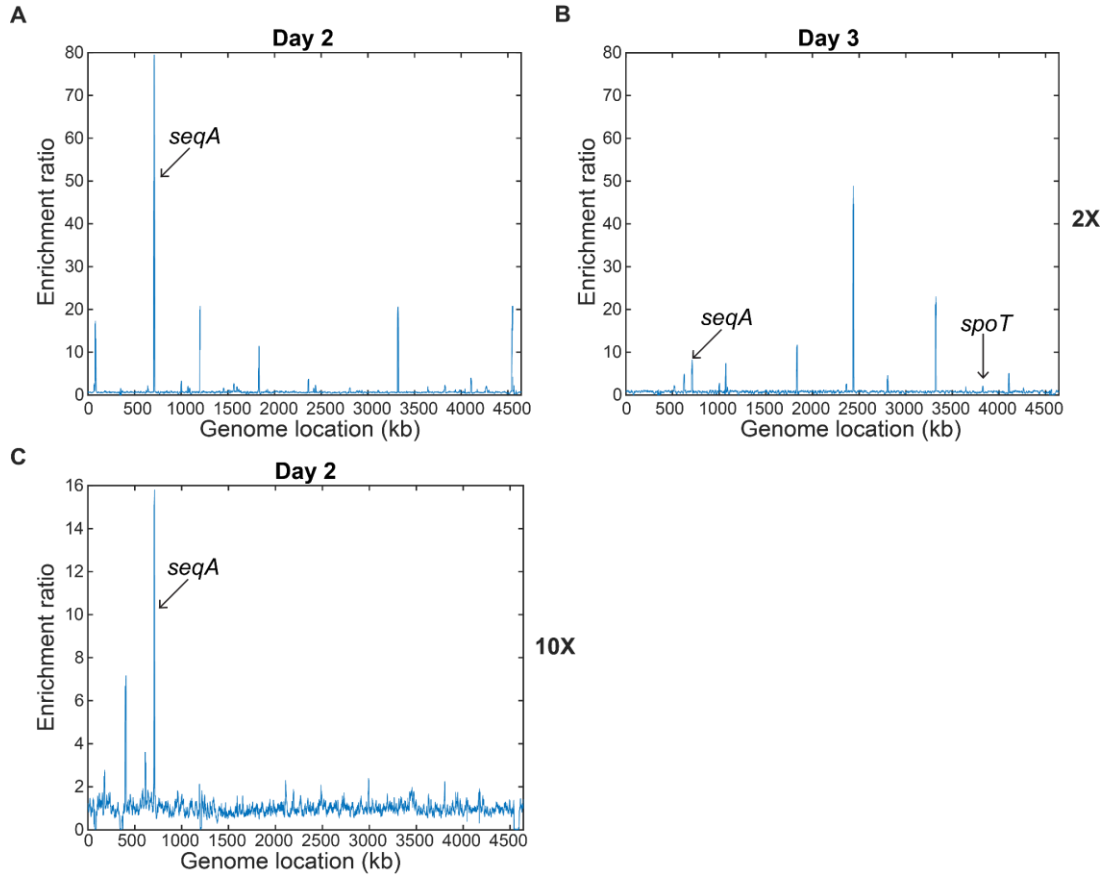

Figure 13: Enriched regions in *E. coli* genome from Experiment 2

Ratio of read depths relative to Day 0 mapped to genome location. **A, B.** Ratio for Day 2 and Day 3 from 2X coverage library. **C.** Ratio for Day 2 from 10X coverage library

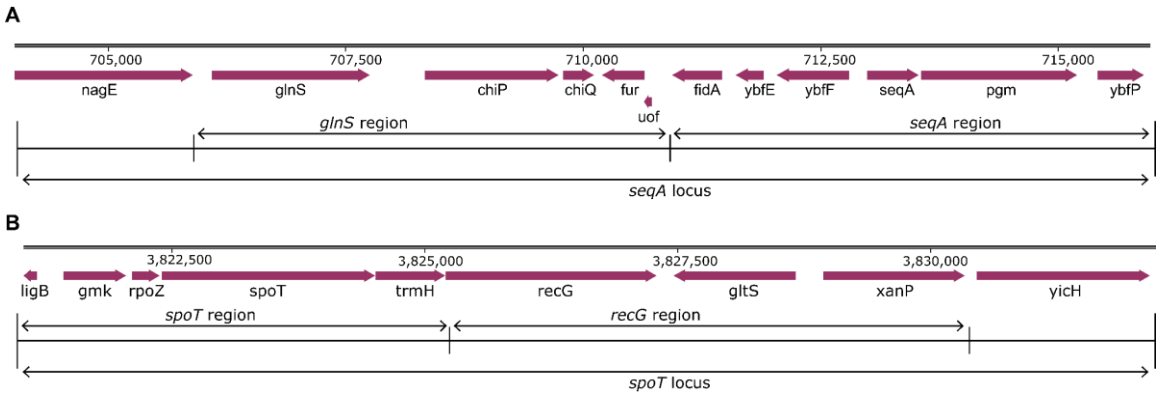

Figure 14: Gene neighbourhood of prominent peaks

A. Genes present at the enriched region near *seqA* locus **B.** Genes present at the enriched region near *spoT* locus

2.5 Plasmids with enriched regions show growth rates comparable to empty vector

To determine whether the enriched regions observed in our selection experiment resulted from increased growth rates, we performed growth curve experiments comparing colonies from Day 0 and Day 4 (**Figure 15**). No significant differences in growth rates were detected between these colonies. However, considering the enrichment process occurred over several days, even a small difference in growth rate could become significant in this time frame. Consequently, the possibility of selection based on growth advantages cannot be ruled out entirely.

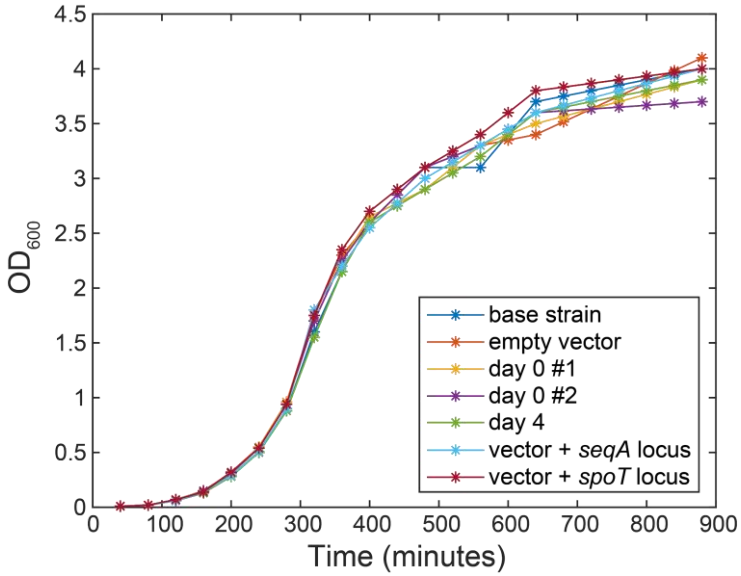

Figure 15: Growth curve of library colonies before and after selection

2.6 Plasmids carrying *spoT* or *seqA* locus exhibit lower plasmid loss in DH10β

To investigate whether the presence of *spoT* or *seqA* locus provides stability to an otherwise unstable plasmid, we cloned the enriched 10 kb regions around these genes (**Figure 14)** into unstable plasmids and transformed them separately into the strain used for preparing the library. We also managed to clone the 10 kb region corresponding to the *spoT* locus as two separate fragments: one containing the 4 kb region including *spoT* (designated as *spoT* region) and another with genes downstream of *spoT* (designated as *recG* region).

We grew these strains in non-selective media for 48 hours, back-diluting into fresh media every 12 hours, to determine plasmid loss rates. After 48 hours, the cells were 10-fold serially diluted and spotted onto agar plates containing both non-selective and selective media. Colonies appearing on the selective media plate correspond to those that retained the plasmid in a given volume. We found that the unstable vector carrying the 10 kb fragment corresponding to the *spoT* or *seqA* locus exhibited lower plasmid loss compared to the empty

vector, corroborating our results from sequence analysis (**Figure 16**). Additionally, the vector containing the smaller fragment from the *spoT* locus (*spoT* region), which contains the *spoT* gene, also showed lower plasmid loss, similar to the 10 kb fragment from the *spoT* locus. In contrast, the sequence downstream of *spoT* (*recG* region) did not show lower plasmid loss. This suggests that the apparent reduction in plasmid loss is associated with the sequence present in the *spoT* region. Nevertheless, the reduction in plasmid loss was not comparable to that of a stable vector with an active partitioning system (*sopABC*), which showed almost no plasmid loss after 48 hours.

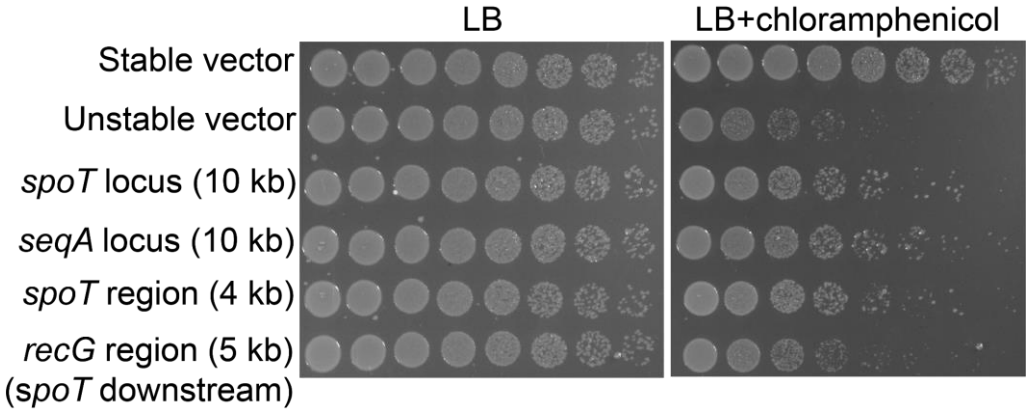

Figure 16: *spoT* or *seqA* loci carrying unstable plasmids show reduced plasmid loss

Furthermore, we assessed plasmid stability based on colony-forming units (CFU) and compared it with an unstable plasmid containing a random fragment (Day 0) and a stable vector. We found that the unstable vector containing the *spoT* region conferred relatively higher stability compared to a random fragment, corroborating the results obtained in the spotting assay (**Figure 17**). Nevertheless, the observed stability is considerably lower than that of a plasmid equipped with an active partitioning system.

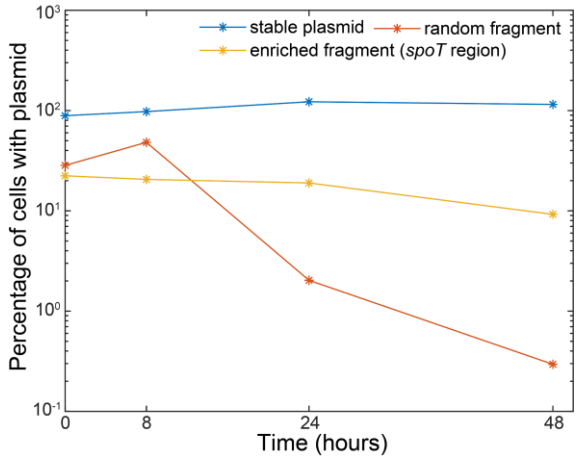

Figure 17: Unstable plasmid with *spoT* locus show reduced plasmid loss

2.7 Unstable vector having *spoT* or *seqA* locus shows random localization inside cells

Following our observation that presence of enriched regions in the unstable plasmid leads to reduction in plasmid loss, we asked whether the apparent reduction in plasmid loss is due to active positioning inside cells, as would be the case for a stable plasmid. Using the $ParB_{pMT1}$/$parS_{pMT1}$ labelling system we visualised their localization under a widefield fluorescence microscope and compared it with that of the unstable (empty) plasmid. Cells that contain plasmids displayed foci inside cells. We measured their long axis position inside cells and found that plasmids containing *spoT* or *seqA* localised randomly inside cells, similar to the empty plasmid (**Figure 18)**. Moreover, they did not show any specific localization indicative of active positioning. Consequently, we infer that the apparent reduction in plasmid loss is likely not due to active partitioning.

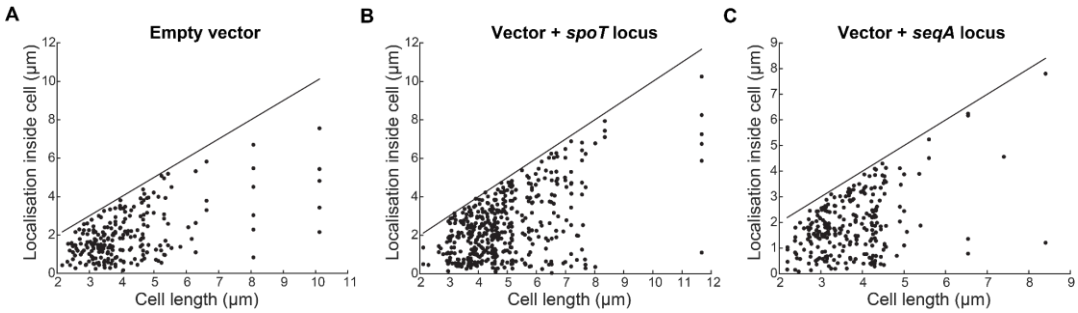

Figure 18: Unstable plasmids with enriched regions does not show specific localisation inside cells

A. Localisation of unstable empty plasmid inside cells. **B.** Localisation of unstable plasmid containing *spoT* locus inside the cells. **C.** Localisation of unstable plasmid containing *seqA* locus inside the cells (n>280)

2.8 Presence of enriched regions in unstable plasmid have a minimal effect on plasmid copy number

Plasmids lacking an active segregation system can potentially be stabilised by increasing their copy number and relying on random diffusion (Köhler et al., 2022; Reyes-Lamothe et al., 2014). We investigated whether the presence of *spoT* or *seqA* regions in the unstable plasmid could lead to an increase in its copy number, thus reducing the plasmid loss. Using data from our plasmid localization experiment, we examined the distribution of foci numbers. Our findings revealed that most cells had either one or two plasmids, similar to the empty vector (**Figure 19**). This suggests that an increase in the copy number of plasmids containing *spoT* and *seqA* regions might not be the primary factor responsible for the observed reduction in plasmid loss.

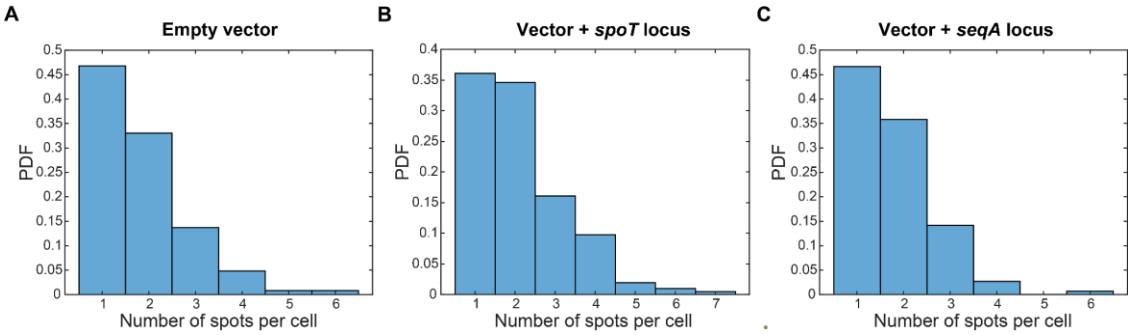

Figure 19: Presence of enriched regions in unstable plasmids have a minimal effect on copy number

A. Number of yGFP-ParB$_{pMT1}$ spots inside cells with unstable empty plasmid. **B.** Number of yGFP-ParB$_{pMT1}$ spots inside cells with unstable plasmid having *spoT* locus. **C.** Number of yGFP-ParB$_{pMT1}$ spots inside cells with unstable plasmid having *seqA* locus. (n>280)

2.9 *seqA* locus but not *spoT* locus shows reduced plasmid loss in MG1655

Considering that all observations made so far have been based on the cloning strain, we questioned whether the results would be consistent when using an MG1655 background strain. To address this, we transformed the unstable vectors with enriched regions into an MG1655 Δ*recA* strain and performed a spotting assay as described for Figure 16. Interestingly, in contrast to the results from the cloning strain (DH10β), plasmids containing the *spoT* locus did not exhibit reduced plasmid loss. However, plasmids containing the *seqA* locus displayed a reduction in plasmid loss, similar to what was observed with the cloning strain (**Figure 20**). The result from the *seqA* locus fragment is consistent with the results from *glnS* region and *seqA* region, which are derived by cloning the *seqA* locus fragment as two smaller fragments (**Figure 14A)**. This suggests that the *seqA* locus contains sequences that provide higher stability to unstable plasmids for unknown reasons that is consistent across strains.

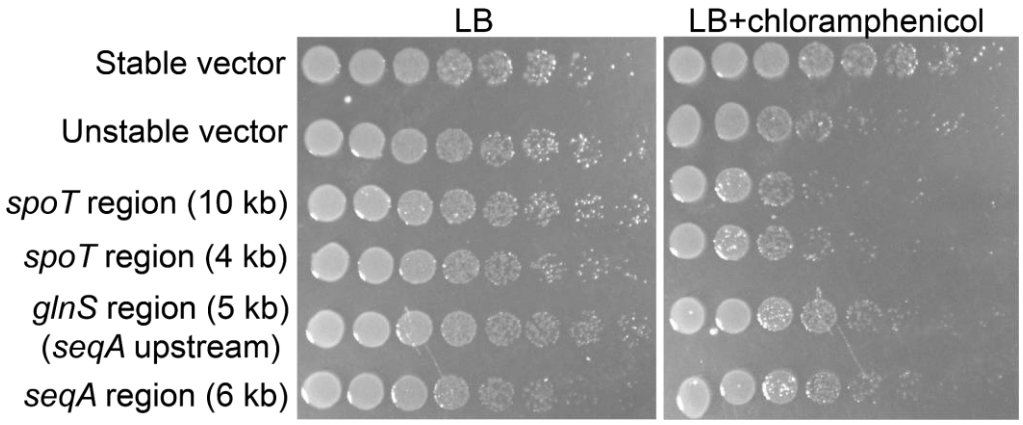

Figure 20: Presence of *seqA* locus in unstable vector shows reduced plasmid loss

The finding where unstable plasmids containing the *spoT* locus did not show a decrease in plasmid loss in a MG1655 strain, implies that the region may not have a centromere-like sequence, despite its proximity to *oriC*. The strain background (DH10β) used to construct the library is known to possess a *spoT1* allele instead of wild-type *spoT* (Durfee et al., 2008). This mutation increases the basal level of (p)ppGpp in cells (Fiil et al., 1977). (p)ppGpp is an alarmone produced in response to nutrient-limiting conditions, which helps bacteria adapt to changing environments. Increased levels of (p)ppGpp are correlated with decreased growth rates (Spira and Ospino, 2020) and it has been suggested that lower growth rate of DH10β compared to MG1655 is likely a consequence of elevated basal (p)ppGpp levels (Durfee et al., 2008). Therefore, it is plausible that DH10β cells carrying a WT copy of the *spoT* gene in the unstable plasmid might have lower levels of (p)ppGpp, which would in turn provide a growth advantage during fluctuating nutrient conditions, as was the case in Experiment 1.

The enriched region near the *seqA* gene contains genes involved in diverse functions, such as sugar uptake and metabolism, protein translation, iron homeostasis, and DNA replication. The consistent results observed between the two strain backgrounds, along with the fact that the *seqA* locus was enriched in both experimental conditions, suggest that the apparent stability associated with the presence of the *seqA* locus is not strain-specific or a consequence of the growth conditions. As for SeqA, a negative modulator of chromosome replication initiation, there is currently no evidence suggesting that it contributes to the stability of F-plasmids. Moreover, given that the stability effect is observed in both of the smaller fragments (*glnS* region and *seqA* region) derived from the *seqA* locus, only one of which contains *seqA*, it seems unlikely at this stage that the effect is due to the activity of SeqA (**Figure 20**). Further experiments are needed to elucidate the identity and mechanism by which sequences in the *seqA* locus confer a modest stability to unstable plasmids.

In this part of the study, we found that presence of the regions near *spoT* and *seqA* genes confer a modest stability to an unstable plasmid. The stability conferred by the *spoT* locus appears to be exclusive to a DH10β strain background, likely attributable to the presence of a mutated *spoT1* allele in this strain. On the other hand, the locus near the *seqA* gene appears to confer a modest stability that is consistent across both DH10β and MG1655 strains. Based on our results, it seems unlikely that the effect is due to the activity of SeqA, even though it has been shown to play roles in chromosome organisation. Unfortunately, due to time constraints, we decided not to pursue a detailed study to understand the mechanism by which sequences present in the *seqA* locus confer a modest stability. Future experiments could further narrow down the *seqA* locus to understand the identity of the sequence that leads to the modest stability. Overall, our results align with the prevalent notion that a centromere-like sequence responsible for chromosome partitioning is absent in the *E. coli* genome.

Part II

3. A high-throughput single-cell imaging and analysis to study chromosome organisation in bacteria

The *ter* region of the *E. coli* chromosome exhibits a set of dynamics and characteristics that differentiate it from the rest of the chromosome. It shows a unique positioning pattern during the cell cycle and has a crucial role in the final stages of cell division, mediated through the interaction with the divisome complex via the *ter*-specific protein MatP (Crozat et al., 2020; Espéli et al., 2012; Li et al., 2003, 2002; Männik et al., 2016; Mercier et al., 2008). Recent studies have shown that the SMC complex MukBEF is excluded from the *ter* by MatP, resulting in a less condensed terminus (Lioy et al., 2018; Nolivos et al., 2016). However, the series of events leading to the unique localisation pattern exhibited by *ter*, as well as the implications of having a decondensed terminus, remain to be fully understood. In this part of the study, we used a high-throughput single-cell imaging approach to quantitatively dissect the various events involving the *ter* region. By capturing and analysing these details, we aimed to expand our understanding of the mechanisms underlying the bacterial chromosome organisation and segregation, particularly the *ter* region.

3.1 The mother machine and 'Mothersegger'

The accurate analysis of *ori* and *ter* dynamics requires the temporal imaging of a large number of cell cycles. We achieved this using a high-throughput single-cell approach based on a 'mother machine' microfluidic device (Wang et al., 2010). Mother machine comprises a series of growth channels, which are oriented at right angles to the flow of media and allow for continuous feeding of cells with fresh media. The cells that grow out of the growth channels are washed away by the media flow and exit through the outlet. The original design of the device features channels with one open end and one closed end. However, we utilised a modified version with both ends open, one of which is constricted to allow media to flow but not cells (Baltekin et al., 2017). This modification provides easier loading of cells and improved exchange of media (**Figure 21**). We were able to image the cells every 5 minutes while maintaining sufficient signal and without significant changes in growth rates for up to three days.

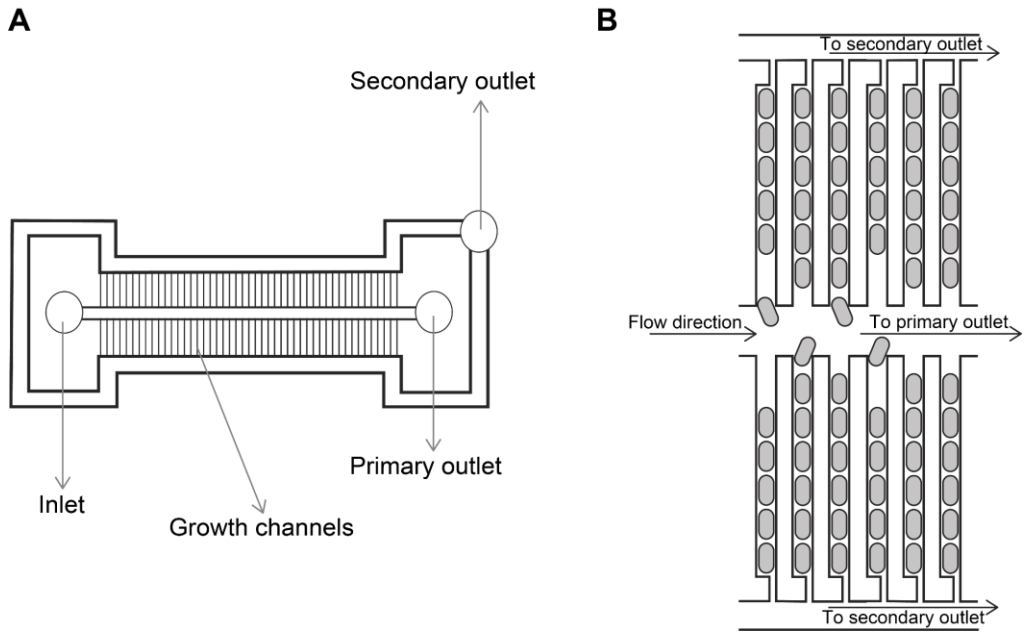

Figure 21: Schematic of the mother machine

A. Blueprint of the mother machine used in this study. **B**. Schematic representation of bacteria growing inside growth channels channels from **A**.

The use of the mother machine together with a custom image analysis pipeline namely 'Mothersegger' (Köhler et al., 2023, 2022), implemented in MATLAB, allowed us to effectively segment and track tens of thousands of cell cycles in steady-state conditions. The Mothersegger pipeline follows a multi-step process. In the initial step, growth channels are identified and cropped from each of the field of views (FOVs) by utilising phase contrast images, followed by background subtraction. In the second step, individual cells are identified by carrying out cell segmentation on the background subtracted phase contrast images. The third step employs data from the previous step to identify cells belonging to the same cell cycle, along with their mothers and daughters (**Figure 22**). Subsequently, foci identification and tracking are performed on images from fluorescence channels in the fourth step. Finally, in the fifth step, all the information from the preceding stages are compiled to generate a combined file, which can be utilised for qualitative and quantitative analysis.

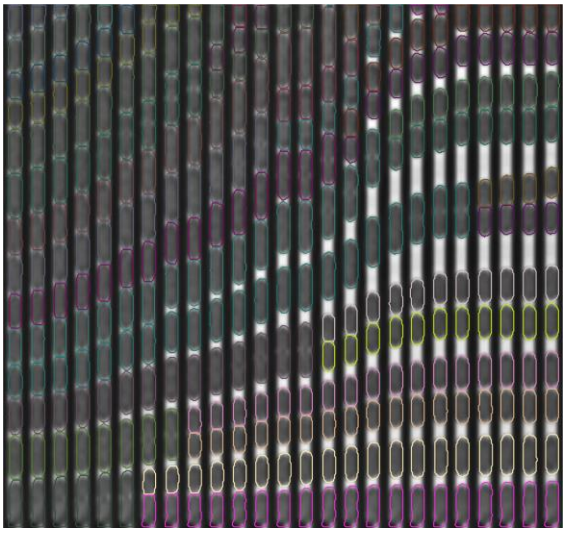

Figure 22: Time-lapse images of *E. coli* in a mothermachine growth channel segmented and tracked using Mothersegger

3.2 Labelling of *ori*, *ter* and nucleoid

Before we began our study we identified and tested existing chromosomal labelling systems for imaging in mother machine conditions (**Figure 23**). Two prevalent techniques for labelling the chromosomal loci are the fluorescent repressor-operator system (FROS) and ParB-*parS* labelling system. FROS involves placing a tandem array of operator sites, such as *lacO* or *tetO*, at a specific location on the chromosome and expressing its corresponding repressor (LacI or TetR respectively) fused with a fluorescent protein under an ectopic promoter in the chromosome or a plasmid. On the other hand, the ParB-*parS* labelling system utilises the ability of the ParB protein to nucleate near the *parS* site. Here, the *parS* site is inserted at a specific location in the chromosome, and the cognate ParB protein fused with a fluorescent protein is expressed from a plasmid or chromosome. For our study, we used the P1 ParB/*parS* labelling system to label the *ori*. It consists of a $parS_{P1}$ inserted near *oriC* and an inducible $ParB_{P1}$ fused to mTurquoise2 or CFP, expressed from a plasmid (Li et al., 2002; Nielsen et al., 2006a). This choice of labelling method was made based on the notion that the ParB-*parS* system is a naturally evolved system, and hence would likely have minimal interference on cellular processes involving DNA transactions. The *ter* region is visualised using a functional endogenous fusion of terminus specific protein MatP-YPet, which has been shown to colocalise well with loci of the terminus region (Bailey et al., 2014; Espéli et al., 2012; Männik et al., 2016; Mercier et al., 2008). The nucleoid was labelled using HU-mCherry through the endogenous fusion of *hupA-mCherry* (Figure 23). HU is a nucleoid associated protein (NAP) that binds DNA non-specifically and exists as a heterodimer of HupA and HupB.

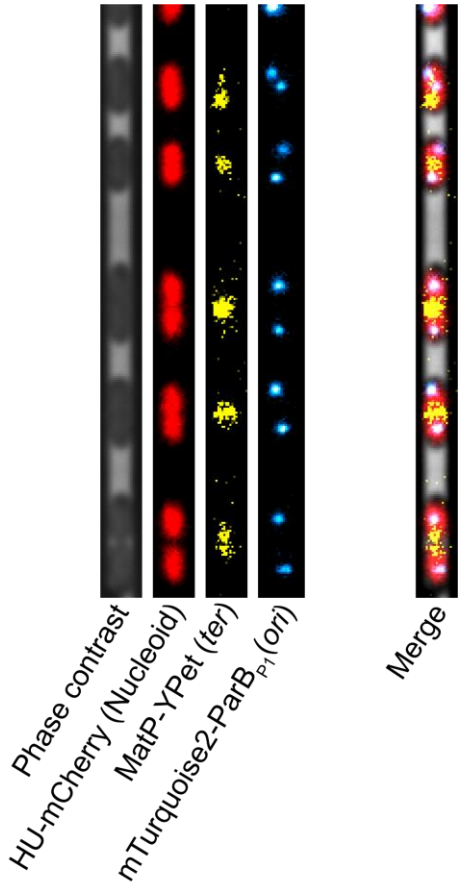

Figure 23: Fluorescence images of chromosomal labels used in this study

3.3 Steady state growth in M9 minimal media

We began our study with the *ori-ter*, dual-labelled strain (IS 130). Under our conditions the cells grew in the device with a mean cell cycle duration of 133 minutes (**Figure 24A**) and a mean birth length of 1.71 µm (**Figure 24B**). The cells had an average growth rate of 5.5 x 10^{-3} min^{-1} which was found to be maintained during the course of imaging, indicating steady state growth conditions throughout the course of imaging (**Figure 24C**). Most of the cells were born with one *ori* focus at birth and had two *ori* foci at division (**Figure 24D**).

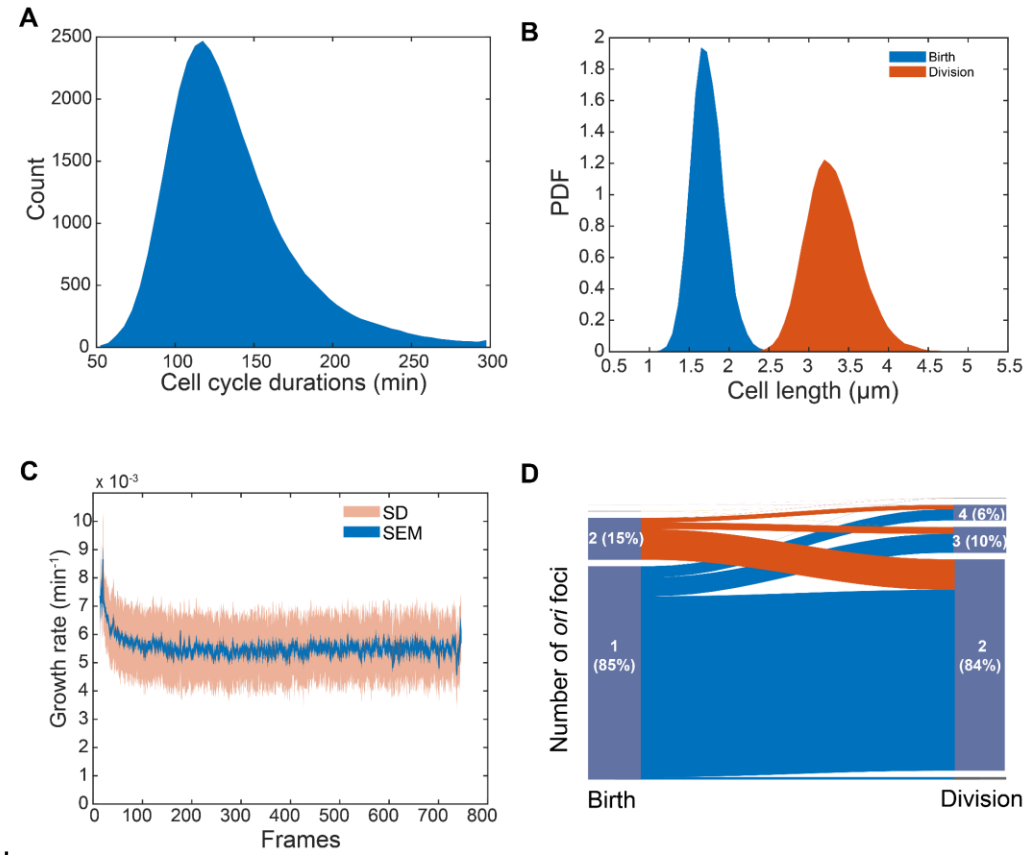

Figure 24: Growth statistics of *ori-ter* labelled strain grown in mother machine

A. Distribution of cell cycle durations (mean ± sd = 132.8 ± 39.1 min) for the IS 130 (*ori-ter* labelled) strain. **B.** Distribution of birth (1.71 ± 0.2 μm) and division lengths (3.31 ± 0.33 μm) for cells. **C.** Mean cellular growth rate showing stable growth conditions throughout the imaging every 5 minutes. **D.** Flow diagram showing the number of *ori* foci at birth and division. Data is from 38066 cell cycles.

Interestingly, we found that 15% of cells were born with more than one *ori* focus (**Figure 24D**), indicating that DNA replication was initiated in the previous cell cycle. This population, however, was not detectable in the population average kymographs or demographs (**Figure 25B, C**). In a recent publication, we have shown that this is consistent with the volume dependence of chromosome replication initiation (Donachie, 1968; Levin and Taheri-Araghi, 2019) and arises from a second replication initiation in the mother cell due to the size of the mother cell crossing the volume per origin initiation threshold for a second time in the same cell cycle (Köhler et al., 2023)

3.4 The cell cycle dynamics of *ori* and *ter*

We first examined the cell cycle dynamics of *ori*, confirming its behaviour as seen in previous studies using agarose pads at similar growth rates (Kuwada et al., 2013; Lau et al., 2003; Li et al., 2002; Nielsen et al., 2006a; Wang et al., 2005). We observed that newborn cells typically

had a single *ori* focus near the midcell, which, upon duplication, segregated outwards to the quarter positions (**Figure 25A**).

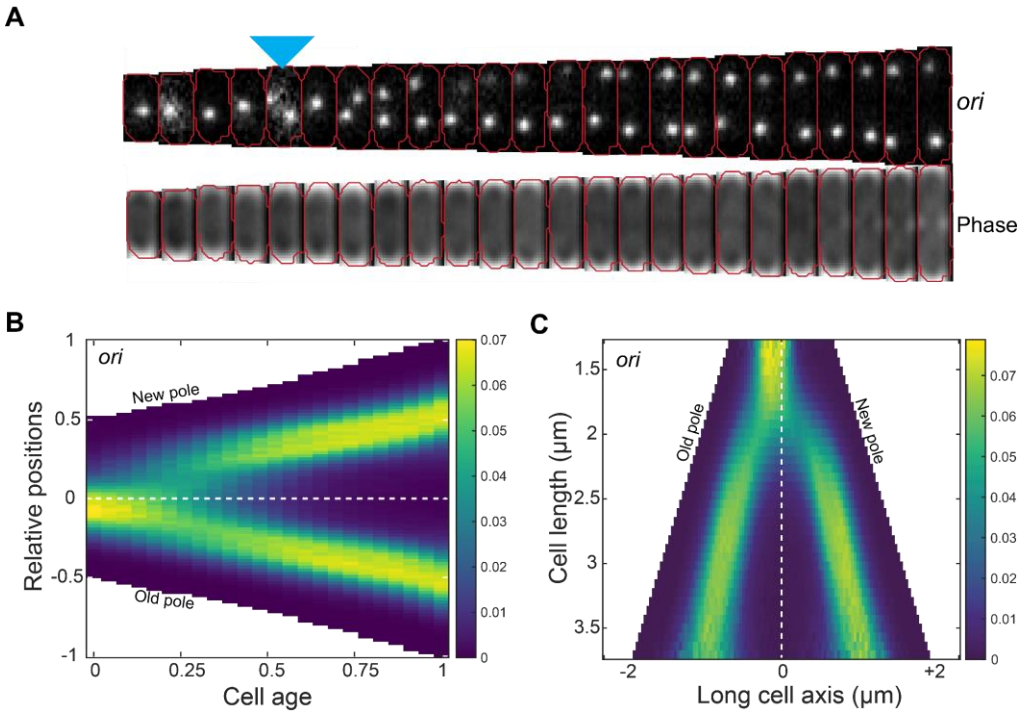

Figure 25: *ori* dynamics during the cell cycle

A. An example cell cycle showing *ori* (mTurquoise2-ParB$_{P1}$) dynamics during the cell cycle. The *ori* duplication frame is marked with a blue arrow. **B.** Population average kymograph of *ori* foci positions along the long axis of the cells. **C.** Demograph of *ori* foci positions along the long axis of cells. The values in the colour scale for the kymographs and demographs represent the frequency of occurrence of foci positions normalised to the number of cell cycles at each cell age. Data as in Figure 24 (n=38066 cell cycles).

To visualise the population-average *ori* dynamics, we created a kymograph (based on cell age) and demograph (based on cell length) to display *ori* foci positions along the long axis of the cell (**Figure 25 B, C**). We combined data from all cell cycles, binning cells according to their cell age (x=0 birth, x=1 division) or cell length, and foci positions according to their positions within the cell. Since we had access to the lineage information of cell cycles, we oriented the cells based on their new pole/old pole orientation. This revealed intriguing details about *ori* dynamics that call into question existing paradigms about *E. coli* chromosome organisation.

In contrast to *ori*, *ter* displayed localisation either at the new pole or at the mid-cell, with the mid-cell localisation being particularly tight. The *ter* (used synonymously with MatP) was observed near the new pole at birth before relocating to the mid-cell, where it remained tightly localised for most of the cell cycle (**Figure 26A**). To visualise the population average dynamics, we created kymographs and demographs for *ter* in a manner similar to *ori*. These localizations correspond to two distinct peaks visible in both the kymograph (**Figure 26B**) and

demograph (**Figure 26C**). The visible separation of MatP foci occurred just before cell division, consistent with its association to the early divisome protein FtsZ (aided by ZapB and ZapA (Espéli et al., 2012)), though the precise timing of this relative to the cell cycle is dependent on our identification of the cell division event. Correspondingly, at birth *ter* is initially found closer to the pole before moving inward to the edge of the nucleoid.

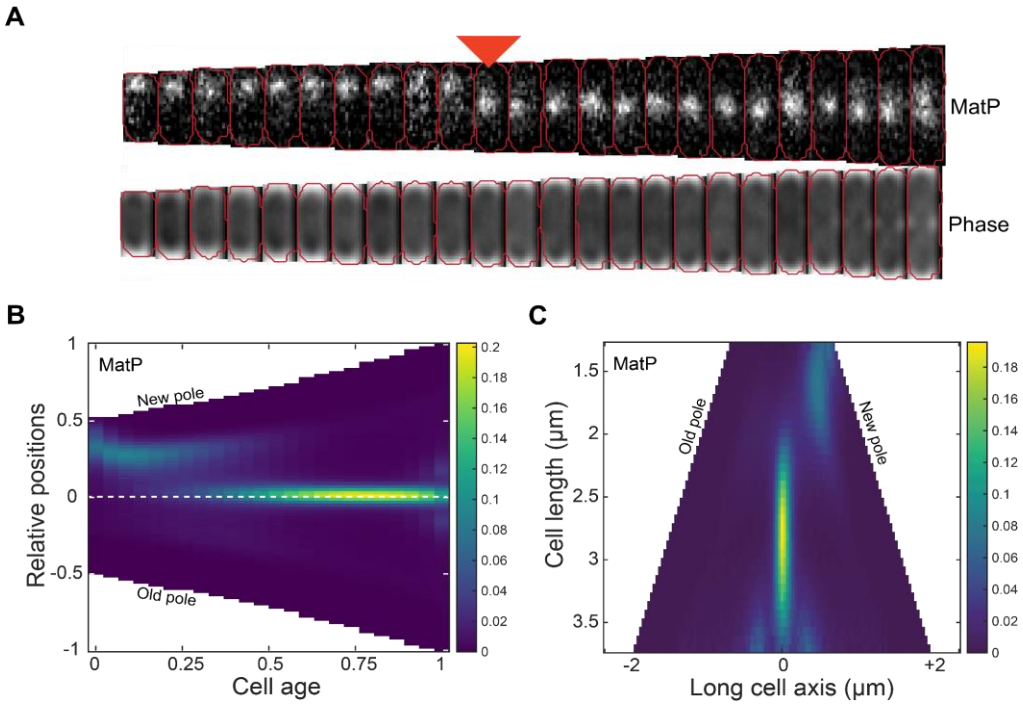

Figure 26: *ter* dynamics during the cell cycle

A. An example cell cycle showing *ter* (MatP-YPet) dynamics during the cell cycle. The *ter* relocalization frame is marked with a red arrow. **B.** Population average kymograph of MatP foci positions along the long axis of the cells. **C.** Demograph of MatP foci positions along the long axis of cells.The colour scale in **B, C** is as in Figure 25. Data as in Figure 24 (n=38066 cell cycles).

3.5 *ter* relocalization occurs after *ori* focus duplication

While these results are known, the high-throughput and temporal nature of our data allows us to quantify *ori-ter* dynamics in detail. As mentioned above, two of the important events related to *ori* and *ter* are *ori* focus duplication and *ter* relocalization to mid-cell. We find that separation of *ori* (T_{ori}), defined by two *ori* foci seen for the first time in the cell cycle, occurred on average 27 min after birth, at a cell length of 2.0 μm but with substantial variation between cells (**Figure 27A, B**).

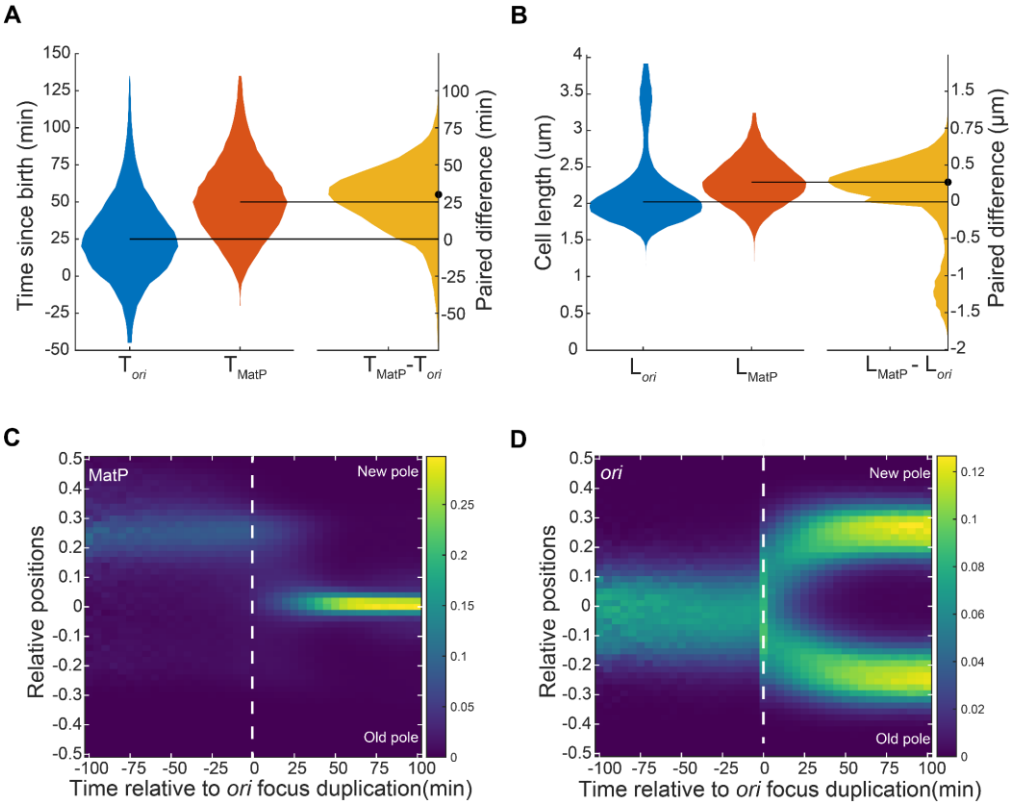

Figure 27: Distributions of time and cell length for *ori* duplication and *ter* centralisation

A. Distribution of the time of *ori* focus duplication (T_{ori}, mean ± sd = 26.6 ± 28.0 min) and *ter* relocalization (T_{MatP}, 52.8 ± 26.1 min) along with the time difference between the two events (T_{MatP}-T_{ori}, 26.5 ± 23.2 min). The negative values in T_{ori} and T_{MatP} correspond to events occurring in the previous cell cycle. The horizontal lines indicate the median values of 25 and 50 minutes for T_{ori} and T_{MatP} respectively. The dot indicates the median (30 minutes) of the paired difference T_{MatP} - T_{ori}. **B.** Distribution of cell lengths at *ori* duplication (L_{ori}) and *ter* centralization (L_{MatP}) along with their paired difference. The smaller peak for L_{ori} near 3.5 µm shows that a portion of cells duplicates *ori* twice in a cell cycle (see **Figure 24D**). **C.** Kymograph of MatP foci positions relative to the frame of *ori* foci duplication. **D.** Kymograph of *ori* foci positions relative to the frame of *ori* foci duplication.The colour scale in **C, D** is as in **Figure 25**. Data as in Figure 24 (n=38066 cell cycles).

Additionally, to visualise *ter* dynamics relative to *ori* focus duplication, we constructed a MatP kymograph synchronised to *ori* focus duplication, which shows that *ter* is localised near the new pole when *ori* focus duplicates (**Figure 27C**).

To quantify the timing of *ter* transition, we defined *ter* arrival at midcell (*ter* centralisation or T_{MatP}) as the first frame at which the MatP-YPet focus is within the middle 4.8 pixels (320 nm) of the cell for three consecutive frames (or 15 minutes). This pixel value is determined from the position distribution of MatP-YPet between cell lengths (2.48 and 3.01 µm) where the focus is found to be localised at mid-cell (**Figure 28**). Using this measure, stable *ter* localisation to mid-cell occurred on average 53 min into the cell cycle and 26 min after *ori* separation (**Figure 27A**). Our timings are consistent with those previously inferred from snapshots (Wang et al.,

2005). Here, however, we follow complete cell cycles and have captured the entire distribution of timings.

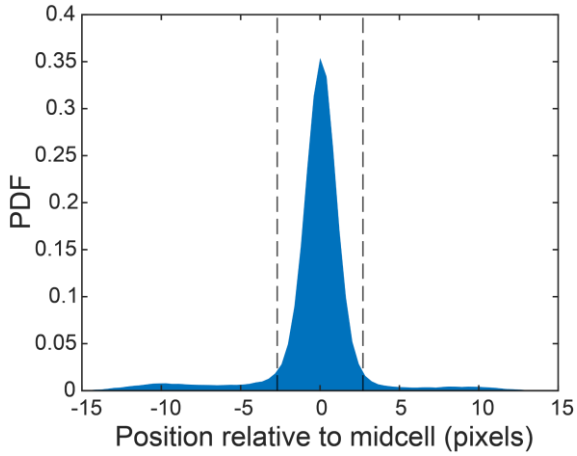

Figure 28: Distribution of MatP foci positions when MatP is at mid-cell
Probability density function of MatP foci positions in cells between 2.5 µm and 3 µm. Dashed lines indicate the width (4.8 pixels) used to define mid-cell position. Data as in Figure 25 (n=38066 cell cycles).

3.6 Origins and nucleoid are asymmetrically positioned

Our data also reveals that *ori* is not precisely positioned at the mid- and quarter-cell positions but rather exhibits a bias towards the old pole (**Figure 25B, C**). The offset is small (approximately 5% of cell length) but reproducible and persistent during the cell cycle, particularly at birth and division. As a consequence, the trajectories of segregating *ori* foci are not symmetric with the new-pole proximal *ori* moving further and faster (discussed later) to reach its target quarter-cell position. It is important to note that the bias at birth is only apparent when cells are ordered according to their polarity. It is not detectable when cells are oriented randomly, as would be the case for a snapshot-based analysis (**Figure 29**). The mid-cell positioning of *ter*, on the other hand, is precise (**Figure 26B, C**).

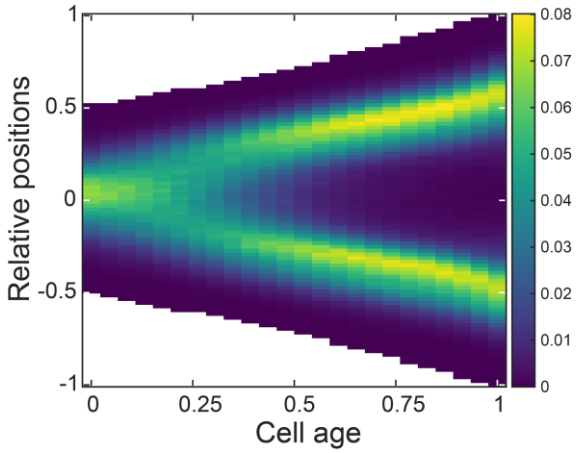

Figure 29: *ori* foci positions kymograph when cells are oriented randomly
Data and colour scale values as in Figure 25.

Since the nucleoid exhibits a new-pole bias during the early part of the cell cycle (Bates and Kleckner, 2005; Fisher et al., 2013; Hadizadeh Yazdi et al., 2012), we sought to determine how *ori* is positioned relative to the nucleoid. To do this, we examined the localisation of *ori* and *ter* in a strain expressing the nucleoid marker HU-mCherry (strain IS 129, **Figure 30A**).

Unlike the *ori* and *ter* labels, the nucleoid marker HU-mCherry forms a diffused signal within the cells. To analyse the nucleoid, we generated line profiles of the HU-mCherry signal along the long axis of the cell by computing the mean signal along its short axis at each point (pixel) on the long axis. We used these line profiles to create the nucleoid kymograph (**Figure 30B**). Additionally, we show the upper 50% (solid contour) and 80% (dashed contour) signal.

Consistent with results from previous studies, we found a clear bias of the nucleoid towards the new pole that gradually decreases during the first half of the cell cycle until the nucleoid is symmetrically positioned within the cell (**Figure 30B**). As a result, at birth the *ori* is positioned at the old-pole proximal periphery of the nucleoid, typically at the outer quarter mark of HU-mCherry signal. After duplication, one *ori* moves to the opposite side of the nucleoid resulting in a symmetric configuration with respect to both the nucleoid and the cell (**Figure 30C**). Interestingly, the position of *ter* is unaffected by the initial bias in the nucleoid position, perhaps because the bias has largely been resolved by the time of *ter* centralisation (**Figure 30D**).

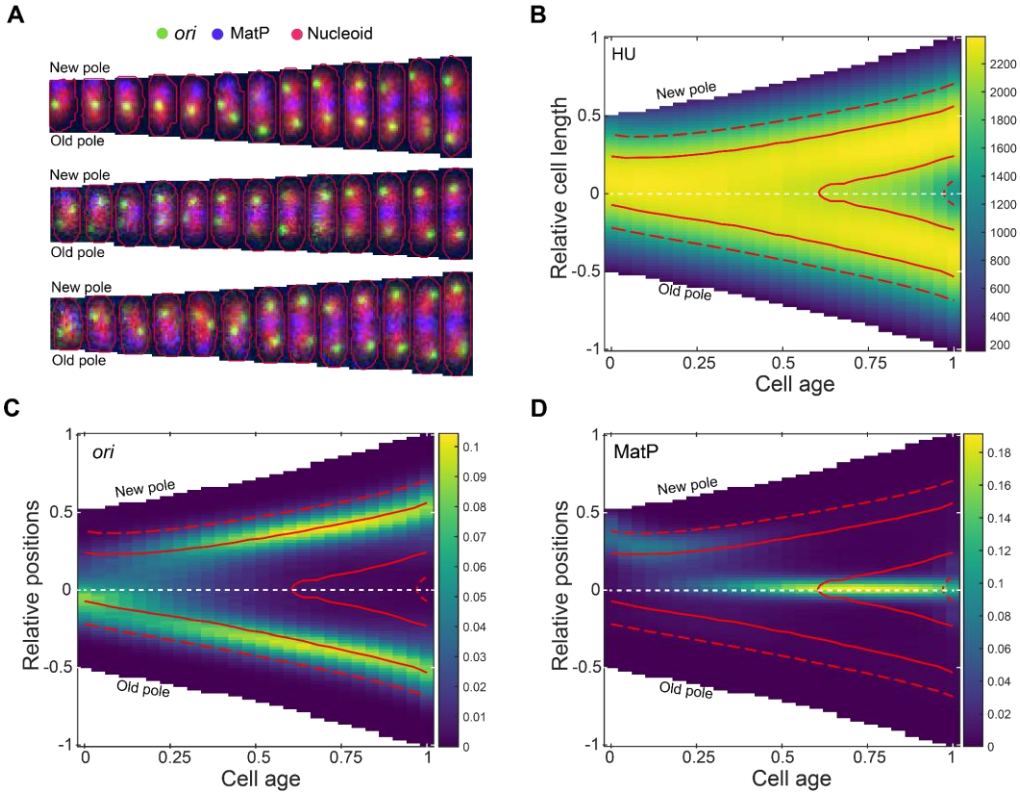

Figure 30: *ori* and *ter* are positioned at the periphery of the nucleoid

A. Representative cell cycles (10-minute intervals) with *ori* in green, HU in red and MatP in blue **B**. Population kymograph of HU-mCherry signal along the long axis of the cell. The solid and dashed contour lines enclose the upper 50 and 80 percent respectively of the total HU-mCherry signal. **C.** Population kymograph of *ori* foci positions (as in **Figure 25B**) with contour lines from **B**. **D**. Population kymograph of MatP foci positions (as in **Figure 26B**) with contour lines from **B**. The values in the colormap scale for **B** represents the mean intensity of line profiles across the cell length. The colour scale in **C** and **D** is as in **Figure 25**. Data is from 33593 cell cycles.

We investigated whether the aforementioned orientation is dependent on media conditions. To this end, we conducted experiments using two different media conditions: AB minimal media with glycerol (Nielsen et al., 2006b, 2006a) and M9 minimal media with glycerol to compare with the results from M9 minimal media with glucose. The cells exhibited average division times of 163 minutes and 170 minutes in AB glycerol and M9 glycerol, respectively (**Figure 31**).

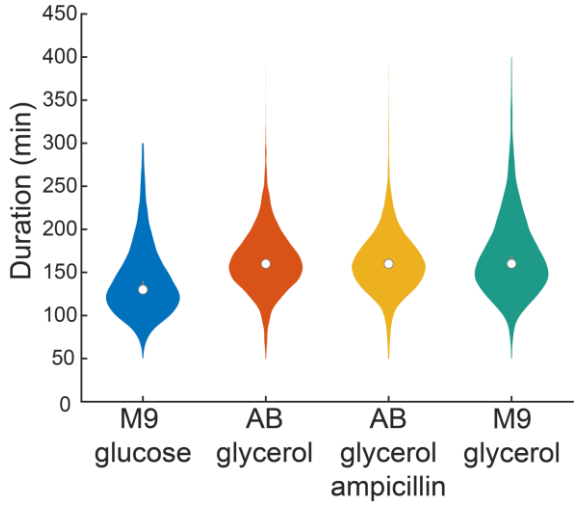

Figure 31: Distribution of cell cycle durations in different media

Growth rate of IS 129 strain in different media conditions. The white dots indicate mean - M9 minimal media with glucose (mean ± s.d = 140.7 ± 41.7 min), AB minimal media (162.8 ± 35.8 min), AB minimal media with ampicillin (161.1 ± 35.9 min) and M9 minimal media with 0.2% glycerol (169.6 ± 48.1 min). All experiments except M9 glucose were done at 32^{o}C.

Under these conditions, we observed that *ori* and *ter* displayed a similar positioning within cells, with *ori* duplication and *ter* centralization occurring later in the cell cycle compared to M9 glucose conditions. Intriguingly, *ori* duplication occurred markedly earlier in M9 glycerol (**Figure 32C**) than in AB glycerol (**Figure 32A, B**), despite nearly identical cell division times in both conditions.

Notably, we found that *ori* is situated at the outer quarter mark of the HU-mCherry signal for approximately 50 percent of the cell cycle duration. The *ori* is found to be positioned at the centre of the nucleoid only during its duplication. Taking these observations into account, we infer that *ori* duplicates at the centre of the nucleoid and subsequently relocates to the periphery following duplication, similar to what we observe in M9 glucose conditions.

A previous study on vegetative *B. subtilis* has shown that during replication, chromosome organisation alternates between *ori-ter* and left-*ori*-right configurations (Wang et al., 2014). Our results suggest that *E. coli* shares a similar pattern of chromosome organisation with *B. subtilis*. Overall, these results refine our understanding of *ori-ter* positioning in slow-growing *E. coli* cells during steady state growth and draw upon similarities between *E. coli* and *B. subtilis* chromosome organisation.

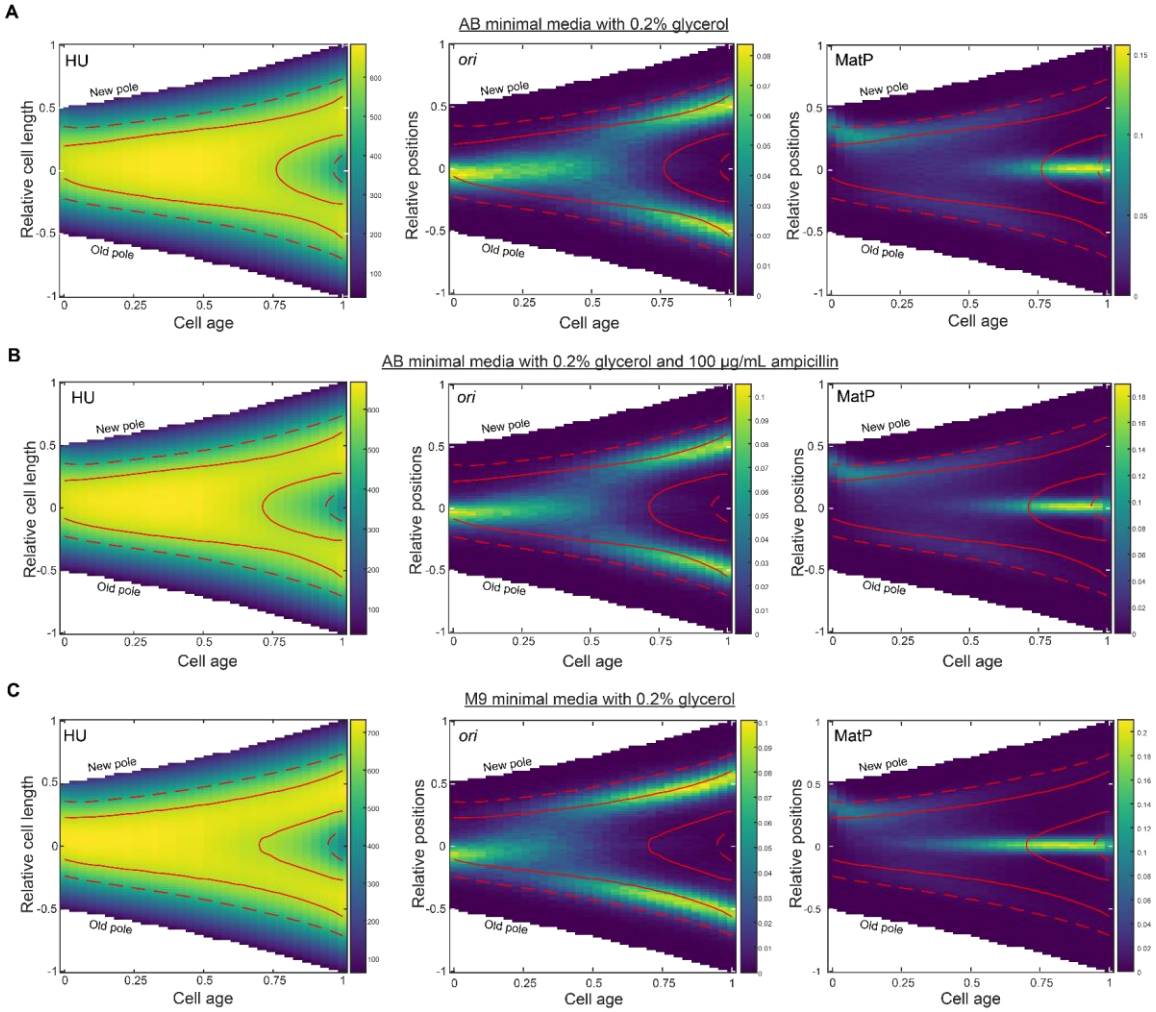

Figure 32: *ori* and *ter* are positioned at the periphery of nucleoid in different media conditions

A. (Left) Average kymograph of HU-mCherry signal along the long axis of the cell. The solid contour lines represent upper 50 percent, and the dashed lines represent upper 80 percent of the total HU-mCherry signal. Average kymograph of *ori* foci positions (middle) and MatP foci positions (right) with contour lines from HU-mCherry grown in AB minimal media with 0.2% glycerol, 1 µg/mL thiamine and 1 µg/mL uracil (n=7281 cell cycles). **B.** Same as **A**, but grown in AB minimal media with 0.2% glycerol, 1 µg/mL thiamine, 1 µg/mL uracil and 100 µg/mL ampicillin (n=8128 cell cycles). **C.** Same as **A, B**, but grown in M9 minimal media supplemented with 0.2% glycerol (n=6973 cell cycles). The colour scales are as in Figure 30.

3.7 Left and right chromosomal arms lie between *ori* and new pole during the cell cycle

Given that we find *ori* foci localising along the outer quarter mark of the nucleoid signal, we asked whether the left and right chromosomal arms localise outside or inside the outer quarter mark. Some of the previous studies have observed that the left and right chromosomal arms occupy opposite cell halves along the long axis, implying that the chromosome would adopt a left-*ori*-right orientation (Mäkelä et al., 2021; Nielsen et al., 2006b; Wang et al., 2006). If true, considering the localization of *ori* along the outer quarter mark of the nucleoid signal during

the cell cycle, the loci belonging to one of the chromosomal arms would need to localise outside the outer quarter mark of the nucleoid signal, which constitutes less than 25 percent of the nucleoid mass. Notably, these studies have not simultaneously probed the localization of arms with respect to the nucleoid and *ori*.

To this end, we investigated the localization of the *rhlE* locus or *elaD* locus, which is located at at 4 o'clock and 8 o'clock, respectively with respect to *ori*, using $parS_{pMT1}$/$ParB_{pMT1}$ chromosomal labelling system. These strains also had their *ori* and nucleoid labelled as described before (**Figure 33**). Additionally, we also generated a strain which had both *rhlE* and *elaD* loci labelled with $parS_{P1}$ and $parS_{pMT1}$, respectively, along with nucleoid. These loci are adjacent to regions R3 and L3, previously observed to reside in separate cell halves with significant distance between them (Wang et al., 2006).

Upon imaging these strains, we observed a similar positioning of the *ori* relative to the nucleoid as in our previous results (**Figure 33B, E**). For reasons not fully understood, the strain with the right-arm label showed earlier *ori* duplication, which did not impact its overall organisation (**Figure 33E**). In contrast to *ori*, both the left and right arms were found towards the opposite edge of the nucleoid, specifically before division when the loci typically resided at the inner quarter mark of the corresponding nucleoids (**Figure 33C, F**). In other words, on average, we find that chromosomal loci belonging to the left and right arms reside between *ori* and new pole (at birth) or *ori* and midcell (towards division) during the cell cycle.

We quantified these observations by measuring the frequency of various possible arrangements of *ori* (O), *elaD* (L), and *rhlE* (R) relative to the new (NP) and old (OP) poles. We found that 84% or 83% of newborn cells showed an NP-L-O-OP or NP-R-O-OP pattern respectively, indicating that the left and right loci were predominantly found closer to the new pole than *ori*. Moreover, 78% or 74% of cells before division displayed an O-L-L-O or O-R-R-O pattern respectively, thereby replicating the predominant arrangement in the daughter cells (**Figure 33J, K**). This pattern deviates from the transverse L-O-R chromosome organisation proposed by several studies, where L and R are equally likely to be close to the new pole at birth, and sister chromosomes relate primarily through translation, yielding an L-O-R-L-O-R pattern before division (**Figure 33L**).

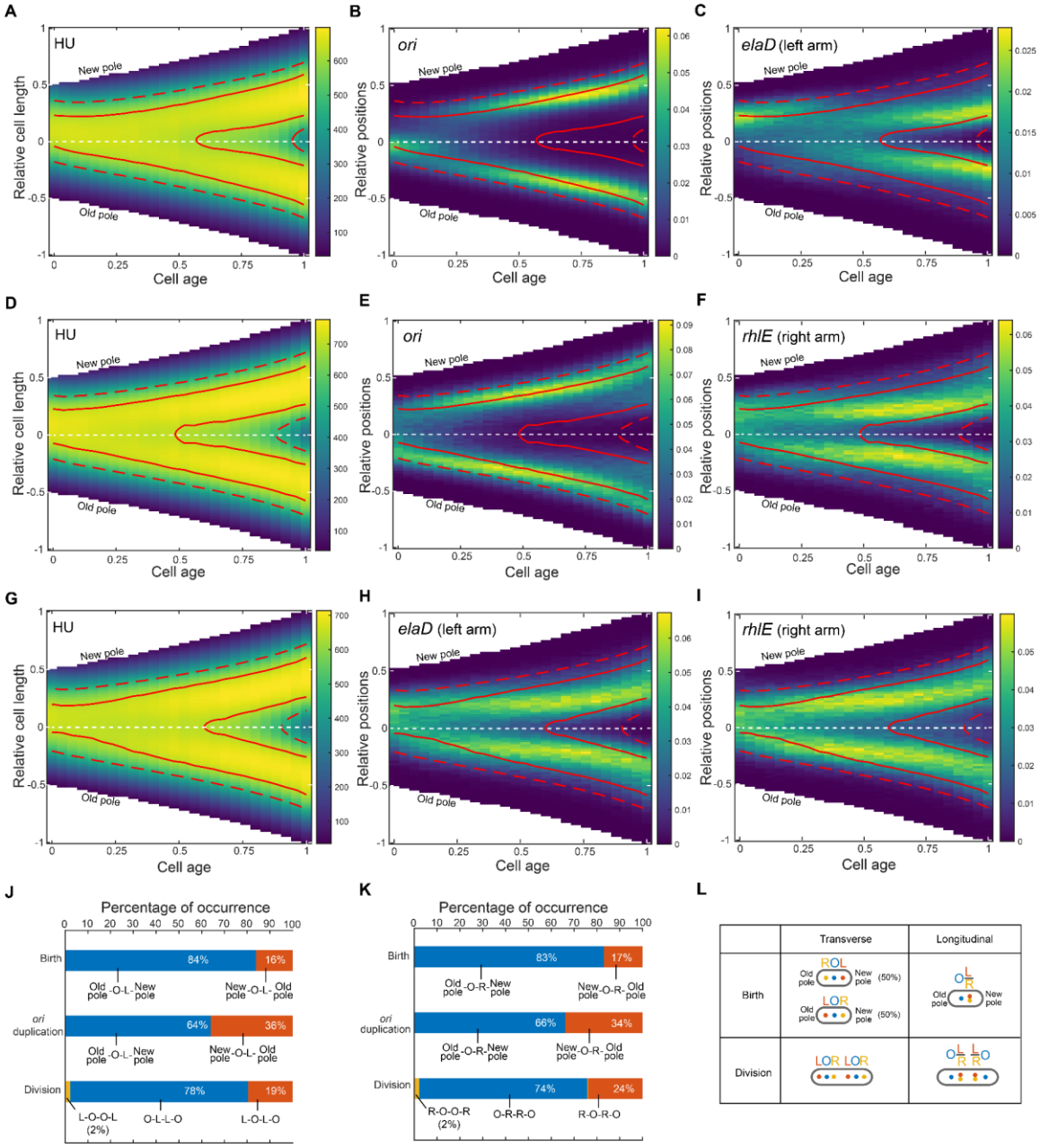

Figure 33: Left and right chromosomal arms localise within the bulk nucleoid signal

A, D, G. Average kymograph of HU-mCherry signal along the long axis of the cell for each of the strains. The solid contour lines represent upper 50 percent, and the dashed lines represent upper 80 percent of the total HU-mCherry signal for the respective strain **B, E.** Average kymograph of foci positions of *ori* labelled with mTurquoise2-ParB$_{P1}$ in strains that has *elaD* locus or *rhlE* locus tagged with mVenus-ParB$_{pMT1}$. The contour lines correspond to the respective HU-mCherry signal in each strain. **C, F.** Average foci kymograph of *elaD* or *rhlE* locus labelled with mVenus-ParB$_{pMT1}$ in strains that has *ori* labelled with mTurquoise2-ParB$_{P1}$. **H, I**. Average kymograph of foci positions of *elaD* and *rhlE* locus labelled using mVenus-ParB$_{pMT1}$ and mTurquoise2-ParB$_{P1}$ respectively in the same strain **J, K**. Percentage of occurrence of different chromosome orientations. **L.** Schematic representation of chromosome orientations in transverse and longitudinal configurations. The colour scales for kymographs are as in Figure 30. (n>3000 cell cycles for each strain)

Overall, our results are largely inconsistent with the transverse L-O-R organisation, proposed to predominate during slow growth conditions, in which the chromosomal arms are expected to occupy opposite cell halves along the long axis. Instead, we observed a pattern reminiscent of a "longitudinal-like" arrangement, where the *ori* and *ter* are situated towards opposite ends of the nucleoid, with chromosomal arms occupying the opposite lateral cell halves between them. Acknowledging the validity of previous results, we propose that both transverse and longitudinal organisations might occur during slow growth. The specific conditions determining one pattern over the other, however, remain unclear.

3.8 *ter* centralisation occurs before nucleoid constriction

In a recent study, it was proposed that the *ter* centralisation occurs shortly before the formation of a stable constricted or bilobed nucleoid structure, which in turn influences the onset of cell division (Männik et al., 2016; Tiruvadi-Krishnan et al., 2022). Our high-throughput dataset allowed us to investigate and quantify this observation in greater detail. We performed a comprehensive analysis of the HU-mCherry signal along the long-axis of the cells. This enabled us to accurately determine the time point at which a stable (i.e., non-transient) nucleoid constriction was established (**Figure 34**).

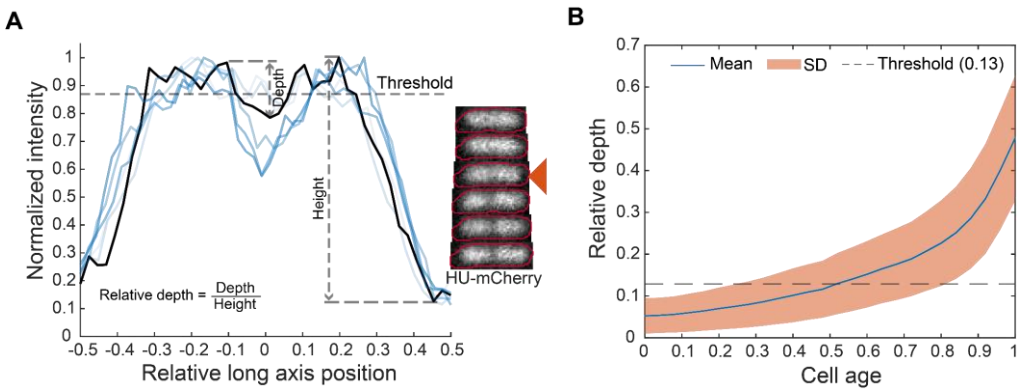

Figure 34: Relative depth of nucleoid constriction during cell cycle

A. Line profile plots of HU-mCherry signal on different frames with corresponding images. The threshold for the stable constriction is shown in a grey dashed line. Red arrow indicates the frame corresponding to the stable constriction for this cell cycle whose line profile indicated in black. Parameters used for determining nucleoid constriction are also shown. **B.** Relative depth of HU-mCherry signal binned according to the cell age (25 bins). The threshold (0.13) for nucleoid constriction is defined as the value at the 95th percentile of the first bin based on the assumptions that no new born cell has a truly constricted nucleoid so that any dips observed are due to random fluctuations. The blue line represents the mean, and the shaded region represents standard deviation. Data as in **Figure 30**.

For this analysis, we created line profiles of the HU-mCherry signal along the long axis of the cell by calculating the mean signal along the short axis at each point (pixel) on the long axis.

A nucleoid constriction, or bilobeness, manifests as a dip in the signal near the mid-cell in the line profile. Nucleoid segregation occurs in stages (Fisher et al., 2013), leading to transient dips in the line profile. In contrast, a stable constriction arises when the nucleoid steadily separates, resulting in a consistent increase in the dip across successive frames. We used this characteristic to define the occurrence of a stable constriction in the nucleoid during the cell cycle. Additionally, we established a threshold value for the dip to be considered as a constriction, which helps filter out noise. The threshold value (0.13) is given by the 95th percentile of the relative depth of the nucleoid signal in new-born cells i.e., the first bin of the plot in **Figure 34B**. Consequently, a signal dip is deemed a stable nucleoid constriction ($T_{nucleoid}$) if its relative depth exceeds the threshold and maintains this state until division.

Our results indicate that the occurrence of stable nucleoid constriction was significantly delayed by approximately 45 minutes compared to the *ter* centralization event (**Figure 35A**). This contrasts with the results from Männik et al., which reported only an 8-minute delay between the two events. The discrepancy in the estimates between the studies could be attributed to differences in constructing the line profile and defining stable constriction. While we used the mean signal across the points in the long axis, Männik et al. used pixel intensities along the long axis of the cell to construct line profiles. Additionally, a recent study has shown that timing of nucleoid constriction varies across conditions (Govers et al., 2023). Nevertheless, our observations call into question the idea of a direct causal relationship between *ter* centralization and nucleoid constriction, implying that other factors or mechanisms may be involved.

Our study has successfully delineated the timing of three critical cell cycle events: (1) the separation of duplicated origins, (2) *ter* centralisation, and (3) the onset of nucleoid constriction (**Figure 36A**). While the timing of these events exhibits considerable variation among individual cells, our findings reveal that, in at least 87 percent of cells, these events occur sequentially in the order described above (**Figure 36B**).

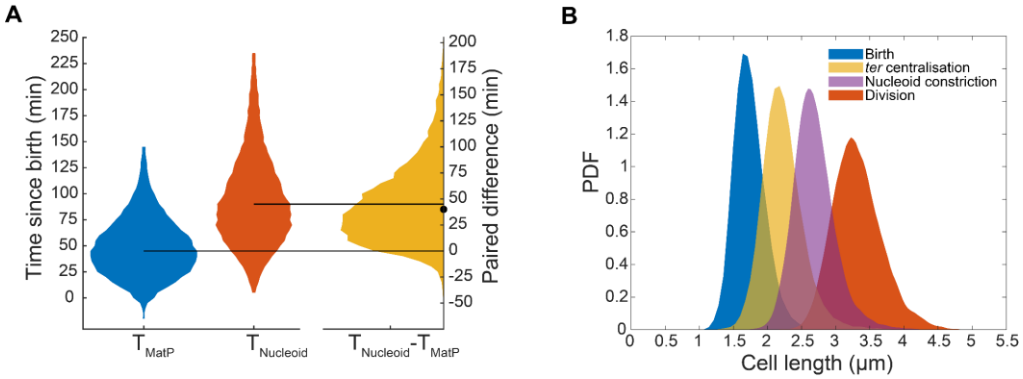

Figure 35: Timing and cell lengths at which *ter* centralisation and nucleoid constriction occur

A. Distribution of the time of MatP centralisation, T_{MatP} (mean ± sd = 49.5 ± 28.4 min) and stable nucleoid constriction, $T_{Nucleoid}$ (94.2 ± 43.7 min) along with the time difference between the two events (51.5 ± 38.1 min) as in **Figure 27**. The horizontal lines indicate the median values of 45 and 90 minutes for T_{MatP} and $T_{Nucleoid}$ respectively. The dot indicates the median (40 minutes) of the paired difference $T_{Nucleoid}$ - T_{MatP}. **B.** Distribution of cell lengths at which T_{MatP} (2.22 ± 0.30 μm) and $T_{Nucleoid}$ (2.68 ± 0.30 μm) occur in cell cycles along with their birth (1.73 ± 0.22 μm) and division lengths (3.32 ± 0.36 μm). Data as in **Figure 30.**

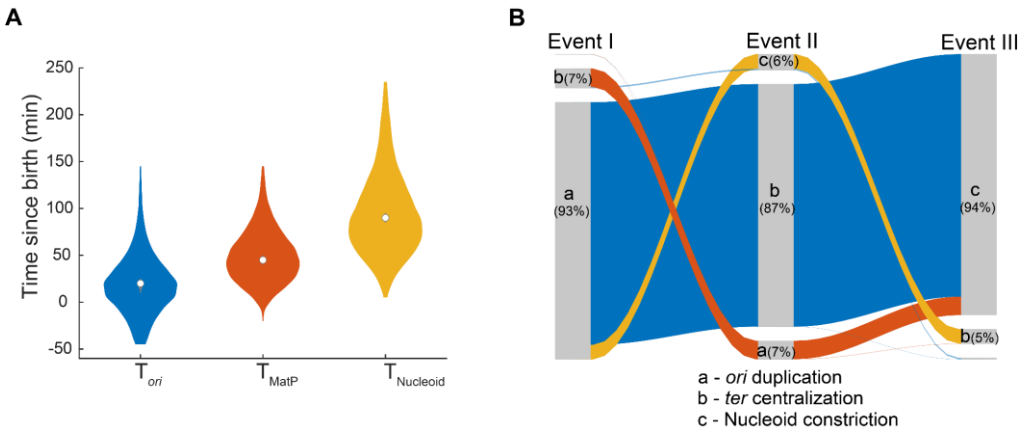

Figure 36: Order of occurrence of events

A. Distribution of time of *ori* focus duplication, T_{ori} (mean ± s.d = 20.0 ± 32.3 min) MatP centralization, T_{MatP} (49.7 ± 28.6 min) and stable nucleoid constriction, $T_{Nucleoid}$ (95.0 ± 44.3 min) for strain IS 129 (*ori*, *ter*, HU labelled). The white dots indicate the mean. **B.** Order of occurrence of events involving *ori* duplication, *ter* centralization and (stable) nucleoid constriction. a, b and c represent the events *ori* duplication, *ter* centralization and nucleoid constriction respectively. The corresponding percentages indicate the proportion of cells in which a particular event was first (Event I), second (Event II) or third (Event III) to occur. Data as in Figure 30.

3.9 *ter* centralisation is a rapid event

The kymographs and demographs of *ter* (**Figure 26B, C**) reveal the presence of distinct peaks, which implies that the migration of the *ter* region from the edge of the nucleoid towards the midcell takes place rapidly in comparison to its movement during other stages of the cell cycle.

In some instances, this transition was observed to occur within a single frame, equivalent to a 5-minute duration (**Figure 26A**). This rapid migration can be clearly visualised by synchronising the cell cycles according to the time of *ter* centralisation (**Figure 37A**).

Upon synchronisation, we observed that the mean stepwise velocity of MatP foci, as measured between consecutive frames, exhibited a sharp peak during the transition, followed by a rapid decline to zero shortly thereafter (**Figure 37B**). It is important to note that this observed pattern is not an artefact of the synchronisation process. In fact, the most significant movement consistently took place during the transition phase, as evidenced by the data presented in **Figure 38**.

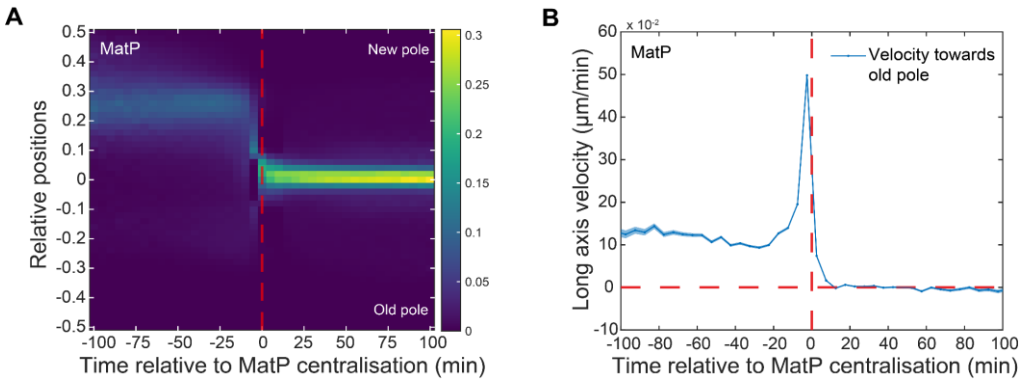

Figure 37: *ter* centralisation is a rapid event

A. Kymograph of MatP foci positions synchronised to MatP centralisation. **B.** Mean velocity of the MatP focus towards the old pole relative to the time of MatP centralisation. The colour scale in **A** is as in **Figure 25**. Shading in **B** indicates standard error of the mean. Data as in Figure 25.

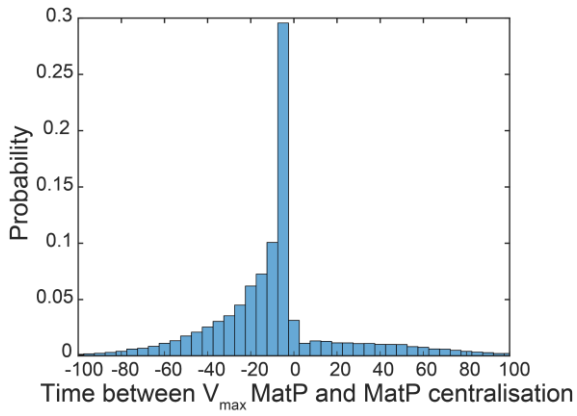

Figure 38: Greatest MatP movement most frequently occurred during *ter* centralisation

Distribution of time between the frame that has maximum MatP focus velocity (stepwise) and the frame in which MatP centralization occurs. Negative values indicate the maximum MatP velocity occurred before MatP centralisation. Bin width is 5 minutes. Data as in Figure 25.

While the migration of *ter* to mid-cell has previously been attributed to the action of the mid-cell localised replication machinery (Espéli et al., 2012), it is unclear if this is consistent with such a rapid transition. Indeed, a study of chromosome organisation during fast growth found that *ter* centralisation was correlated with cell length rather than progression of the replication fork and that, irrespective of when the transition occurred the remaining unreplicated DNA migrates with it (Youngren et al., 2014). This is consistent with the large variation we observe in the timing of the transition (**Figure 27A**), which can occur even before visible origin separation or as late as 75 min afterwards.

3.10 *ter* centralisation coincides with completion of *ori* segregation

The kymographs in Figures 25, 26 and 30 indicate that *ter* centralisation occurs at approximately the same time as *ori* segregation. In fact, after synchronising the *ori* foci positions relative to *ter* centralisation, it became clear that centralisation is coincident with the completion of *ori* segregation, i.e, with the arrival of the replicated ori at the quarter positions of the cell (**Figure 39A**). The average velocity of both the new pole and old-proximal ori increased steadily up to the *ter* transition before dropping rapidly, with the peak occurring at the same time as that of *ter* (**Figure 39B**). We additionally note that the new pole-proximal *ori* exhibits a higher mean velocity than its sister, consistent with our previous observation of asymmetric *ori* segregation (**Figure 25A, 30C**). Overall these results indicate a coupling between *ter* centralization and the completion of origin segregation and it is tempting to speculate a causative relationship between the two events, namely that the final stage of *ori* segregation somehow triggers *ter* to rapidly move to midcell.

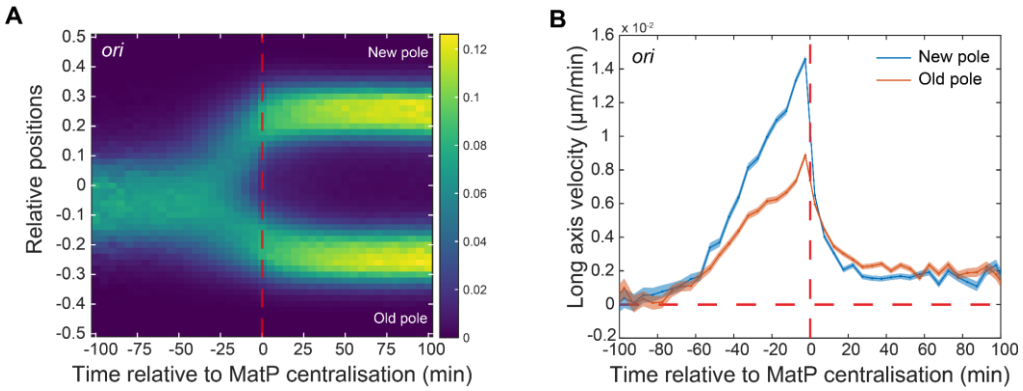

Figure 39: *ter* centralisation coincides with completion of *ori* segregation
A. Kymograph of *ori* foci positions synchronised to MatP centralisation **B.** Mean velocity of *ori* foci towards the nearest pole relative to the time of MatP centralisation. The colour scale in **A** as in Figure 25. Shading in **B** indicate standard error of the mean. Data as in Figure 25.

3.11 *ter-ori* coupling does not depend on the *ter* linkage

If the processes of *ter* centralisation and *ori* segregation are genuinely interconnected, disrupting one or both of these processes may provide insights into their mutual dependence. To investigate the interconnection, our study initially focused on the process of *ter* centralisation. Previous research has indicated that upon arrival at the midcell, *ter* is partially anchored to the divisome by a protein linkage involving FtsZ, ZapA, ZapB, and MatP (Espéli et al., 2012). It has been shown that disrupting this linkage can reduce the duration of *ter* centralization and modify the timing of sister *ter* segregation (Espéli et al., 2012; Männik et al., 2016; Nolivos et al., 2016).

However, when we analysed a *zapB* deletion strain, we observed that the impact on MatP foci positioning was relatively minor, with only a slight broadening of its position distribution and marginally earlier segregation (compare **Figure 26B** and **Figure 40C**).

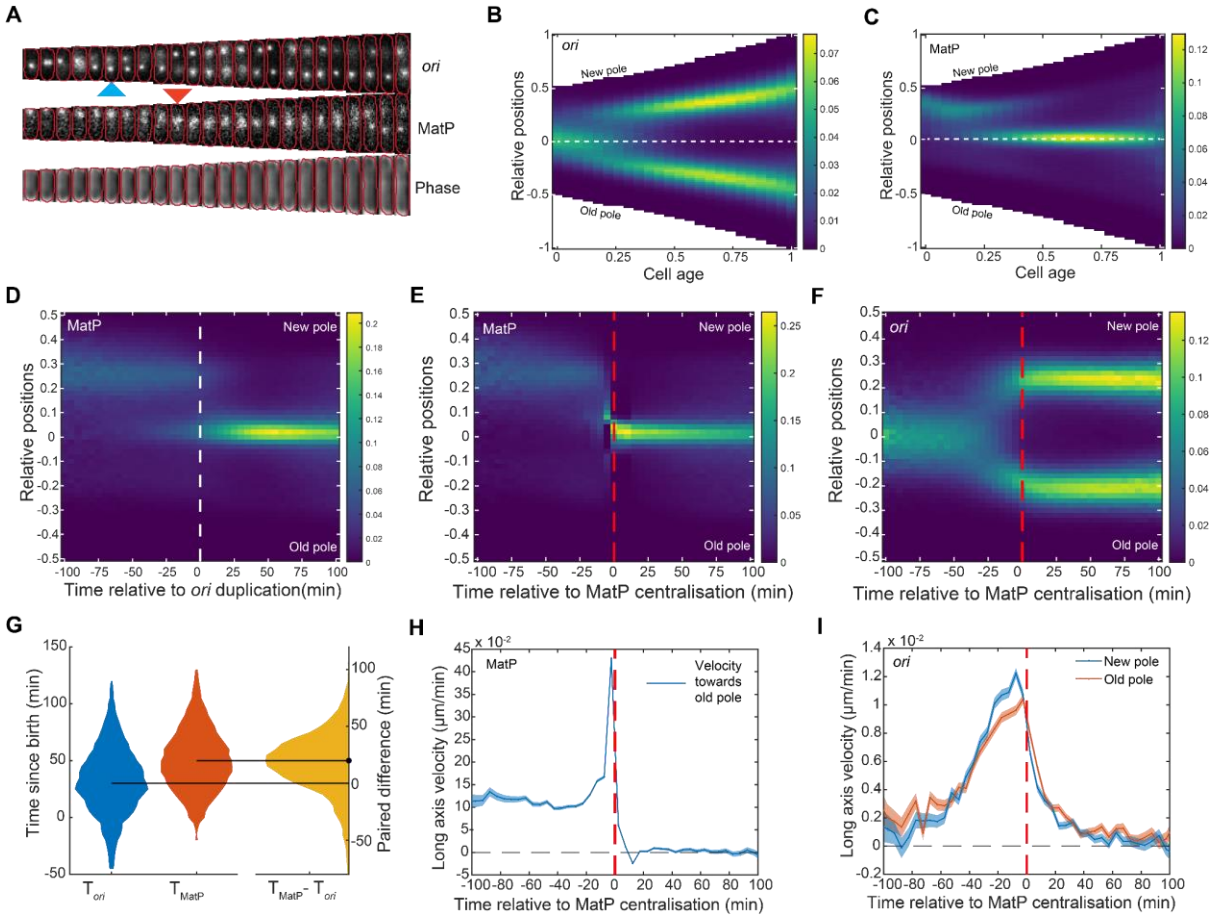

Figure 40: *ter*-linkage is not involved in MatP relocalization

A. An example cell cycle of Δ*zapB* strain with *ori* and MatP labelled. The blue arrow indicates *ori* focus duplication and the red arrow indicates MatPΔC20 relocalization to midcell. **B.** Kymograph of *ori* foci positions in a Δ*zapB* strain. **C.** Kymograph of MatP foci positions in a Δ*zapB* strain. **D.** Kymograph of MatP foci positions synchronised to ori focus duplication in a Δ*zapB* strain. **E.** Kymograph of MatP foci positions in a Δ*zapB* strain synchronised to MatP centralisation. **F.** Kymograph of *ori* foci positions synchronised to MatP centralisation in a Δ*zapB* strain **G.** Distribution of the time of *ori* focus duplication,

T_{ori} (mean ± sd = 32.6 ± 29.9 min) and MatP centralization, T_{MatP} (50.5 ± 27.2 min) along with the time difference between the two events (17.9 ± 27.2 min) similar to Figure 27A. The horizontal lines indicate the median values of 30 and 50 minutes for T_{ori} and T_{MatP} respectively. The dot indicates the median (20 minutes) of the paired difference T_{MatP} - T_{ori} . **H.** Mean step-wise velocity of MatP focus tracks towards the old pole relative to MatP centralisation in a Δ*zapB* strain. **I.** Mean velocity of *ori* foci tracks towards the nearest pole relative to the time of MatP centralisation in a Δ*zapB* strain. Shading in **H** and **I** indicate standard error of the mean. The colour scale in **B**, **C**, **D**, **E** and **F** as in Figure 25. Data is from 20183 cycles.

Nonetheless, the transition to mid-cell still occurred rapidly (**Figure 40E**). Interestingly, the asymmetry in *ori* positioning was almost non-existent, with only a slight difference in the velocity of sister *ori* detectable (**Figure 40B, F, I**). This would imply that in the absence of *ter*-linkage sister *ori* segregation is symmetric compared to wild-type and that *ter*-linkage affects *ori* positioning. Despite this, *ter* centralisation was still coincident with the completion of origin segregation (**Figure 40F**).

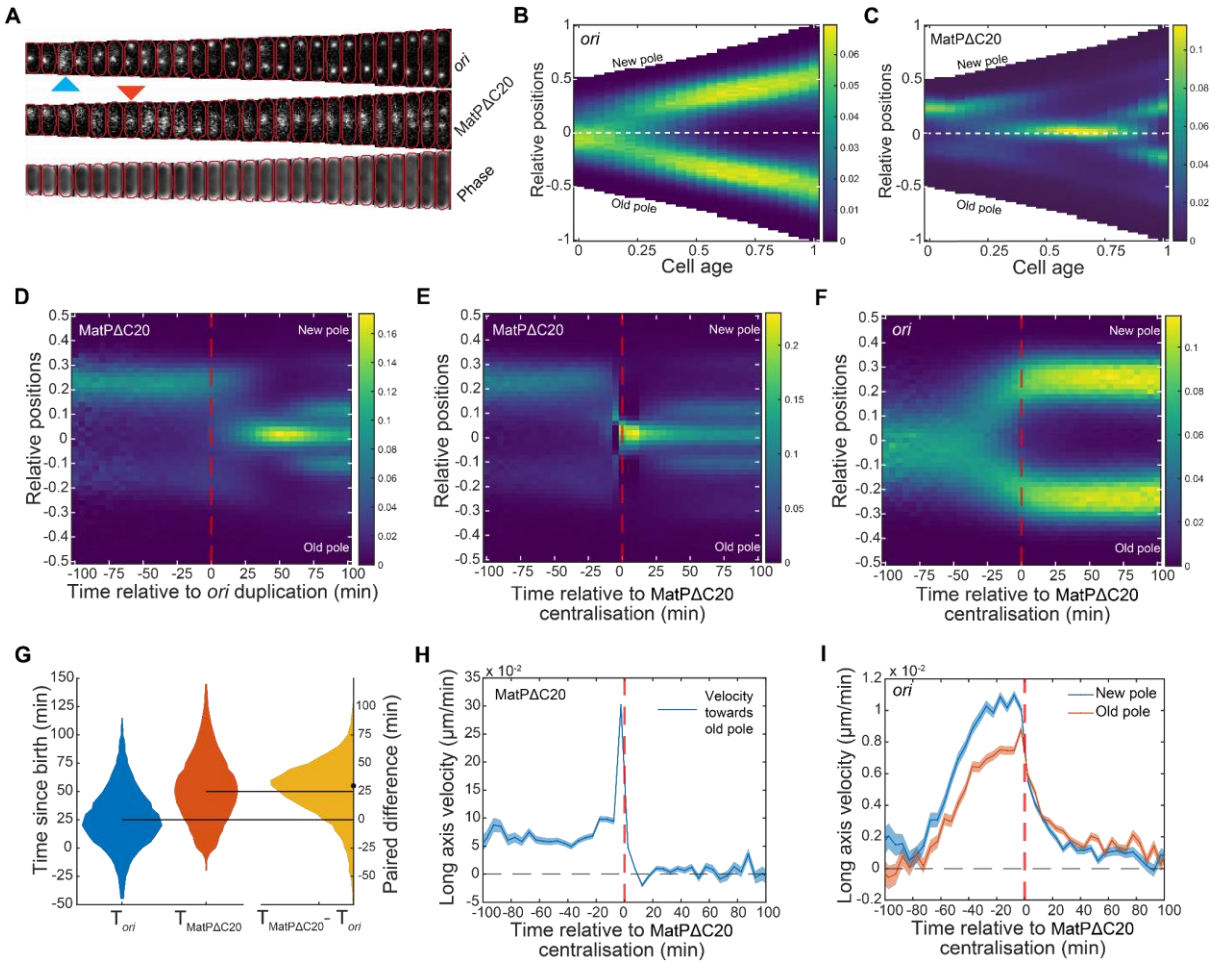

Figure 41: *ter* centralisation coincides with *ori* segregation in MatPΔC20 strain

A. An example cell cycle of *matPΔC20* strain with *ori* and MatPΔC20 labeled. The blue arrow indicates *ori* focus duplication and the red arrow indicates MatPΔC20 relocalization to midcell. **B.** Average foci position kymograph of *ori* in a *matPΔC20* strain **C.** Average foci position kymograph of MatPΔC20 in a

matPΔC20 strain. **D.** Kymograph of MatPΔC20 foci positions synchronized to *ori* focus duplication. **E.** Kymograph of MatPΔC20 foci positions synchronized to MatPΔC20 centralization. **F.** Kymograph of *ori* foci positions relative to MatPΔC20 centralization. **G.** Distribution of the time of *ori* focus duplication, T_{ori} (mean ± sd = 26.7 ± 26.8 min) and MatPΔC20 centralization, $T_{MatP\Delta C20}$ (52.4 ± 30.0 min) along with the time difference between the two events (25.8 ± 27.0 min) similar to Figure 27A. The horizontal lines indicate the median values of 25 and 50 minutes for T_{ori} and $T_{MatP\Delta C20}$ respectively. The dot indicates the median (30 minutes) of the paired difference $T_{MatP\Delta C20}$ - T_{ori}. **G.** Mean velocity of MatPΔC20 focus track towards the old pole relative to MatPΔC20 centralisation. **H.** Mean velocity of *ori* foci tracks towards the nearest pole relative to the time of MatPΔC20 centralisation. Shading in **H** and **I** indicate standard error of the mean. The colour scale in **B**, **C**, **D**, **E** and **F** as in Figure 25. Data is from 18202 cell cycles.

A more pronounced phenotype was observed in *matPΔC20* cells, in which MatP lacks 20 amino acids from its C-terminal. This is believed to prevent its multimerisation and interaction with ZapB, which is required for the formation of *ter*-linkage, but not its binding to *matS* (Crozat et al., 2020; Dupaigne et al., 2012; Espéli et al., 2012; Nolivos et al., 2016). We found that, although the timing of *ter* centralisation is very similar to that of the wild type, *ter* is more dynamic and often overshoots the mid-cell before returning (**Figure 41A**). This was apparent at the population level, as indicated by a smear in the kymograph (**Figure 41C**). The segregation of sister *ter* occurs noticeably earlier, resulting in a correspondingly shorter period of centralisation (**Figure 41C, D, E**). Despite these irregularities, *ori* positioning seems largely unaffected **(Figure 41B**), and importantly, the completion of *ori* segregation remains coincident with *ter* centralisation (**Figure 41F, I**). We also noted that the time between *ori* duplication and *ter* centralisation is slightly reduced in *ΔzapB* mutant compared to the wild type. As it seems unlikely that this mutation would increase the duration of duplicated *ori* cohesion or accelerate DNA replication, this supports the idea that *ter* migration is not directly triggered by replication fork progression.

In summary, these findings provide further evidence that the *ter*-linkage isn't necessary for the movement of *ter* to mid-cell or its sustained presence there. They also illustrate the robustness and predictability of the relationship between the centralisation of *ter* and the completion of *ori* segregation.

3.12 MatP centralisation occurs in the absence of SMC complex MukBEF

One possible explanation for this observed coupling between *ori* and *ter* could lie in the activity of the Structural Maintenance of Chromosomes complex MukBEF. This complex plays a key role in *E. coli* chromosomal organisation and is instrumental in ensuring correct *ori* positioning (Badrinarayanan et al., 2012a; Danilova et al., 2007; Hofmann et al., 2019). MukBEF forms DNA-associated clusters that co-localize with *ori*, but are displaced from the terminus region due to their interaction with MatP (Lioy et al., 2018; Nolivos et al., 2016). As such, MukBEF

could feasibly act as the mediator of the observed coupling. However, our findings suggest that *ter* positioning largely persists in the absence of MukBEF (**Figure 42**), aligning with the findings of a recent study (Mäkelä et al., 2021). Importantly, even without MukBEF, *ter* continues to exhibit a similar rapid transition from the new pole to mid-cell.

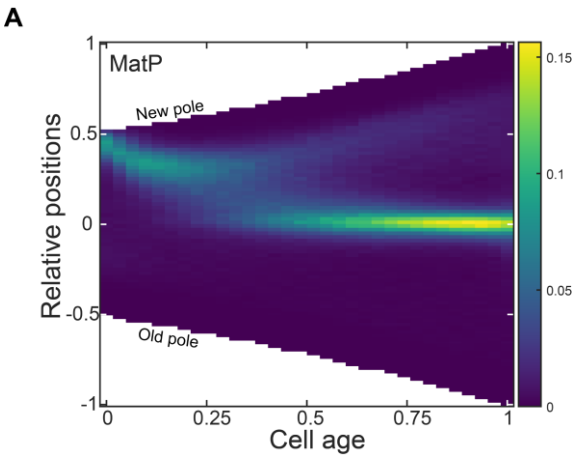

Figure 42: MatP localization to mid-cell is not affected by loss of MukBEF
Foci position kymograph of MatP in a Δ*mukB* strain in a strain without *ori* labelled. The colour scale as in Figure 25. Data is from 11062 cell cycles.

Unfortunately, our *ori* labelling system (mTurquoise2-ParB$_{P1}$) seemed to introduce defects in the absence of MukBEF. This was indicated by a significant increase in anucleate cells, occurring in around 25% of divisions, and a somewhat disrupted *ter* positioning when *ori* was additionally labelled (**Figure 43**). This might suggest that TopoIV recruitment by MukBEF is needed to counterbalance the supercoiling instigated by ParB (Lemonnier et al., 2000). As a result, we are unable to discern any potential differences in the relative timing of *ter* centralisation and *ori* segregation. However, the snapshot demographs from Mäkelä et al., which are based on FROS labelling of loci and offer somewhat limited resolution, appear to suggest that the segregation of *ori* from mid-cell to the poles generally coincides with *ter* centralisation, even in the absence of MukBEF. While further investigation is necessary, these findings hint that MukBEF is likely not the agent responsible for the observed coupling. It is important to note that we have no reason to suspect any artefacts stemming from the mTurquoise2-ParB$_{P1}$ labelling system in the other strains we studied. The focus distributions we achieved are consistent with previous studies, and no phenotypic changes were detected when we applied a lower induction level.

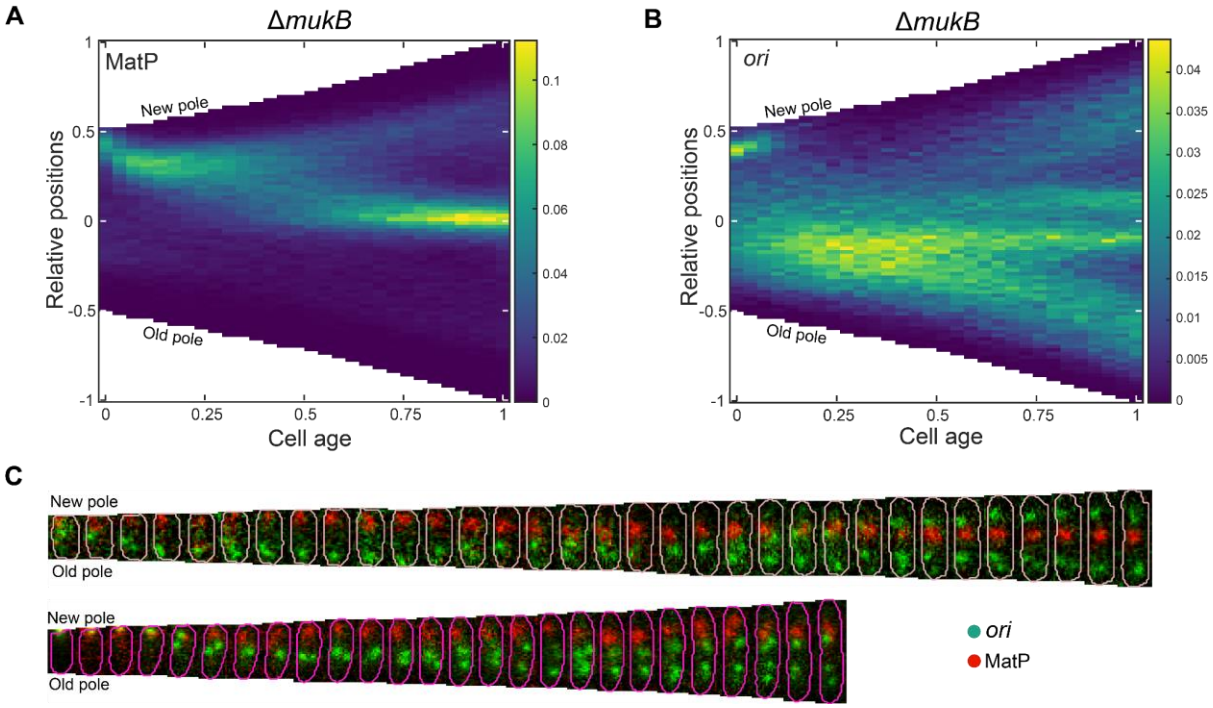

Figure 43: *ori-ter* dynamics in a *ΔmukB* strain

Foci position kymograph of MatP (**A**) and *ori* (**B**) in a Δ*mukB* strain with *ori* additionally labelled using mTurquoise2-ParB$_{P1}$. Cell cycles producing anucleate daughters (detected by the absence of MatP foci) are not included in the analysis. **C.** Representative cell cycles showing MatP (red) and *ori* (green) dynamics in the Δ*mukB* strain. The colour scale in **A** and **B** is as in Figure 25. Data is from 3122 cell cycles.

3.13 CFP-ParB$_{P1}$, but not mTurquoise2-ParB$_{P1}$ negatively affects *ori* segregation

At the beginning of our study, we used the CFP-ParB$_{P1}$ fusion protein to track the *parS*$_{P1}$-labelled *ori* before switching to mTurquoise2-ParB$_{P1}$. Regulated by the *lac* promoter and expressed from a plasmid, we initially chose a 30 µM IPTG induction concentration based on a recent publication using the same construct (Crozat et al., 2020). However, we found that induction of CFP-ParB$_{P1}$ caused a delay in *ori* segregation (**Figure 44**), indicated by the presence of a single *ori* focus for most of the cell cycle.

This issue was not observed under uninduced conditions, but the signal from leaky expression was too weak for effective foci tracking. While increasing the excitation power of the blue light improved the signal, it also negatively impacted cell growth and led to cell cycle arrest or cell death, as shown in a recent study (El Najjar et al., 2020). Consequently, we opted to substitute CFP with a more advanced, brighter fluorophore, mTurquoise2, to allow for *ori* imaging without compromising *ori* segregation. Intriguingly, the mTurquoise2-ParB$_{P1}$ signal was weaker than the CFP-ParB$_{P1}$ signal under uninduced conditions, despite the former being at least twice as bright as the latter (Goedhart et al., 2012).

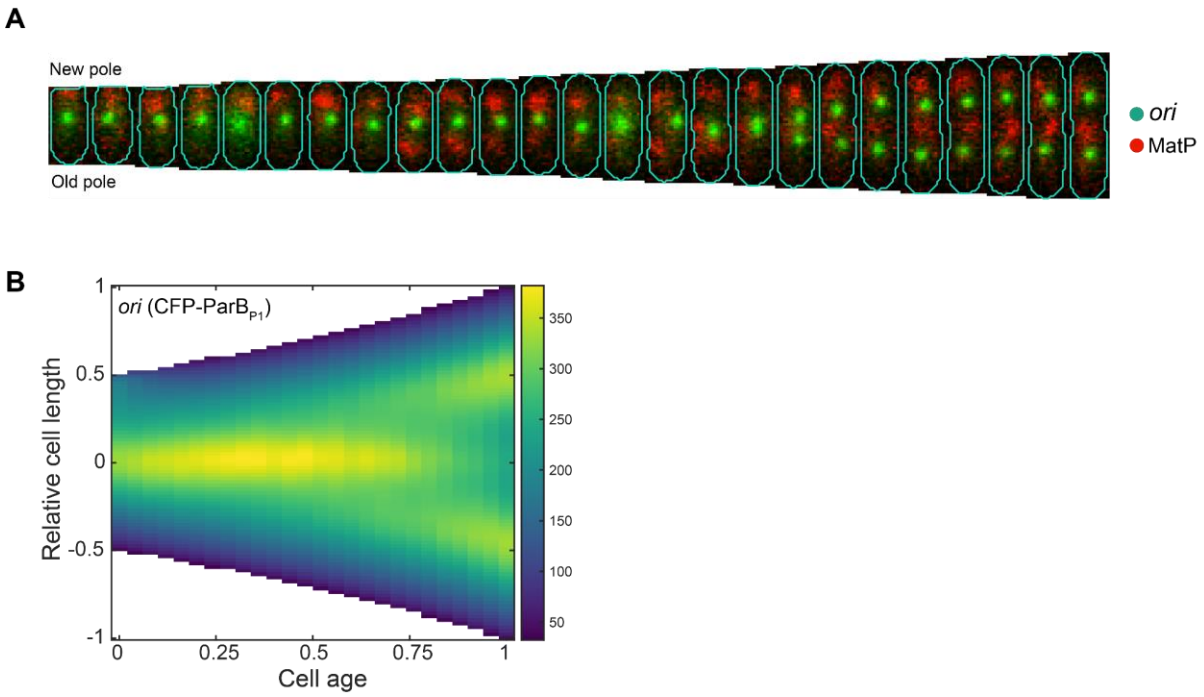

Figure 44: *ori* segregation is delayed in a CFP-ParB$_{P1}$ labelled strain

A. Representative cell cycles showing MatP (red) and *ori* (green) dynamics in a strain that has *ori* labelled with CFP-ParB$_{P1}$. **B.** Population kymograph of CFP-ParB$_{P1}$ signal along the long axis of the cell. The colour scale is as in Figure 30B. Data in **B** corresponds to more than 1000 cell cycles.

Subsequently, we assessed a range of IPTG concentrations between 0 and 50μM to pinpoint the optimal level of induction that would not interfere with normal *ori* dynamics. Trackable foci were detectable at a 30 μM induction concentration, and unlike CFP-ParB$_{P1}$, mTurquoise2-ParB$_{P1}$ did not result in *ori* segregation defects. Interestingly, even when the induction level was raised to 50 μM, *ori* segregation remained consistent with the 30 μM condition (**Figure 45**), suggesting that the *ori* segregation defect observed for CFP-ParB$_{P1}$ was likely due to the CFP component. It should be noted that we were unable to utilise fluorophores in the green/yellow and red spectrums, as they were already designated for labelling *ter* and nucleoid, respectively.

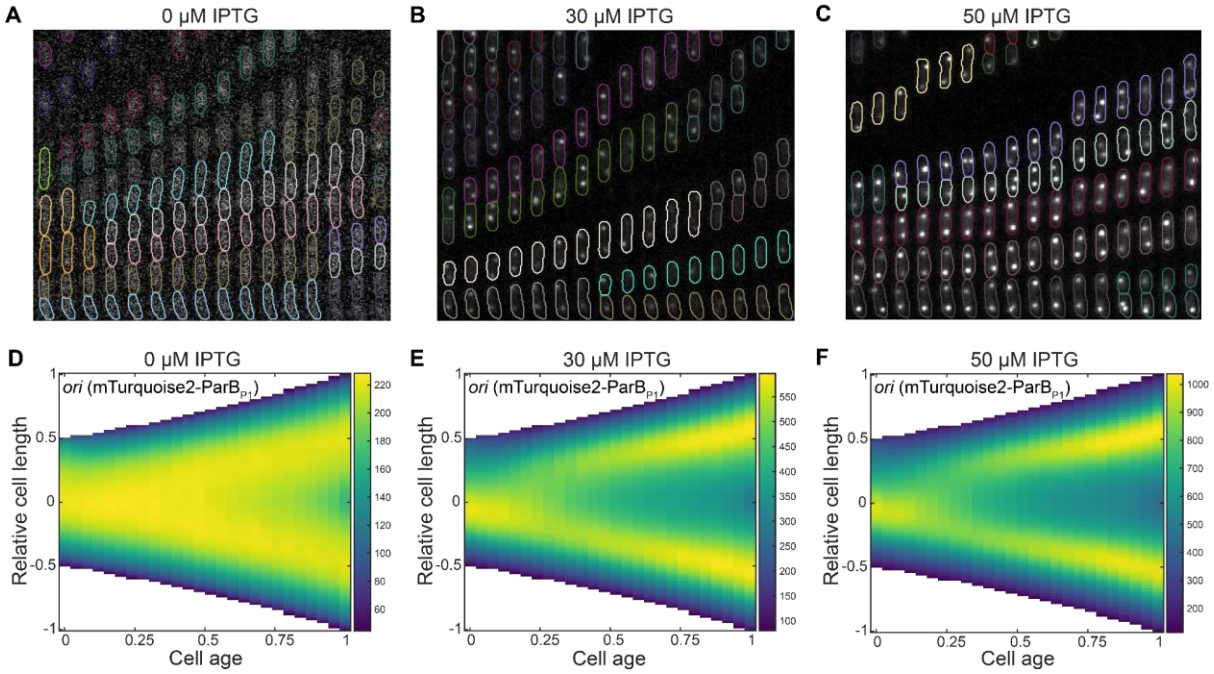

Figure 45: *ori* segregation remains consistent upon mTurquoise2-ParB$_{P1}$ induction

mTurquoise2-ParB$_{P1}$ signal in cells without induction (**A**) with 30uM IPTG (**B**) with 50uM IPTG (**C**) along with their corresponding line profile kymographs (**D, E, F**). Data in **D, E** and **F** corresponds to more than 1000 cell cycles each. The colour scale is as in Figure 30B.

What could be the underlying cause of the impaired *ori* segregation induced by CFP-ParB$_{P1}$? The most plausible explanation arises from the oligomeric differences between CFP and mTurquoise2. CFP, a derivative of GFP, forms dimers, while mTurquoise2, evolved from mVenus and carrying the A206K mutation characteristic of all monomeric GFP variants, is monomeric (Goedhart et al., 2012; Zacharias et al., 2002). It is possible that the dimeric nature of CFP results in the aggregation of CFP-ParB$_{P1}$ bound to *parS*$_{P1}$ near *oriC*, thereby impeding the separation of newly replicated *ori*. It is important to note that this effect is local and does not impede the segregation of the rest of the chromosome (discussed in the next section). In previous studies employing CFP-ParB$_{P1}$ fusion, continuous induction throughout imaging was not required, as experiments were conducted on agarose pads and had a duration of no more than a few hours (Crozat et al., 2020; Mercier et al., 2008; Nielsen et al., 2006a). Under such conditions, a 30-minute induction prior to imaging sufficed. Moreover, any phototoxic or photobleaching effects resulting from the use of a higher power lamp would not have been noticeable due to the shorter imaging duration. Our imaging conditions required cells to be monitored for several days, necessitating optimisation of both the induction concentration and lamp power to establish a steady-state condition that would allow for cell imaging over extended periods. Thus, our specific requirements unveiled a previously unrecognised artefact associated with chromosome labelling.

This serendipitous discovery provided us with an opportunity to manipulate *ori* segregation and investigate its impact on chromosome organisation, which we subsequently employed. This has advantages over, for example, depleting TopoIV (Nicolas et al., 2014) as the direct effect of the perturbation should be local to the *ori* region.

3.14 *ori* segregation is a requirement for stable MatP relocalization to mid-cell

In the dataset used for Figure 25, 30 (IS 130, IS 129 strains respectively), we encountered a consistent small population (<1%) in which *ori* segregation occurred late in the cell cycle (>0.75 cell age). Thanks to our high-throughput dataset, we were able to identify a common characteristic among these cells. We observed that in this subpopulation, the prolonged mid-cell localisation of *ter* was absent. Instead, following its duplication near mid-cell, *ter* localisation shifted from the mid-cell towards the poles. We examined whether this positioning was connected to *ori* segregation by leveraging our fortuitous discovery with CFP-ParB$_{P1}$ labelling where we observed a prolonged *ori* cohesion during cell cycles (**Figure 44A, 46A**).

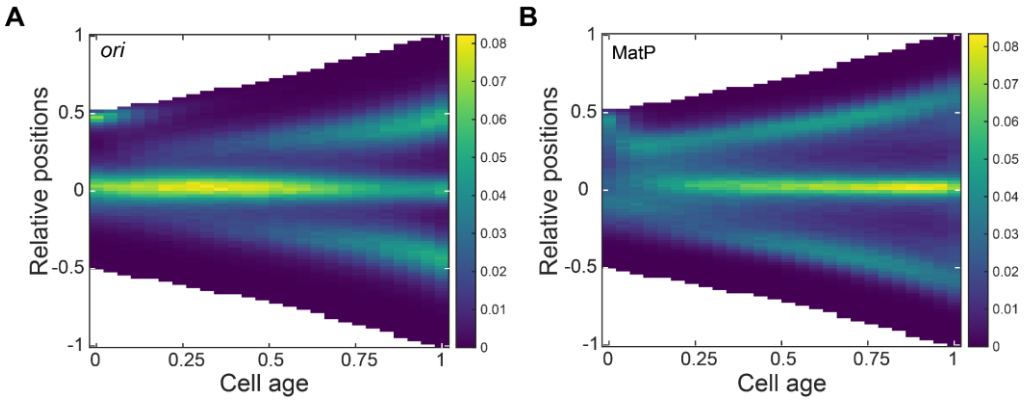

Figure 46: CFP-ParB$_{P1}$ affects chromosome organisation

A. Average foci position kymograph of *ori* labelled with CFP-ParB$_{P1}$ **B.** Average foci position kymograph of MatP in the same strain. The colour scale is as in Figure 25. Data is from 19511 cell cycles.

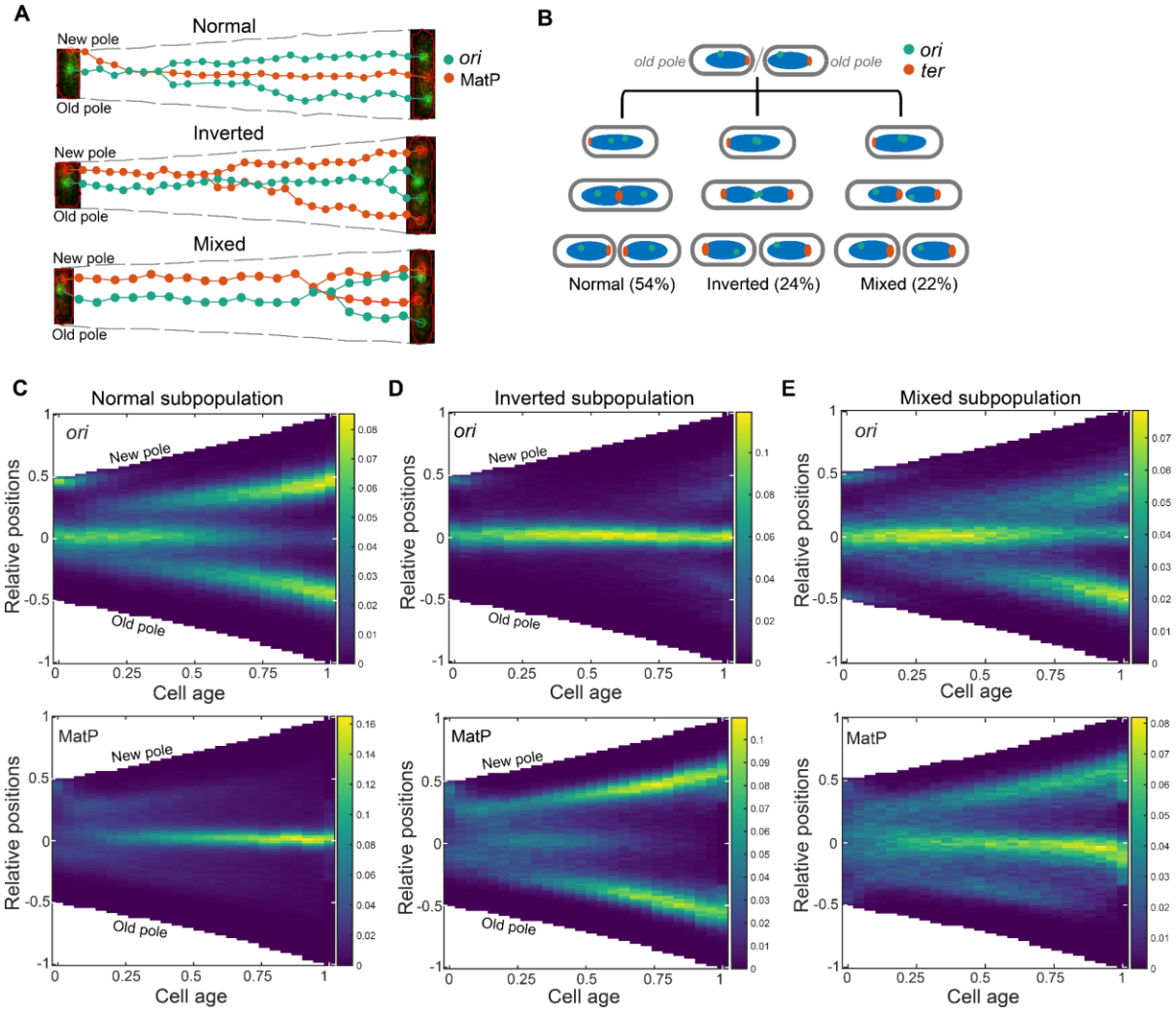

Figure 47: Subpopulations of cells resulting from CFP-ParB$_{P1}$ labelling of *ori*

A. Example cell cycles beginning with a normal chromosome orientation but with daughter cells inheriting either normal, inverted or mixed (one normal, one inverted) orientations. Foci position of *ori* (green) and MatP (red) are shown with a composite fluorescent image of the first and last frame of the cell cycle. **B.** A schematic representation of *ori-ter* organisation based on **A** and the previous nucleoid imaging**. C, D, E.** Foci position kymographs of the normal (n=8269 cell cycles), inverted (n=3774 cell cycles) and mixed subpopulations (n=3407 cell cycles). The colour scale is as in Figure 25.

To study the *ori-ter* dynamics dynamics in a CFP-ParB$_{P1}$ strain, we classified the cell cycles based on the localisation of MatP in the last frame. We categorised chromosome organisation in these cell cycles into three categories - Normal, Inverted and Mixed orientations. More than half of the cells displayed normal orientation, wherein *ori-ter* dynamics were similar to that of mTurquoise2-ParB$_{P1}$ labelling (**Figure 47A** (top)**, C**). The remaining ~46% comprising the inverted and mixed orientations showed a defect in *ori* segregation, with only a single mid-cell localised *ori* for most of the cell cycle (**Figure 47A** (middle, bottom), **D, E**). In these cells, *ter* (MatP-YPet) does not maintain a sustained mid-cell localisation as in normal cells. It still moves to mid-cell but only for a short time, likely in order to be replicated, as evidenced by the appearance of two foci shortly afterwards. These MatP foci were often found to rapidly move

outward towards opposite poles, resulting in both daughter cells having an inverted *ori-ter* axis (inverted orientation) i.e. with *ter* at the old rather than new poles (**Figure 47A** (middle), **D**). Alternatively, in the mixed orientation one chromosome manages to correct itself before division resulting in only one daughter cell having an inverted orientation (**Figure 47A** (bottom), **E**).

Interestingly, despite these anomalies, the growth rate and the duration of the cell cycles were similar to those of normal cells (**Figure 48**). This suggests that while the usual arrangement has *ter* oriented towards the new pole, it is not an absolute requirement for successful cell cycle completion. Neither is the segregation of *ori* away from the mid-cell. Furthermore, there appears to be no hereditary influence on orientation - cells born with an inverted orientation are just as likely to produce inverted offspring as those born with normal orientation (**Figure 49**).

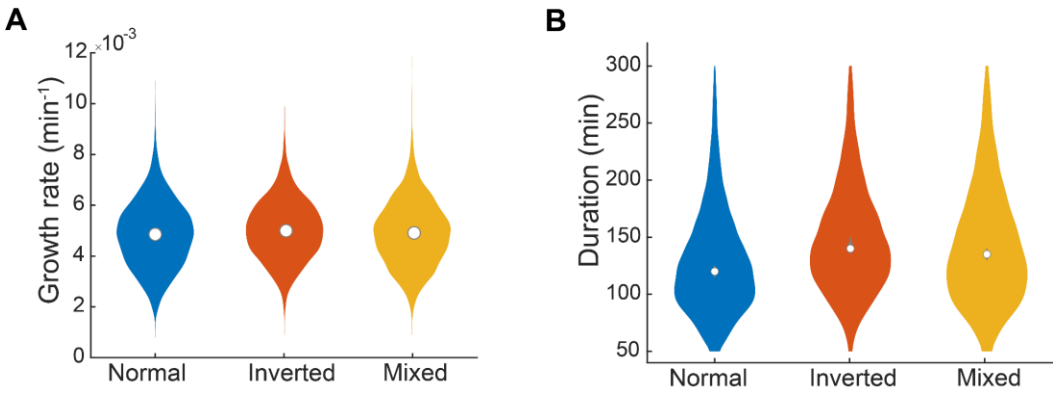

Figure 48: Growth rate and duration of CFP-ParB$_{P1}$ labelled cells

A. The distributions of growth rates of the normal (mean ± sd = (4.9 ± 1.3) x 10^{-3} min^{-1}), inverted ((5.0 ± 1.2) x 10^{-3} min^{-1}) and mixed ((4.9 ± 1.3) x 10^{-3} min^{-1}) subpopulations. The white circle indicates the mean. **B.** The distributions of cell cycle durations in normal (129 ± 46 min), inverted (148 ± 46 min) and mixed (142 ± 50 min) subpopulations. The white circles indicate the mean. The normal, inverted and mixed subpopulations had 8269, 3774 and 3407 cell cycles respectively. Cell cycles shorter than 50 minutes and longer than 300 minutes were excluded from analysis.

Figure 49: No hereditary effect on chromosome orientation observed between subpopulations

It is worth noting that while the kymographs show some period of *ter* localisation at mid-cell, it is due to the averaging of cell-to-cell variation. *ter* spends on average, one-third of the time at the mid-cell compared to the normal subpopulation or cells labelled with mTurquoise2-ParB$_{P1}$ at *ori* (**Figure 50A**). Moreover, the co-localisation with *ori* does not increase compared to normal cells (**Figure 50B**). Taken together, these results suggest that the segregation of sister *ori* away from the mid-cell is a prerequisite for the stable localisation of *ter* at that position.

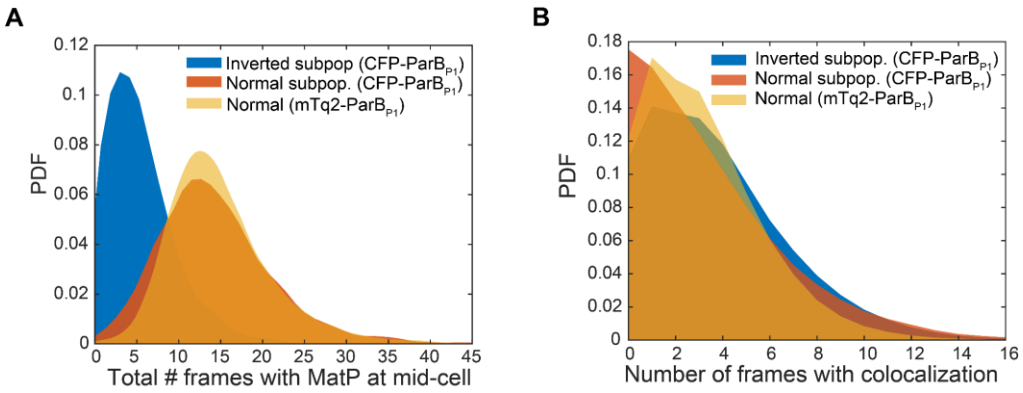

Figure 50: MatP localisation at mid-cell is reduced in inverted subpopulations
A. Distribution of the total number of frames in which MatP foci is found at mid-cell in each cell cycle of the inverted subpopulation (*ori*-CFP-ParB, n=3774 cell cycles), normal subpopulation (*ori*-CFP-ParB$_{P1}$, n=8269 cell cycles) and for the data from Figure 25 (*ori*-mTq2-ParB, n=38066 cell cycles). **B.** Total number of frames in each cell cycle where MatP and *ori* foci are colocalized for the data shown in **A**.

Overall, in this study we explored the dynamics of chromosomal organisation in slow-growing *E. coli*, focusing particularly on the migration of the chromosomal terminus from the new pole to midcell during replication. Our high-throughput time-lapse microscopy approach quantified this transition, its timing, and its relationship with *ori* segregation. The terminus centralisation emerged as a rapid, discrete event occurring approximately 25 minutes after origin separation and roughly 50 minutes prior to bulk nucleoid segregation, albeit with notable cell-to-cell

variation. Intriguingly, this movement closely coincided with the completion of origin segregation, regardless of *ter*-linkage, indicating a possible coupling between these two events. Disruptions to origin segregation away from midcell led to an inability of the terminus to move to midcell, resulting in inverted chromosome organisation in the daughter cells. Our findings have elucidated the precise choreography of origin-terminus positioning and unveiled a previously unexplored connection between these loci, significantly enriching our understanding of chromosome segregation in *E. coli*.

III. Discussion

4.1 A novel approach to identify potential centromere-like sequences in bacteria

Previous studies that identified centromere-like *parS* sequences in various bacteria leveraged on two main factors: firstly, the known characteristic of ParB proteins that bind to *parS* sequences, and secondly, the understanding that centromere-like sequences should be situated near the *oriC* because the *ori* region is the first to segregate after replication initiation. However, in the case of *E. coli* and several other *gammaproteobacteria*, no *parABS* homolog has been identified. (Fogel and Waldor, 2006; Lin and Grossman, 1998; Toro and Shapiro, 2010). Even so, much like other bacteria that possess a *parABS* system, the *ori* region of *E. coli* is the first to segregate after replication initiation. Based on this observation, former studies have examined the *oriC* and its flanking regions for the presence of centromere-like sequences (Valens et al., 2016; Yamaichi and Niki, 2004). The *migS* and *maoS* sequences that were identified in this regard, while influencing mild polar positioning and *ori* mobility respectively, are non-essential and chromosome segregation proceeds uninhibited in their absence. Though previous studies were not able to find a centromere-like sequence in the *ori* region so far, the recent finding that *ori* is attracted to MukBEF, (with which it colocalises throughout the cell cycle) which is found to be positioned near midcell or quarter positions, reignited the search for a (centromere-like) sequence that would help explain the positioning of *ori* in bacteria such as *E. coli* (Hofmann et al., 2019).

In our study, we introduced a novel approach to identify potential centromeric sites in bacterial genomes. This method merges the potency of classical genetics with the competencies of NGS to address a fundamental question. One advantage of using this proposed technique is its capability to scan the entire genome for potential centromeric sites, rather than just the region near the *oriC*, which is found to contain centromeric *parS* sequences in many bacteria. We successfully generated a genomic library in an unstable plasmid and executed the selection experiment to pinpoint potential centromeric regions in the *E. coli* genome. We found that regions near the *spoT* and *seqA* genes became enriched in the population. The enrichment of the *spoT* locus is likely attributable to the presence of a mutated *spoT1* allele in the strain used for the experiment. This is supported by the observation that the apparent stability of plasmids containing the *spoT* locus is confined only to the experimental strain, not extending to the MG1655 wild-type strain. Conversely, the presence of *seqA* locus in an unstable plasmid appears to confer a moderate stability compared to the unstable vector that lacks this locus. This stability, however, does not match the level provided by an active segregation system, such as *parABS*. There appears to be no mutations in any of the genes present in this locus in the experimental strain, indicating that the enrichment of the *seqA* locus is unlikely to be resulting from the genetic differences between MG1655 and DH10β. Furthermore, the marginally higher stability seems to persist in the MG1655 wild-type strain unlike the *spoT* locus.

Among the genes present in the *seqA* locus, only *seqA* itself is known to have roles in DNA replication, segregation, and organisation. It has been reported that the presence of additional copies of *seqA* and its immediate upstream region have little or no effect on growth (Lu et al., 1994). Moreover, there is no existing evidence which suggests that *seqA* or the genes present in its locus influence the stability of the F plasmid. Thus, the reason for the higher stability of unstable plasmids in the presence of sequences from the *seqA* locus requires further investigation.

Intriguingly, none of the enriched sequences in our screening coincide with the locations of previously identified sequences (like *migS*, *maoS*) known for their roles in the organisation of the *ori* region. A succinct follow-up study performed by an intern in our lab probed some of the regions exhibiting less conspicuous peaks in our experiments for their potential to stabilise an unstable plasmid. Yet, none of these sequences were found to lend stability to the unstable plasmid into which they were cloned. Overall, our results in this part of study agrees with the absence of a centromere-like sequence that directs *ori* (or the chromosome) for its positioning.

4.2 Quantitative analysis of cell cycle events

In the second part of our study, we introduced a high-throughput analysis that allows for the comprehensive investigation of the entire spatiotemporal dynamics associated with *ori*, *ter*, and the nucleoid. This robust method captured thousands of cell cycles, providing quantitative data on the spatiotemporal dynamics of chromosomal loci relative to both birth and various cell cycle events. Besides the advantage of high temporal resolution and consistent signal quality, our datasets contain cells imaged under steady-state growth conditions.

A unique feature of our approach is its ability to identify mother and daughter cells throughout the cell cycles, thereby shedding light on intriguing findings. One such observation was that despite slow growth conditions, 15% of cells were born with two *ori* foci. Intriguingly, of this subgroup, the majority (73%) did not undergo *ori* foci duplication. The depth of our dataset allowed us to pinpoint with significant statistical confidence that this deviation from normal behaviour was due to the volume dependence of replication initiation, corroborating previous research.

Our high-throughput time-lapse methodology enabled us to determine the full distribution of timings and durations of steady-state cell cycle events. Specifically, we recorded a median time of 30 minutes between *ori* focus duplication and *ter* centralisation, and 45 minutes between *ter* centralisation and stable nucleoid constriction. These events occurred sequentially in 87% of cell cycles. Our findings build on recent research on the relative timing of replication termination and cell constriction commencement, enriching our understanding of cell cycle progression.

4.3 The chromosome organisation in *E. coli*

Two distinct organisational patterns of the chromosome have been reported for *E. coli* under slow-growing conditions. The older perspective is based on FISH analysis of ori and ter, along with nucleoid labelling (Bates and Kleckner, 2005; Fisher et al., 2013; Niki and Hiraga, 1998). Here, at the beginning of the cell cycle chromosome is longitudinally arranged, with *ori* and *ter* at opposing ends of the nucleoid along the long axis of the cell. The *ori* then shifts towards midcell for replication, and post-replication, the sister *ori* migrates to the opposite edges of the nucleoid, aligning with the quarter positions of the cell. This pattern is also observed in *B. subtilis* (Wang et al., 2014).

The second pattern primarily relies on snapshot imaging of live cells (Nielsen et al., 2006b, 2006a; Wang et al., 2006, 2005). Here, initially the chromosome adopts a 'transverse' or left-ori-right orientation, with the *ori* at mid-cell and chromosomal arms on either side connected by a stretched *ter* region. As the chromosome replicates, the sister *ori* segregate to the cell quarters, replicating the left-*ori*-right pattern in each cell half, thereby ensuring inheritance by the daughter cells. This model, the 'transverse' or 'sausage' model, has gained acceptance as the model of chromosome organisation in slow-growing *E. coli* due to subsequent supporting studies (Wiggins et al., 2010; Woldringh et al., 2015). However, longitudinal organisation remains pertinent, as two live-cell studies have reported its occurrence at faster growth rates (around 1 hour doubling time), with and without overlapping replication (Cass et al., 2016; Youngren et al., 2014).

Our study adds another dimension, showing that longitudinal organisation can occur even during slow growth. But the *ori* aren't at the nucleoid's extreme edge; instead, they are closer to the outer quarter positions. This implies that 25 percent of the nucleoid mass resides between each *ori* and the nearest pole while the left arm lies within the upper 50 percent of nucleoid mass. Additionally, chromosomal loci at 4 o’clock (right arm) and 8 o'clock (left arm) are found between *ori* and the new-pole in majority of cells at birth and in between two *ori* towards division, leading us to refer to this as a 'mixed' or 'longitudinal-like' organisation. This could potentially reconcile the studies based on imaging loci from each chromosomal arm, which didn't include the nucleoid and concluded a transverse organisation, with other studies (including ours) that suggest a more longitudinal arrangement.

We have also considered whether the unique growing conditions in our approach could contribute to this observation. The mother machine continuously feeds cells with fresh media, ensuring steady-state growth (**Figure 24C**). However, as growth on agarose pads should remain stable for a few generations, we find this explanation less likely. Another potential reason could be a difference in growth media. Nevertheless, our observations of position

distributions remained consistent when cells were grown in AB media supplemented with glycerol (**Figure 32A, B**), as in prior studies using the same MG1655 wildtype strain (Nielsen et al., 2006b, 2006a). Similar results were obtained using M9 supplemented with glycerol (**Figure 32C**). Yet, compared to M9 glucose, we noticed that the *ori* positioning distributions are found in the upper 50 percent of the nucleoid mass for a relatively longer period. This observation leads us to hypothesise that the transition from longitudinal-like to transverse (left-*ori*-right) organisation might be dependent on media conditions and growth rate. Further experiments needed to be performed under growth conditions with a growth rate lower than that of M9 glycerol (or AB glycerol), coupled with studies analysing the position distributions of the left and right arms of the chromosome, to obtain a comprehensive understanding of chromosome organisation.

4.4 *ter* centralisation is coupled to, and requires *ori* segregation

Previous studies based on fluorescence in-situ hybridization (FISH) identified several transitions in the organisational patterns of the *E. coli* cycle during slow growth (Bates and Kleckner, 2005; Joshi et al., 2011). The T1 transition begins with the initial separation of sister *ori* at midcell, with one sister moving to the *ter*-distal end of the nucleoid and the other remaining near the midcell. The T2 transition occurs approximately 20 minutes later, marking the rapid movement of the remaining midcell-proximal *ori* to the *ter*-proximal edge of the nucleoid, coinciding with the movement of the *ter* to the midcell. The outcome of T1 and T2 transitions is symmetrically positioned sister *ori* at opposite ends of the nucleoid, corresponding to the cell's quarter positions.

Our findings broadly concur with this study. However, while we also notice an asymmetry in *ori* positioning and movement, our data demonstrate both sister *ori* simultaneously reaching their target positions at the edge of the nucleoid. Moreover, our high-resolution tracking of tens of thousands of cell cycles enables us to establish that *ter* centralisation is substantially quicker than *ori* movement, taking place in about 5 minutes (1 frame), and more specifically, is concurrent with the completion of the more gradual *ori* segregation process.

What could possibly underlie such a rapid transition? It seems unlikely that it would result from the typically midcell located replisomes 'pulling in' the *ter* region, considering the significant variation in the time between initial separation of *ori* foci and *ter* centralisation (**Figure 27A**). The same conclusion was drawn in a study on chromosome organisation during fast growth (Youngren et al., 2014). It suggested that the transition could occur at diverse stages in the replication process, but regardless of when it happens, any unreplicated DNA is carried with the terminus to midcell. This was attributed to the entropic properties of a replicating ring polymer. In fact, polymer simulations have illustrated that a partially replicated chromosome

in a rod-shaped cell organises itself to position the unreplicated terminus region at midcell (Jun and Mulder, 2006; Jun and Wright, 2010), which could lead to the rapid movement of the terminus region from the pole to midcell (on the timescale of the stochastic fluctuations in the position of the terminus region) (Männik et al., 2016).

Our findings align with this perspective. We observe a distinct connection between *ori* segregation and *ter* centralisation, implying an entropically-induced global chromosome rearrangement (Bates and Kleckner, 2005; Joshi et al., 2011). Although an *ori*-specific mechanism cannot be completely ruled out, our results from the genomic screen as well as the observation that *ori* segregation is not strictly necessary for bulk chromosome segregation (see below) also endorses a locus-agnostic process. Polymer modelling studies in the future could help clarify whether the abruptness and relative timing of the *ter* transition (that is coupled to the completion of *ori* segregation) that we witness could indeed originate from entropy.

4.5 The role of the *ter*-linkage

The *ter* region is considered to be anchored to the septal ring via a MatP-ZapB-ZapA-FtsZ protein linkage. However, it's been found that disrupting this linkage shortens the duration of (and not completely abolishes) *ter* centralisation, resulting in earlier separation of sister *ter* loci in the cell cycle (Espéli et al., 2012; Männik et al., 2016). In line with this, our findings for the *matPΔC20* strain show a similar pattern, although, the deletion of *zapB* had a rather mild impact on *ter* centralisation, resulting in only a slightly broader position distribution and a marginally earlier separation of sister *ter*. This observation implies that MatP may be engaging with other divisome components through the same C-terminal domain, or that a portion of its anchoring effect may demand its C-terminal domain independently of its linkage to the divisome. The latter possibility might be linked to the multimerisation capacity of MatP and bridging of sister *ter* loci (Dupaigne et al., 2012; Mercier et al., 2008).

4.6 *ori* segregation is not required for bulk chromosome segregation

In *E. coli*, like the other bacteria that have been studied, chromosome segregation commences with the origin and proceeds progressively as the chromosome undergoes replication. The significance of initial origin segregation is underscored by the existence of a dedicated system (ParABS) found in many species (such as *C. crescentus*) solely responsible for this process. Hence, it was rather unexpected to find that an impairment in origin segregation, observed in roughly half the cells employing the CFP-$ParB_{P1}$ labelling system (and around 0.5% of cells using mTurquoise2-$ParB_{P1}$), did not prevent the successful completion of the cell cycle. These

cells retained the unsegregated *ori* at the mid-cell for the majority of the cell cycle, yet they were nonetheless capable of distributing the rest of the replicated chromosomes into each cell half, yielding daughter cells with a reversed chromosome orientation i.e., *ter* near the old and *ori* at the new pole.

These findings suggest that while origin segregation typically spearheads the process of chromosome segregation, it is not an obligatory requirement for this process and furthermore aligns with the idea that entropy is the fundamental driver of segregation. In this regard, the driving role of physical forces in chromosome segregation could also underlie active segregation systems. The fact that chromosome segregation occurs in *B. subtilis*, *P. aeruginosa*, and *V. cholerae*, even in the absence of their chromosomally encoded *parABS* system, points in this direction.

It is worth noting that since we label one specific locus (14 kb from *oriC*), it remains plausible that the remainder of the Ori macrodomain segregates properly, with the *parS* proximal regions kept together at the midcell. It would be interesting to see if this observation remains consistent when the *parS* location is moved elsewhere within the Ori macrodomain, especially near the *migS* sequence which was shown to play a minor role in polar localisation of *ori* (Yamaichi and Niki, 2004). Future work could also explore how the localisation of MukBEF is affected in cells that result in an inverted chromosome orientation.

In conclusion, our combined results reinforces the prevalent consensus that the segregation and positioning of the *ori* in *E. coli* may not be directed by a centromere-like sequence. This is supported by our findings that *ori* positioning and segregation is not required for bulk chromosome segregation, instead it is required for positioning of the terminus region at midcell. We also demonstrated that a longitudinal-like chromosome organisation similar to what is reported for *B. subtilis* is possible for *E. coli* under slow growth conditions. Collectively, our results are in line with the theory of spontaneous demixing of confined polymers which suggests that chromosome organisation and segregation in *E. coli* are driven by physical forces.

IV. Materials and Methods

5.1 Strains, plasmids and media (Part I)

All genomic library preparations were done using BAC-Optimized Replicator v2.0 cells (Lucigen Corporation), a derivative of DH10β. All experiments were conducted in Lysogeny Broth (LB) media at 37ºC unless specified otherwise. The MG1655Δ*recA* strain was generated by P1 transduction from the Keio collection knockout strain into an MG1655 WT strain, and the kanamycin resistance was removed using the pCP20 plasmid. The plasmid pBAC-sacB was generated by removing the *sopABC* and *lacZ* genes from the pBAC-lacZ plasmid and replacing them with an engineered *sacB* gene containing a BamHI site. The pBAC-parS was generated by removing the *sacB* cassette from pBAC-sacB and replacing it with a *lacI^{q}-ygfp-parB$_{PMT1}$-parS* cassette, which was generated by combining fragments from the pGBKD3-parS$_{pMT1}$ and pFHC2973 plasmids. For the isolation of pBAC plasmids in BAC-Optimized Replicator v2.0 cells, overnight cultures were back-diluted 1:100, and 10 mM arabinose was added to induce *trfA*, to increase the copy number of the plasmids. The plasmids were isolated after 6 hours.

5.2 Preparation of gDNA library

For genomic gDNA isolation, Δ*recA* (MG1655) cells were grown until saturation. The gDNA was isolated using QIAGEN Genomic tip 100/G and subjected to partial digestion using the Sau3AI restriction enzyme. Time course experiments with varying amounts of Sau3AI and gDNA were done under standard conditions in order to find the appropriate digestion conditions suitable for getting maximum yield (**Figure 51**). The gDNA was partially digested for 80 minutes for optimal yield and ran on a 0.8% agarose gel. The gel fragment in the range between 8kb and 11kb excised was isolated using QIAEX II Gel Extraction Kit. The gel purified DNA was then used to ligate into the vector to create the library.

For the ligation, the vector was initially cut using BamHI, dephosphorylated with Calf Intestinal Phosphatase (CIP) and gel purified. A ligation reaction was then set up between gDNA fragments isolated from partial digestion and the vector and gDNA fragments in 1:2 (vector: insert) molar ratio. The ligation mixture was dialyzed and then electroporated into BAC-Optimized Replicator v2.0 cells. The optimised reaction mixture used in the partial digestion and ligation are listed in Table 2 and Table 3 respectively.

Cells were subjected to recovery for 1 hour and plated on LB-Agar plates without NaCl having 10% (w/v) sucrose (for counter selection) and 17 µg/mL chloramphenicol. Individual colonies were picked using inoculation loops and pooled into 200 mL LB media and kept for shaking at 37ºC for homogenization. After two hours, cryostocks were made for library stocks (Day 0).

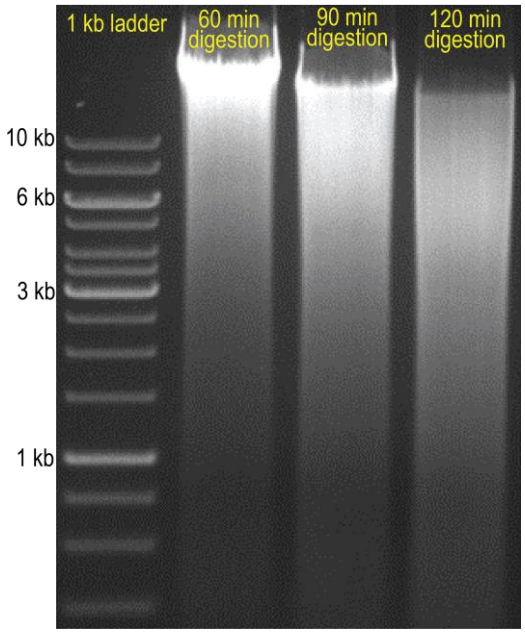

Figure 51: Partial digestion of *E. coli* gDNA using Sau3AI

Table 2: Standardised protocol for digestion

Reagent	Amount
Buffer 1.1	3 µL
gDNA	10 µg
50 U/mL Sau3AI	2.5 µL
Nuclease-free H_2O	to make up 30 uL

Table 3: Standardised protocol for ligation

Reagent	Amount
T4 DNA ligase buffer	2 µL
Vector	200 ng
Insert (gDNA)	965 ng
T4 DNA ligase	1 µL
Nuclease-free H_2O	to make up 20 uL

5.3 Plasmid enrichment assay (Selection experiment)

For enrichment of plasmids that contain centromere-like sequences, cells were grown in LB medium for up to 4 days, backdiluting 1:1000 twice a day for Experiment 1, and every 8 hours for Experiment 2. This included a 16-hour media alone phase and an 8-hour media with antibiotic phase. The latter step was included to ensure maintenance of the population pool that retained the plasmid. A cryostock was made after antibiotic phase each day to extract the plasmid for sequencing.

5.4 Plasmid isolation and next generation sequencing

Cryostocks were revived in LB medium with antibiotic for 2 hours for plasmid isolation. Plasmids were isolated using GeneJET Plasmid Miniprep Kit (Thermo Fisher Scientific). To remove any fragmented or unwanted DNA a gel extraction of plasmid library was performed before doing NGS. The sequencing was done using Illumina HiSeq platform and the average read length of the NGS library was 75 bp.

5.5 Strains, plasmids and media (Part II)

All strains used in this study are derivatives of *E. coli* M1655. For imaging origin and terminus, a new strain was constructed by transduction of *glmS::parS*$_{P1}$::kan from strain RM29 (Li et al., 2002; Mercier et al., 2008) and *matP-YPet*::frt::kan::frt from strain RH3 (Männik et al., 2016) into MG1655 (lab collection) respectively. Two plasmids - pFHCP1-CFP and pFHCP1-mTurquoise2, derived from plasmid pFHC2973 (Nielsen et al., 2006b) by deletion of *ygfp-parB*$_{pMT1}$, were used to drive the expression of CFP-ParB$_{P1}$ and mTurquoise2-ParB$_{P1}$ respectively. Additionally, a plasmid derived from pFHC2973 by replacing the *cfp* with *mTurquoise2* and *ygfp* with mVenus was also created to visualise *parS*$_{P1}$ and *parS*$_{pMT1}$ labels in the same strain. To create the triple labelled strain IS129, strain RH3 was transduced with *glmS::parS*$_{P1}$::kan after removal of the kanamycin resistance. A detailed list of strains and plasmids used in this study can be found in Table 4 and 5. All experiments, unless otherwise mentioned, were performed at 30^{o}C using M9 minimal media (1x M9 salts supplemented with 0.2% glucose, 2 mM $MgSO_4$, 0.1 mM $CaCl_2$). For experiments involving AB minimal media, the recipe and growth conditions of (Nielsen et al., 2006b) were followed. For mother machine experiments, media were supplemented with 0.5 mg/mL BSA (for passivation to reduce cell adhesion to PDMS) and 50 μM IPTG (for induction of ParB fusions).

5.6 Microscopy

Strains were grown overnight in the respective minimal media without BSA and IPTG. For induction of ParB fusions for loci visualization, 50 μM IPTG was added 3 hours before loading into the mother machine microfluidics device. The microfluidics device was prepared and loaded as described previously (Köhler et al., 2022). The cells in exponential phase were then loaded into the mother machine using a 1 mL syringe. After loading, cells were fed with fresh M9 minimal media supplemented with 0.5 mg/mL BSA and 50 μM IPTG at a rate of 2 μL/min, and data was acquired after 3 hours. Time-lapse images were taken every 5 minutes using a Nikon Eclipse Ti-E with a 100x oil-immersion objective and a Hamamatsu Photonics camera. Both phase contrast and fluorescence signals were captured as mentioned above for up to 72 hours. Visualisation of *ori* required blue light excitation (wavelength 436 ± 20 nm), which is known to cause cell cycle arrest (El Najjar et al., 2020). We optimised our imaging settings to avoid this and allow sustained imaging over several days. With these settings, cells divided on average 13% later but we saw no evidence of cell cycle arrest or other defects. The same imaging settings were used for all strains in this study (even for strain IS173, in which mTurquoise2-ParB$_{P1}$ is not present). The IPTG concentration used for induction of mTurquoise2-ParB$_{P1}$ or CFP-ParB$_{P1}$ did not result in a change in growth rate or cell cycle duration under our imaging conditions.

5.7 Image analysis

All analyses were performed using MATLAB. Time-lapse microscopy images were analyzed using our custom-built pipeline called Mothersegger, as previously described (Köhler et al., 2023, 2022). Briefly, time-lapse images acquired using the method described above were saved as TIFF stacks. The pipeline then identifies and isolates individual growth channels, performs background subtraction, and runs segmentation. The segmented data is used to identify cells belonging to the same cell cycle, along with their parent and daughters. A hard cut-off was put in place to discard cell cycles that are less than 10 frames (50 minutes) and greater than 60 frames (300 minutes) for experiments in glucose media. For experiments in glycerol media, the upper limit was raised to 80 frames (400 minutes). After identifying cell cycles, foci detection is performed on relevant fluorescence channels.

5.8 Data analysis

While we have focused on time-based measurements, given that there is a known dependence of chromosome replication initiation on cell size (Levin and Taheri-Araghi, 2019), we also considered the cell length at which cell cycle events occurred. However, comparing kymographs (based on relative cell age) and demographs (based on cell length) we saw no

indication that cell size is a better metric for studying *ter* centralisation. On the other hand, since *ter* centralisation was proposed to be coordinated with its replication (Espéli et al., 2012), we reasoned that a time-based analysis would be most appropriate.

5.9 *ori* duplication

To define the *ori* focus duplication, we analyzed complete cell cycles to identify the first frame in which two *ori* foci were detected for the first time. For cells that have an *ori* focus duplication recorded before the first 4 frames, we go back to its mother cell to identify or confirm the correct timing of *ori* focus duplication. In cases where the duplication is recorded in the mother cell, a negative frame number is recorded for *ori* duplication for the daughter cell.

5.10 MatP relocalization

We defined MatP relocalization (centralization) time point as the first of the three consecutive frames (15 min) in which MatP is seen at the midcell for the first time in the cell cycle. The midcell region is defined as the central 4.8 pixels (0.32 μm) in each cell. This value is identified by analyzing the spread of MatP foci positions in the demograph (**Figure 38**) when it is tightly localized at midcell (between 2.48 and 3.01 μm long cells).

5.11 Nucleoid constriction and HU contours

The line profiles of HU-mCherry are obtained by plotting the mean signal along the short axis. A constricted nucleoid is defined by a dip in the middle one third of the HU-mCherry signal greater than the threshold value. The threshold value (0.13) is given by the 95th percentile of the relative depth of the nucleoid signal in new-born cells i.e., the first bin of the plot in Figure 34B. The threshold intensity values defining the contour lines of the HU-mCherry kymographs were chosen such that that 50% or 80% of the HU-mCherry signal was above the threshold, averaged over each cell age bin of the kymograph.

Appendix

Table 4: List of strains

Strain name	Genotype	Source
BAC-Optimized Replicator v2.0	F¯ mcrA Δ(mrr-hsdRMS-mcrBC) endA1 recA1 Φ80dlacZ ΔM15 ΔlacX74 araD139 Δ(ara,leu)7697 galU galK rpsL (StrR) nupG (attL araC-PBADtrfA250 bla attR) λ	https://shop.biosearchtech.com/competent-cells-for-transformation/large-or-difficult-cloning/bac-optimised-electrocompetent-cells/p/60210
IS 11 (MG1655)	F- lambda- ilvG- rfb-50 rph-1	Lab collection
IS 18	MG1655 Δ*recA::frt-kan-frt*	This study
IS 29	MG1655 *glmS::parS*$_{P1}$::*kan*	Li et al., 2002
IS 57	MG1655 *matP-YPet::frt::kan::frt hupA-mCh::frt*	Männik et al., 2016
IS 79	MG1655 Δ*recA::frt*	This study
IS 111	MG1655 *matP-YPet::frt glmS::parS*$_{P1}$::*kan* + pFHCP1-CFP	This study
IS 129	MG1655 *hupA-mCherry::frt matP-YPet::frt glmS::parS*$_{P1}$::*kan* + pFHCP1-mTurquoise2	This study
IS 130	MG1655 *matP-YPet::frt glmS::parS*$_{P1}$::*kan* + pFHCP1-mTurquoise2	This study
IS 146	MG1655 *matPΔC20-YPet::frt glmS::parS*$_{P1}$::*kan* + pFHCP1-mTurquoise2	This study
IS 161	MG1655 *ΔzapB::frt::cat::frt matP-YPet::frt glmS::parS*$_{P1}$::*kan* + pFHCP1-mTurquoise2	This study
IS 173	MG1655 *ΔmukB::frt::kan::frt matP-YPet::frt glmS::parS*$_{P1}$::*frt::cat::frt*	This study
IS 174	MG1655 *ΔmukB::frt::kan::frt matP-YPet::frt glmS::parS*$_{P1}$::*frt::cat::frt* + pFHCP1-mTurquoise2	This study
IS 233	MG1655 *glmS::parS*$_{P1}$::*kan rhlE::parS*$_{pMT1}$::*frt::cat::frt*	This study
IS 234	MG1655 *rhlE::parS*$_{P1}$::*frt elaD::parS*$_{pMT1}$::*frt::cat::frt*	This study

IS 243	MG1655 *glmS::parS*$_{P1}$*::kan elaD::parS*$_{pMT1}$*::frt::cat::frt*	This study

Table 5: List of plasmids

Plasmid name	Description/use	Source
pBAC-lacZ	Original plasmid from which the unstable plasmid (pBAC-sacB) was derived	Addgene plasmid # 13422
pBAC-sacB	Creation of genomic library	This study
pBAC-parS	Screening of enriched sequences	This study
pBAC-parS+IS_oligo_106-107 product	Unstable plasmid with 10kb *seqA* locus	This study
pBAC-parS+IS_oligo_118-119 product	Unstable plasmid with 10kb *spoT* locus	This study
pBAC-parS+IS_oligo_136-137 product	Unstable plasmid with ~5 kb genomic region around *spoT*	This study
pBAC-parS+IS_oligo_138-139 product	Unstable plasmid with ~5 kb downstream of *spoT*	This study
pBAC-parS+IS_oligo_142-143 product	Unstable plasmid with ~5 kb genomic region upstream of *seqA*	This study
pBAC-parS+IS_oligo_144-107 product	Unstable plasmid with ~5 kb genomic region around *seqA*	This study
pFHC2973	Labeling of *parS*$_{P1}$ and *parS*$_{pMT1}$ loci	Nielsen et al., 2006b
pFHCP1-CFP	Used to express CFP-ParB$_{P1}$ needed to visualize *ori*. Inducible with IPTG.	This study; Derived from plasmid pFHC2973
pFHCP1-mTurquoise2	Used to express mTurquoise2-ParB$_{P1}$ needed to visualize *ori*. Inducible with IPTG.	This study; Made by replacement of CFP with mTurquoise2 in pFHCP1-CFP
pFHCP1-mTurquoise2-T1-mVenus	Used to express mTurquoise2-ParB$_{P1}$ and mVenus-ParB$_{pMT1}$ needed to visualize *parS*$_{P1}$ and *parS*$_{pMT1}$ tagged loci respectively. Inducible with IPTG.	This study; Derived from plasmid pFHC2973 by replacement of *CFP* with *mTurquoise2* and *yGFP* with *mVenus*
pGBKD3-parSP1	Used to amplify *parS*$_{P1}$ sequence for chromosome labeling	Espeli et al., 2008

pGBKD3-parSpMT1	Used to amplify *parS*$_{P1}$ sequence for chromosome labeling	Mercier et al., 2008

Table 6: Primers used in this study

Primer name	Sequence	Notes
IS_oligo_55	TTATAAGCTTatgcgagagtagggaactgccagg	pFH2973 forward for creating pFHCP1-CFP
IS_oligo_ 59	TTATAAGCTTTCTAGAGGATCCCCGGGTTAATAG	pFH2973 reverse for creating pFHCP1-CFP
IS_oligo_85	ctcaacgatgaaaccgaagagaatcagccagatagcggagaggaagaaTAgtcttgagcgattgtgtaggctgga	*mukB* knockout forward from pKD4
IS_oligo_86	gaaacggagttttcggaaaaagaaaaggcggcattgctgccgccttaaTTcatatgaatatcctccttagttcctattcc	*mukB* knockout reverse from pKD4
IS_oligo_89	aatcgggacgaggatttttatccatcaacgcctgcaattcaggagagGTgtcttgagcgattgtgtaggctgga	*zapB* knockout forward from pKD3
IS_oligo_90	ttacctgttggcctacacagtaaagaaattacgcggaagatgaagcgtAAcatatgaatatcctccttagttcctattcc	*zapB* knockout reverse from pKD3
IS_oligo_106	atcacgaggccctttcgtcttcaaGAATTCcactgttgctgcgattcggtc	Forward for cloning 10kb *seqA* locus
IS_oligo_107	aatttatctgcgtgatgggttaaaGGATCCacactgtatggtctggtatcacca	Reverse for cloning 10kb *seqA* locus
IS_oligo_117	aatttatctgcgtgatgggttaaaGGATCCtccagttcatcggcaatacgcg	Forward for cloning 10kb *spoT* locus
IS_oligo_118	atcacgaggccctttcgtcttcaaGAATTCcttccttccagtagtcatcgtccc	Reverse for cloning 10kb *spoT* locus
IS_oligo_136	atcacgaggccctttcgtcttcaaGAATTCcatcatcacctccgctgtagatag	Forward for cloning ~5 kb genomic region around *spoT*
IS_oligo_137	aatttatctgcgtgatgggttaaaGGATCCcattaatttcggtttcgggtgact	Reverse for cloning ~5 kb genomic region around *spoT*
IS_oligo_138	atcacgaggccctttcgtcttcaaGAATTCatgaacccaacacgttatgcacg	Forward for cloning ~5 kb downstream of *spoT*

IS_oligo_139	aatttatctgcgtgatgggttaaaGGATCCg ctgttttgagtctgcgcaacc	Reverse for cloning ~5 kb downstream of *spoT*
IS_oligo_142	atcacgaggccctttcgtcttcaaGAATTCt ctgctttatgcctgatgcgacgc	Forward for cloning ~5 kb genomic region upstream of *seqA*
IS_oligo_143	aatttatctgcgtgatgggttaaaGGATCCc aatgcctgatgtgatgcggcgta	Reverse for cloning ~5 kb genomic region upstream of *seqA*
IS_oligo_144	atcacgaggccctttcgtcttcaaGAATTCt acgccgcatcacatcaggcattg	Forward for cloning ~5 kb genomic region around *seqA*
IS_oligo_155	GAATTCGAGCTCAGTGTCGAGC AG	pFHCP1-CFP forward from parB linker for creation of pFHCP1-mTurquoise2
IS_oligo_156	GGTCTGTTTCCTGTGTGAAATT GTTAT	pFHCP1-CFP reverse upstream CFP for creation of pFHCP1-mTurquoise2
IS_oligo_157	CGGATAACAATTTCACACAGGA AACAGACCatggtttctaaaggtgaagaa ctgtttacc	mTurquoise2 forward with pFHCP1-CFP overhang
IS_oligo_158	GAATACCTGCTCGACACTGAGC TCGAATTCtttgtacagttcatccatacct aaggtaat	mTurquoise2 reverse with pFHCP1-CFP overhang
IS_oligo_204	aagcacttgtcagcaatttgagaacacGGG gattgtgtaggctggagctgc	Forward primer with overhang from *rhlE* locus (4 o'clock) to amplify $parS_{P1}$ or $parS_{pMT1}$ from pGBKD3P1 or pGBKD3T1 plasmid respectively
IS_oligo_205	tctcggtggcttatgggcggtaaaacaGATt atcccgtgacaggtcattcagac	Reverse primer with overhang from *rhlE* locus (4 o'clock) to amplify $parS_{P1}$ or $parS_{pMT1}$ from pGBKD3P1 or pGBKD3T1 plasmid respectively
IS_oligo_206	tcattgttaattaattcgaccagtcagCAAgat tgtgtaggctggagctgc	Forward primer with overhang from *elaD* locus (8 o'clock) to amplify $parS_{P1}$ or $parS_{pMT1}$ from pGBKD3-parSP1 or pGBKD3-parSpMT1 plasmid respectively
IS_oligo_207	actgtttagcaaactatgttcgaccagTCAtat cccgtgacaggtcattcagac	Reverse primer with overhang from *elaD* locus (8 o'clock) to amplify $parS_{P1}$ or $parS_{pMT1}$ from pGBKD3-parSP1 or pGBKD3-parSpMT1 plasmid respectively

List of figures

List of tables

References

Ali Azam T, Iwata A, Nishimura A, Ueda S, Ishihama A. 1999. Growth phase-dependent variation in protein composition of the Escherichia coli nucleoid. *J Bacteriol* **181**:6361–6370. doi:10.1128/JB.181.20.6361-6370.1999

Aussel L, Barre F-X, Aroyo M, Stasiak A, Stasiak AZ, Sherratt D. 2002. FtsK Is a DNA Motor Protein that Activates Chromosome Dimer Resolution by Switching the Catalytic State of the XerC and XerD Recombinases. *Cell* **108**:195–205. doi:10.1016/S0092-8674(02)00624-4

Austin S, Abeles A. 1983. Partition of unit-copy miniplasmids to daughter cells: I. P1 and F miniplasmids contain discrete, interchangeable sequences sufficient to promote equipartition. *J Mol Biol* **169**:353–372. doi:10.1016/S0022-2836(83)80055-2

Badrinarayanan A, Le TB, Laub MT. 2015. Bacterial chromosome organization and segregation. *Annu Rev Cell Dev Biol* **31**:171–199. doi:10.1146/annurev-cellbio-100814-125211

Badrinarayanan A, Lesterlin C, Reyes-Lamothe R, Sherratt D. 2012a. The Escherichia coli SMC Complex, MukBEF, Shapes Nucleoid Organization Independently of DNA Replication. *J Bacteriol* **194**:4669–4676. doi:10.1128/JB.00957-12

Badrinarayanan A, Reyes-Lamothe R, Uphoff S, Leake MC, Sherratt DJ. 2012b. In Vivo Architecture and Action of Bacterial Structural Maintenance of Chromosome Proteins. *Science* **338**:528–531. doi:10.1126/science.1227126

Bahng S, Kumar R, Marians KJ. 2022. Intersubunit and intrasubunit interactions driving the MukBEF ATPase. *J Biol Chem* **298**:101964. doi:10.1016/j.jbc.2022.101964

Bailey MW, Bisicchia P, Warren BT, Sherratt DJ, Männik J. 2014. Evidence for Divisome Localization Mechanisms Independent of the Min System and SlmA in Escherichia coli. *PLoS Genet* **10**. doi:10.1371/journal.pgen.1004504

Baltekin Ö, Boucharin A, Tano E, Andersson DI, Elf J. 2017. Antibiotic susceptibility testing in less than 30 min using direct single-cell imaging. *Proc Natl Acad Sci* **114**:9170–9175. doi:10.1073/pnas.1708558114

Bates D, Kleckner N. 2005. Chromosome and Replisome Dynamics in E. coli: Loss of Sister Cohesion Triggers Global Chromosome Movement and Mediates Chromosome Segregation. *Cell* **121**:899–911. doi:10.1016/j.cell.2005.04.013

Bock FP, Liu HW, Anchimiuk A, Diebold-Durand M-L, Gruber S. 2022. A joint-ParB interface promotes Smc DNA recruitment. *Cell Rep* **40**. doi:10.1016/j.celrep.2022.111273

Brézellec P, Hoebeke M, Hiet M-S, Pasek S, Ferat J-L. 2006. DomainSieve: a protein domain-based screen that led to the identification of dam-associated genes with potential link to DNA maintenance. *Bioinforma Oxf Engl* **22**:1935–1941. doi:10.1093/bioinformatics/btl336

Britton RA, Lin DC-H, Grossman AD. 1998. Characterization of a prokaryotic SMC protein involved in chromosome partitioning. *Genes Dev* **12**:1254–1259.

Bürmann F, Funke LFH, Chin JW, Löwe J. 2021. Cryo-EM structure of MukBEF reveals DNA loop entrapment at chromosomal unloading sites. *Mol Cell* **81**:4891-4906.e8. doi:10.1016/j.molcel.2021.10.011

Bürmann F, Lee B-G, Than T, Sinn L, O'Reilly FJ, Yatskevich S, Rappsilber J, Hu B, Nasmyth K, Löwe J. 2019. A folded conformation of MukBEF and cohesin. *Nat Struct Mol Biol* **26**:227–236. doi:10.1038/s41594-019-0196-z

Bürmann F, Shin H-C, Basquin J, Soh Y-M, Giménez-Oya V, Kim Y-G, Oh B-H, Gruber S. 2013. An asymmetric SMC–kleisin bridge in prokaryotic condensin. *Nat Struct Mol Biol* **20**:371–379. doi:10.1038/nsmb.2488

Cass JA, Kuwada NJ, Traxler B, Wiggins PA. 2016. Escherichia coli Chromosomal Loci Segregate from Midcell with Universal Dynamics. *Biophys J*. doi:10.1016/j.bpj.2016.04.046

Castillo F, Benmohamed A, Szatmari G. 2017. Xer Site Specific Recombination: Double and Single Recombinase Systems. *Front Microbiol* **8**:453. doi:10.3389/fmicb.2017.00453

Claret L, Rouviere-Yaniv J. 1997. Variation in HU composition during growth of Escherichia coli: the heterodimer is required for long term survival11Edited by M. Gottesman. *J Mol Biol* **273**:93–104. doi:10.1006/jmbi.1997.1310

Costa A, Hood IV, Berger JM. 2013. Mechanisms for Initiating Cellular DNA Replication. *Annu Rev Biochem* **82**:25–54. doi:10.1146/annurev-biochem-052610-094414

Crozat E, Tardin C, Salhi M, Rousseau P, Lablaine A, Bertoni T, Holcman D, Sclavi B, Cicuta P, Cornet F. 2020. Post-replicative pairing of sister ter regions in Escherichia coli involves multiple activities of MatP. *Nat Commun* **11**:3796. doi:10.1038/s41467-020-17606-6

Dages S, Zhi X, Leng F. 2020. Fis protein forms DNA topological barriers to confine transcription-coupled DNA supercoiling in Escherichia coli. *FEBS Lett* **594**:791–798. doi:10.1002/1873-3468.13643

Danilova O, Reyes-Lamothe R, Pinskaya M, Sherratt D, Possoz C. 2007. MukB colocalizes with the oriC region and is required for organization of the two Escherichia coli chromosome arms into separate cell halves. *Mol Microbiol* **65**:1485–1492. doi:10.1111/j.1365-2958.2007.05881.x

Davis MA, Radnedge L, Martin KA, Hayes F, Youngren B, Austin SJ. 1996. The P1 ParA protein and its ATPase activity play a direct role in the segregation of plasmid copies to daughter cells. *Mol Microbiol* **21**:1029–1036. doi:10.1046/j.1365-2958.1996.721423.x

Dillon SC, Dorman CJ. 2010. Bacterial nucleoid-associated proteins, nucleoid structure and gene expression. *Nat Rev Microbiol* **8**:185–195. doi:10.1038/nrmicro2261

Drlica K, Rouviere-Yaniv J. 1987. Histonelike proteins of bacteria. *Microbiol Rev* **51**:301–319.

Dupaigne P, Tonthat NK, Espéli O, Whitfill T, Boccard F, Schumacher MA. 2012. Molecular basis for a protein-mediated DNA-bridging mechanism that functions in condensation of the E. coli chromosome. *Mol Cell* **48**:560–571. doi:10.1016/j.molcel.2012.09.009

Durfee T, Nelson R, Baldwin S, Plunkett G, Burland V, Mau B, Petrosino JF, Qin X, Muzny DM, Ayele M, Gibbs RA, Csörgő B, Pósfai G, Weinstock GM, Blattner FR. 2008. The Complete Genome Sequence of Escherichia coli DH10B: Insights into the Biology of a Laboratory Workhorse. *J Bacteriol* **190**:2597–2606. doi:10.1128/JB.01695-07

El Najjar N, van Teeseling MCF, Mayer B, Hermann S, Thanbichler M, Graumann PL. 2020. Bacterial cell growth is arrested by violet and blue, but not yellow light excitation during fluorescence microscopy. *BMC Mol Cell Biol* **21**:35. doi:10.1186/s12860-020-

00277-y

Espéli O, Borne R, Dupaigne P, Thiel A, Axel Thiel, Axel Thiel, Gigant E, Mercier R, Boccard F. 2012. A MatP–divisome interaction coordinates chromosome segregation with cell division in E. coli. *EMBO J* **31**:3198–3211. doi:10.1038/emboj.2012.128

Espeli O, Mercier R, Boccard F. 2008. DNA dynamics vary according to macrodomain topography in the E. coli chromosome. *Mol Microbiol* **68**:1418–1427. doi:10.1111/j.1365-2958.2008.06239.x

Fiil NP, Willumsen BM, Friesen JD, von Meyenburg K. 1977. Interaction of alleles of therelA, relC andspoT genes inEscherichia coli: Analysis of the interconversion of GTP, ppGpp and pppGpp. *Mol Gen Genet MGG* **150**:87–101. doi:10.1007/BF02425329

Finkel SE, Johnson RC. 1992. The Fis protein: it's not just for DNA inversion anymore. *Mol Microbiol* **6**:3257–3265. doi:10.1111/j.1365-2958.1992.tb02193.x

Fisher JK, Bourniquel A, Witz G, Weiner B, Prentiss M, Kleckner N. 2013. Four-dimensional imaging of E. coli nucleoid organization and dynamics in living cells. *Cell* **153**:882–895. doi:10.1016/j.cell.2013.04.006

Fogel MA, Waldor MK. 2006. A dynamic, mitotic-like mechanism for bacterial chromosome segregation. *Genes Dev* **20**:3269–3282. doi:10.1101/gad.1496506

Ganji M, Shaltiel IA, Bisht S, Kim E, Kalichava A, Haering CH, Dekker C. 2018. Real-time imaging of DNA loop extrusion by condensin. *Science* **360**:102–105. doi:10.1126/science.aar7831

Gligoris T, Löwe J. 2016. Structural Insights into Ring Formation of Cohesin and Related Smc Complexes. *Trends Cell Biol* **26**:680–693. doi:10.1016/j.tcb.2016.04.002

Gloyd M, Ghirlando R, Matthews LA, Guarné; A. 2007. MukE and MukF Form Two Distinct High Affinity Complexes*. *J Biol Chem* **282**:14373–14378. doi:10.1074/jbc.M701402200

Goedhart J, von Stetten D, Noirclerc-Savoye M, Lelimousin M, Joosen L, Hink MA, van Weeren L, Gadella TWJ, Royant A. 2012. Structure-guided evolution of cyan fluorescent proteins towards a quantum yield of 93%. *Nat Commun* **3**:751. doi:10.1038/ncomms1738

Gogou C, Japaridze A, Dekker C. 2021. Mechanisms for Chromosome Segregation in Bacteria. *Front Microbiol* **12**:685687. doi:10.3389/fmicb.2021.685687

Govers SK, Campos M, Tyagi B, Laloux G, Jacobs-Wagner C. 2023. Apparent simplicity and emergent robustness in bacterial cell cycle control. doi:10.1101/2023.01.16.524295

Grainge I, Lesterlin C, Sherratt DJ. 2011. Activation of XerCD-dif recombination by the FtsK DNA translocase. *Nucleic Acids Res* **39**:5140–5148. doi:10.1093/nar/gkr078

Grainger DC, Goldberg MD, Lee DJ, Busby SJW. 2008. Selective repression by Fis and H-NS at the Escherichia coli dps promoter. *Mol Microbiol* **68**:1366–1377. doi:10.1111/j.1365-2958.2008.06253.x

Grainger DC, Hurd D, Goldberg MD, Busby SJW. 2006. Association of nucleoid proteins with coding and non-coding segments of the Escherichia coli genome. *Nucleic Acids Res* **34**:4642–4652. doi:10.1093/nar/gkl542

Grainger DC, Hurd D, Harrison M, Holdstock J, Busby SJW. 2005. Studies of the distribution of Escherichia coli cAMP-receptor protein and RNA polymerase along the E. coli chromosome. *Proc Natl Acad Sci U S A* **102**:17693–17698. doi:10.1073/pnas.0506687102

Gruber S, Errington J. 2009. Recruitment of condensin to replication origin regions by ParB/SpoOJ promotes chromosome segregation in B. subtilis. *Cell* **137**:685–696. doi:10.1016/j.cell.2009.02.035

Hadizadeh Yazdi N, Guet CC, Johnson RC, Marko JF. 2012. Variation of the folding and dynamics of the Escherichia coli chromosome with growth conditions. *Mol Microbiol* **86**:1318–1333. doi:10.1111/mmi.12071

Haering CH, Löwe J, Hochwagen A, Nasmyth K. 2002. Molecular Architecture of SMC Proteins and the Yeast Cohesin Complex. *Mol Cell* **9**:773–788. doi:10.1016/S1097-2765(02)00515-4

Hiraga S, Niki H, Ogura T, Ichinose C, Mori H, Ezaki B, Jaffé A. 1989. Chromosome partitioning in Escherichia coli: novel mutants producing anucleate cells. *J Bacteriol* **171**:1496–1505. doi:10.1128/jb.171.3.1496-1505.1989

Hirano M, Hirano T. 2002. Hinge-mediated dimerization of SMC protein is essential for its dynamic interaction with DNA. *EMBO J* **21**:5733–5744. doi:10.1093/emboj/cdf575

Hofmann A, Mä kelä J, Sherratt DJ, Heermann D, Murray SM. 2019. Self-organised segregation of bacterial chromosomal origins. doi:10.7554/eLife.46564.001

Ireton K, Gunther NW, Grossman AD. 1994. spo0J is required for normal chromosome segregation as well as the initiation of sporulation in Bacillus subtilis. *J Bacteriol* **176**:5320–5329. doi:10.1128/jb.176.17.5320-5329.1994

Jalal AS, Tran NT, Le TB. 2020. ParB spreading on DNA requires cytidine triphosphate in vitro. *eLife* **9**:e53515. doi:10.7554/eLife.53515

Jalal AS, Tran NT, Stevenson CE, Chimthanawala A, Badrinarayanan A, Lawson DM, Le TB. 2021. A CTP-dependent gating mechanism enables ParB spreading on DNA. *eLife* **10**:e69676. doi:10.7554/eLife.69676

Japaridze A, Gogou C, Kerssemakers JWJ, Nguyen HM, Dekker C. 2020. Direct observation of independently moving replisomes in Escherichia coli. *Nat Commun* **11**:3109. doi:10.1038/s41467-020-16946-7

Jensen RB, Shapiro L. 1999. The Caulobacter crescentus smc gene is required for cell cycle progression and chromosome segregation. *Proc Natl Acad Sci* **96**:10661–10666. doi:10.1073/pnas.96.19.10661

Joshi MC, Bourniquel A, Fisher J, Ho BT, Magnan D, Kleckner N, Bates D. 2011. Escherichia coli sister chromosome separation includes an abrupt global transition with concomitant release of late-splitting intersister snaps. *Proc Natl Acad Sci* **108**:2765–2770. doi:10.1073/pnas.1019593108

Jun S, Mulder B. 2006. Entropy-driven spatial organization of highly confined polymers: Lessons for the bacterial chromosome. *Proc Natl Acad Sci* **103**:12388–12393. doi:10.1073/pnas.0605305103

Jun S, Wright A. 2010. Entropy as the driver of chromosome segregation. *Nat Rev Microbiol* **8**:600–607. doi:10.1038/nrmicro2391

Kahramanoglou C, Seshasayee ASN, Prieto AI, Ibberson D, Schmidt S, Zimmermann J, Benes V, Fraser GM, Luscombe NM. 2011. Direct and indirect effects of H-NS and

Fis on global gene expression control in Escherichia coli. *Nucleic Acids Res* **39**:2073–2091. doi:10.1093/nar/gkq934

Kamada K, Su'etsugu M, Takada H, Miyata M, Hirano T. 2017. Overall Shapes of the SMC-ScpAB Complex Are Determined by Balance between Constraint and Relaxation of Its Structural Parts. *Structure* **25**:603-616.e4. doi:10.1016/j.str.2017.02.008

Kavenoff R, Ryder OA. 1976. Electron microscopy of membrane-associated folded chromosomes of Escherichia coli. *Chromosoma* **55**:13–25. doi:10.1007/BF00288323

Kleckner NE, Chatzi K, White MA, Fisher JK, Stouf M. 2018. Coordination of Growth, Chromosome Replication/Segregation, and Cell Division in E. coli. *Front Microbiol* **9**.

Köhler R, Kaganovitch E, Murray SM. 2022. High-throughput imaging and quantitative analysis uncovers the nature of plasmid positioning by ParABS. *eLife* **11**:e78743. doi:10.7554/eLife.78743

Köhler R, Sadhir I, Murray SM. 2023. ★Track: Inferred counting and tracking of replicating DNA loci. *Biophys J*. doi:10.1016/j.bpj.2023.03.033

Kuwada NJ, Cheveralls KC, Traxler B, Wiggins PA. 2013. Mapping the driving forces of chromosome structure and segregation in Escherichia coli. *Nucleic Acids Res* **41**:7370–7377. doi:10.1093/nar/gkt468

Lau IF, Filipe SR, Søballe B, Økstad O-A, Barre F-X, Sherratt DJ. 2003. Spatial and temporal organization of replicating Escherichia coli chromosomes. *Mol Microbiol* **49**:731–743. doi:10.1046/j.1365-2958.2003.03640.x

Le TBK, Imakaev MV, Mirny LA, Laub MT. 2013. High-Resolution Mapping of the Spatial Organization of a Bacterial Chromosome. *Science* **342**:731–734. doi:10.1126/science.1242059

Lee PS, Grossman AD. 2006. The chromosome partitioning proteins Soj (ParA) and Spo0J (ParB) contribute to accurate chromosome partitioning, separation of replicated sister origins, and regulation of replication initiation in Bacillus subtilis. *Mol Microbiol* **60**:853–869. doi:10.1111/j.1365-2958.2006.05140.x

Lemonnier M, Bouet J-Y, Libante V, Lane D. 2000. Disruption of the F plasmid partition complex in vivo by partition protein SopA. *Mol Microbiol* **38**:493–503. doi:10.1046/j.1365-2958.2000.02101.x

Levin PA, Taheri-Araghi S. 2019. One is Nothing without the Other: Theoretical and Empirical Analysis of Cell Growth and Cell Cycle Progression. *J Mol Biol* **431**:2061–2067. doi:10.1016/j.jmb.2019.04.004

Li Y, Sergueev K, Austin S. 2002. The segregation of the Escherichia coli origin and terminus of replication. *Mol Microbiol* **46**:985–996. doi:10.1046/j.1365-2958.2002.03234.x

Li Y, Youngren B, Sergueev K, Austin S. 2003. Segregation of the Escherichia coli chromosome terminus. *Mol Microbiol* **50**:825–834. doi:10.1046/j.1365-2958.2003.03746.x

Lin DC-H, Grossman AD. 1998. Identification and Characterization of a Bacterial Chromosome Partitioning Site. *Cell* **92**:675–685. doi:10.1016/S0092-8674(00)81135-6

Lioy VS, Cournac A, Marbouty M, Duigou S, Mozziconacci J, Espéli O, Boccard F, Koszul R. 2018. Multiscale Structuring of the E. coli Chromosome by Nucleoid-Associated and Condensin Proteins. *Cell*. doi:10.1016/j.cell.2017.12.027

Lioy VS, Junier I, Lagage V, Vallet I, Boccard F. 2020. Distinct Activities of Bacterial Condensins for Chromosome Management in Pseudomonas aeruginosa. *Cell Rep* **33**. doi:10.1016/j.celrep.2020.108344

Livny J, Yamaichi Y, Waldor MK. 2007. Distribution of Centromere-Like parS Sites in Bacteria: Insights from Comparative Genomics. *J Bacteriol* **189**:8693–8703. doi:10.1128/JB.01239-07

Lu M, Campbell JL, Boye E, Kleckner N. 1994. SeqA: A negative modulator of replication initiation in E. coli. *Cell* **77**:413–426. doi:10.1016/0092-8674(94)90156-2

Lucchini S, Rowley G, Goldberg MD, Hurd D, Harrison M, Hinton JCD. 2006. H-NS mediates the silencing of laterally acquired genes in bacteria. *PLoS Pathog* **2**:e81. doi:10.1371/journal.ppat.0020081

Mäkelä J, Sherratt D. 2020a. SMC complexes organize the bacterial chromosome by lengthwise compaction. *Curr Genet* **66**:895–899. doi:10.1007/s00294-020-01076-w

Mäkelä J, Sherratt DJ. 2020b. Organization of the Escherichia coli Chromosome by a MukBEF Axial Core. *Mol Cell* **78**:250-260.e5. doi:10.1016/j.molcel.2020.02.003

Mäkelä J, Uphoff S, Sherratt DJ. 2021. Nonrandom segregation of sister chromosomes by Escherichia coli MukBEF. *Proc Natl Acad Sci* **118**. doi:10.1073/PNAS.2022078118

Männik Jaana, Castillo DE, Yang D, Siopsis G, Männik Jaan. 2016. The role of MatP, ZapA and ZapB in chromosomal organization and dynamics in Escherichia coli. *Nucleic Acids Res* **44**:1216–1226. doi:10.1093/nar/gkv1484

Mascarenhas J, Soppa J, Strunnikov AV, Graumann PL. 2002. Cell cycle-dependent localization of two novel prokaryotic chromosome segregation and condensation proteins in Bacillus subtilis that interact with SMC protein. *EMBO J* **21**:3108–3118. doi:10.1093/emboj/cdf314

Melby TE, Ciampaglio CN, Briscoe G, Erickson HP. 1998. The Symmetrical Structure of Structural Maintenance of Chromosomes (SMC) and MukB Proteins: Long, Antiparallel Coiled Coils, Folded at a Flexible Hinge. *J Cell Biol* **142**:1595–1604.

Mercier R, Petit MA, Schbath S, Robin S, El Karoui M, Boccard F, Espéli O. 2008. The MatP/matS Site-Specific System Organizes the Terminus Region of the E. coli Chromosome into a Macrodomain. *Cell* **135**:475–485. doi:10.1016/j.cell.2008.08.031

Mohl DA, Gober JW. 1997. Cell Cycle–Dependent Polar Localization of Chromosome Partitioning Proteins in Caulobacter crescentus. *Cell* **88**:675–684. doi:10.1016/S0092-8674(00)81910-8

Monterroso B, Zorrilla S, Sobrinos-Sanguino M, Robles-Ramos MÁ, Alfonso C, Söderström B, Meiresonne NY, Verheul J, den Blaauwen T, Rivas G. 2019. The Bacterial DNA Binding Protein MatP Involved in Linking the Nucleoid Terminal Domain to the Divisome at Midcell Interacts with Lipid Membranes. *mBio* **10**:e00376-19. doi:10.1128/mBio.00376-19

Mulcair MD, Schaeffer PM, Oakley AJ, Cross HF, Neylon C, Hill TM, Dixon NE. 2006. A Molecular Mousetrap Determines Polarity of Termination of DNA Replication in E. coli. *Cell* **125**:1309–1319. doi:10.1016/j.cell.2006.04.040

Murray SM, Sourjik V. 2017. Self-organization and positioning of bacterial protein clusters. *Nat Phys* **13**:1006–1013. doi:10.1038/nphys4155

Nair S, Finkel SE. 2004. Dps protects cells against multiple stresses during stationary phase. *J Bacteriol* **186**:4192–4198. doi:10.1128/JB.186.13.4192-4198.2004

Nielsen HJ, Li Y, Youngren B, Hansen FG, Austin S. 2006a. Progressive segregation of the Escherichia coli chromosome. *Mol Microbiol* **61**:383–393. doi:10.1111/j.1365-2958.2006.05245.x

Nielsen HJ, Ottesen JR, Youngren B, Austin SJ, Hansen FG. 2006b. The Escherichia coli chromosome is organized with the left and right chromosome arms in separate cell halves. *Mol Microbiol* **62**:331–338. doi:10.1111/j.1365-2958.2006.05346.x

Niki H, Hiraga S. 1998. Polar localization of the replication origin and terminus in Escherichia coli nucleoids during chromosome partitioning. *Genes Dev* **12**:1036–1045.

Niki H, Imamura R, Kitaoka M, Yamanaka K, Ogura T, Hiraga S. 1992. E.coli MukB protein involved in chromosome partition forms a homodimer with a rod-and-hinge structure having DNA binding and ATP/GTP binding activities. *EMBO J* **11**:5101–5109. doi:10.1002/j.1460-2075.1992.tb05617.x

Niki H, Yamaichi Y, Hiraga S. 2000. Dynamic organization of chromosomal DNA in Escherichia coli. *Genes Dev* **14**:212–223.

Nolivos S, Sherratt D. 2014. The bacterial chromosome: architecture and action of bacterial SMC and SMC-like complexes. *FEMS Microbiol Rev* **38**:380–392. doi:10.1111/1574-6976.12045

Nolivos S, Upton AL, Badrinarayanan A, Müller J, Zawadzka K, Wiktor J, Gill A, Arciszewska L, Nicolas E, Sherratt D. 2016. MatP regulates the coordinated action of topoisomerase IV and MukBEF in chromosome segregation. *Nat Commun* **7**. doi:10.1038/ncomms10466

Orban K, Finkel SE. 2022. Dps Is a Universally Conserved Dual-Action DNA-Binding and Ferritin Protein. *J Bacteriol* **204**:e0003622. doi:10.1128/jb.00036-22

Osorio-Valeriano M, Altegoer F, Steinchen W, Urban S, Liu Y, Bange G, Thanbichler M. 2019. ParB-type DNA Segregation Proteins Are CTP-Dependent Molecular Switches. *Cell* **179**:1512-1524.e15. doi:10.1016/j.cell.2019.11.015

Petrushenko ZM, She W, Rybenkov VV. 2011. A new family of bacterial condensins. *Mol Microbiol* **81**:881–896. doi:10.1111/j.1365-2958.2011.07763.x

Pradhan S, Bipinachandran SV, Kumari P, Suguna M, Prasad MD, Kumar R. 2020. MksB, an alternate condensin from Mycobacterium smegmatis is involved in DNA binding and condensation. *Biochimie* **171–172**:136–146. doi:10.1016/j.biochi.2020.03.002

Prieto AI, Kahramanoglou C, Ali RM, Fraser GM, Seshasayee ASN, Luscombe NM. 2012. Genomic analysis of DNA binding and gene regulation by homologous nucleoid-associated proteins IHF and HU in Escherichia coli K12. *Nucleic Acids Res* **40**:3524–3537. doi:10.1093/nar/gkr1236

Reyes-Lamothe R, Tran T, Meas D, Lee L, Li AM, Sherratt DJ, Tolmasky ME. 2014. High-copy bacterial plasmids diffuse in the nucleoid-free space, replicate stochastically and are randomly partitioned at cell division. *Nucleic Acids Res* **42**:1042–1051. doi:10.1093/nar/gkt918

Rice PA, Yang S, Mizuuchi K, Nash HA. 1996. Crystal structure of an IHF-DNA complex: a protein-induced DNA U-turn. *Cell* **87**:1295–1306. doi:10.1016/s0092-8674(00)81824-3

Rouvière-Yaniv J, Gros F. 1975. Characterization of a novel, low-molecular-weight DNA-binding protein from Escherichia coli. *Proc Natl Acad Sci U S A* **72**:3428–3432.

Rybenkov VV, Herrera V, Petrushenko ZM, Zhao H. 2015. MukBEF, a Chromosomal Organizer. *J Mol Microbiol Biotechnol* **24**:371–383. doi:10.1159/000369099

Sakai Y, Miyauchi K, Kimura S, Suzuki T. 2016. Biogenesis and growth phase-dependent alteration of 5-methoxycarbonylmethoxyuridine in tRNA anticodons. *Nucleic Acids Res* **44**:509–523. doi:10.1093/nar/gkv1470

Santero E, Hoover TR, North AK, Berger DK, Porter SC, Kustu S. 1992. Role of integration host factor in stimulating transcription from the sigma 54-dependent nifH promoter. *J Mol Biol* **227**:602–620. doi:10.1016/0022-2836(92)90211-2

Soh Y-M, Bürmann F, Shin H-C, Oda T, Jin KS, Toseland CP, Kim C, Lee H, Kim SJ, Kong M-S, Durand-Diebold M-L, Kim Y-G, Kim HM, Lee NK, Sato M, Oh B-H, Gruber S. 2015. Molecular basis for SMC rod formation and its dissolution upon DNA binding. *Mol Cell* **57**:290–303. doi:10.1016/j.molcel.2014.11.023

Soh Y-M, Davidson IF, Zamuner S, Basquin J, Bock FP, Taschner M, Veening J-W, De Los Rios P, Peters J-M, Gruber S. 2019. Self-organization of parS centromeres by the ParB CTP hydrolase. *Science*. doi:10.1126/science.aay3965

Spira B, Ospino K. 2020. Diversity in E. coli (p)ppGpp Levels and Its Consequences. *Front Microbiol* **11**.

Stouf M, Meile J-C, Cornet F. 2013. FtsK actively segregates sister chromosomes in Escherichia coli. *Proc Natl Acad Sci U S A* **110**:11157–11162. doi:10.1073/pnas.1304080110

Sullivan NL, Marquis KA, Rudner DZ. 2009. Recruitment of SMC by ParB-parS Organizes the Origin Region and Promotes Efficient Chromosome Segregation. *Cell* **137**:697–707. doi:10.1016/j.cell.2009.04.044

Surovtsev IV, Jacobs-Wagner C. 2018. Subcellular Organization: A Critical Feature of Bacterial Cell Replication. *Cell* **172**:1271–1293. doi:10.1016/j.cell.2018.01.014

Swinger KK, Rice PA. 2007. Structure-based analysis of HU-DNA binding. *J Mol Biol* **365**:1005–1016. doi:10.1016/j.jmb.2006.10.024

Tani TH, Khodursky A, Blumenthal RM, Brown PO, Matthews RG. 2002. Adaptation to famine: a family of stationary-phase genes revealed by microarray analysis. *Proc Natl Acad Sci U S A* **99**:13471–13476. doi:10.1073/pnas.212510999

Tiruvadi-Krishnan S, Männik Jaana, Kar P, Lin J, Amir A, Männik Jaan. 2022. Coupling between DNA replication, segregation, and the onset of constriction in Escherichia coli. *Cell Rep* **38**:110539. doi:10.1016/j.celrep.2022.110539

Toro E, Shapiro L. 2010. Bacterial Chromosome Organization and Segregation. *Cold Spring Harb Perspect Biol* **2**:a000349. doi:10.1101/cshperspect.a000349

Valens M, Penaud S, Rossignol M, Cornet F, Boccard F. 2004. Macrodomain organization of the Escherichia coli chromosome. *EMBO J* **23**:4330–4341. doi:10.1038/sj.emboj.7600434

Valens M, Thiel A, Boccard F. 2016. The MaoP/maoS Site-Specific System Organizes the Ori Region of the E. coli Chromosome into a Macrodomain. *PLoS Genet*. doi:10.1371/journal.pgen.1006309

Vallet-Gely I, Boccard F. 2013. Chromosomal Organization and Segregation in Pseudomonas aeruginosa. *PLoS Genet* **9**:e1003492. doi:10.1371/journal.pgen.1003492

Waldminghaus T, Skarstad K. 2009. The Escherichia coli SeqA protein. *Plasmid* **61**:141–150. doi:10.1016/j.plasmid.2009.02.004

Wang P, Robert L, Pelletier J, Dang WL, Taddei F, Wright A, Jun S. 2010. Robust Growth of Escherichia coli. *Curr Biol* **20**:1099–1103. doi:10.1016/j.cub.2010.04.045

Wang X, Brandão HB, Le TBK, Laub MT, Rudner DZ. 2017. Bacillus subtilis SMC complexes juxtapose chromosome arms as they travel from origin to terminus. *Science* **355**:524–527. doi:10.1126/science.aai8982

Wang X, Liu X, Possoz C, Sherratt DJ. 2006. The two Escherichia coli chromosome arms locate to separate cell halves. *Genes Dev* **20**:1727–1731. doi:10.1101/gad.388406

Wang X, Llopis PM, Rudner DZ. 2014. Bacillus subtilis chromosome organization oscillates between two distinct patterns. *Proc Natl Acad Sci U S A* **111**:12877–12882. doi:10.1073/pnas.1407461111

Wang X, Llopis PM, Rudner DZ. 2013. Organization and segregation of bacterial chromosomes. *Nat Rev Genet* **14**:191–203. doi:10.1038/nrg3375

Wang X, Possoz C, Sherratt DJ. 2005. Dancing around the divisome: asymmetric chromosome segregation in Escherichia coli. *Genes Dev* **19**:2367–2377. doi:10.1101/gad.345305

Wang X, Rudner DZ. 2014. Spatial organization of bacterial chromosomes. *Curr Opin Microbiol*, Growth and development: eukaryotes/ prokaryotes **22**:66–72. doi:10.1016/j.mib.2014.09.016

Weiß M, Giacomelli G, Assaya MB, Grundt F, Haouz A, Peng F, Petrella S, Wehenkel AM, Bramkamp M. 2023. The MksG nuclease is the executing part of the bacterial plasmid defense system MksBEFG. *Nucleic Acids Res* **51**:3288–3306. doi:10.1093/nar/gkad130

Wiggins PA, Cheveralls KC, Martin JS, Lintner R, Kondev J. 2010. Strong intranucleoid interactions organize the Escherichia coli chromosome into a nucleoid filament. *Proc Natl Acad Sci* **107**:4991–4995. doi:10.1073/pnas.0912062107

Wilhelm L, Bürmann F, Minnen A, Shin H-C, Toseland CP, Oh B-H, Gruber S. 2015. SMC condensin entraps chromosomal DNA by an ATP hydrolysis dependent loading mechanism in Bacillus subtilis. *eLife* **4**:e06659. doi:10.7554/eLife.06659

Woldringh CL, Hansen FG, Vischer NOE, Atlung T. 2015. Segregation of chromosome arms in growing and non-growing Escherichia coli cells. *Front Microbiol* **6**.

Woo J-S, Lim J-H, Shin H-C, Suh M-K, Ku B, Lee K-H, Joo K, Robinson H, Lee J, Park S-Y, Ha N-C, Oh B-H. 2009. Structural Studies of a Bacterial Condensin Complex Reveal ATP-Dependent Disruption of Intersubunit Interactions. *Cell* **136**:85–96. doi:10.1016/j.cell.2008.10.050

Wu LJ, Lee S, Park S, Eland LE, Wipat A, Holden S, Errington J. 2020. Geometric principles underlying the proliferation of a model cell system. *Nat Commun* **11**:4149. doi:10.1038/s41467-020-17988-7

Yamaichi Y, Niki H. 2004. migS, a cis-acting site that affects bipolar positioning of oriC on the Escherichia coli chromosome. *EMBO J* **23**:221–233. doi:10.1038/sj.emboj.7600028

Yamanaka K, Ogura T, Niki H, Hiraga S. 1996. Identification of two new genes, mukE and mukF, involved in chromosome partitioning in Escherichia coli. *Mol Gen Genet MGG* **250**:241–251. doi:10.1007/BF02174381

Yamanaka K, Ogura T, Niki H, Hiraga S. 1995. Characterization of the smtA gene encoding an S-adenosylmethionine-dependent methyltransferase of Escherichia coli. *FEMS Microbiol Lett* **133**:59–63. doi:10.1111/j.1574-6968.1995.tb07861.x

Yatskevich S, Rhodes J, Nasmyth K. 2019. Organization of Chromosomal DNA by SMC Complexes. *Annu Rev Genet* **53**:445–482. doi:10.1146/annurev-genet-112618-043633

Youngren B, Nielsen HJ, Jun S, Austin S. 2014. The multifork Escherichia coli chromosome is a self-duplicating and self-segregating thermodynamic ring polymer. *Genes Dev* **28**:71–84. doi:10.1101/gad.231050.113

Zacharias DA, Violin JD, Newton AC, Tsien RY. 2002. Partitioning of Lipid-Modified Monomeric GFPs into Membrane Microdomains of Live Cells. *Science* **296**:913–916. doi:10.1126/science.1068539

Zawadzka K, Zawadzki P, Baker R, Rajasekar KV, Wagner F, Sherratt DJ, Arciszewska LK. 2018. MukB ATPases are regulated independently by the N- and C-terminal domains of MukF kleisin. *eLife* **7**:e31522. doi:10.7554/eLife.31522

Zawilak-Pawlik A, Nowaczyk M, Zakrzewska-Czerwińska J. 2017. The Role of the N-Terminal Domains of Bacterial Initiator DnaA in the Assembly and Regulation of the Bacterial Replication Initiation Complex. *Genes* **8**:136. doi:10.3390/genes8050136

Zhao H, Bhowmik BK, Petrushenko ZM, Rybenkov VV. 2020. Alternating Dynamics of oriC, SMC, and MksBEF in Segregation of Pseudomonas aeruginosa Chromosome. *mSphere* **5**:e00238-20. doi:10.1128/mSphere.00238-20

Acknowledgements

Firstly, I want to extend my deepest thanks to my supervisor, Dr. Sean Murray. His patient teaching and guidance played a vital role in introducing me to programming and equipping me with quantitative image analysis skills. Without his foundational guidance, my project's notable outcomes wouldn't have been possible.

I'm truly grateful for the support and friendship I've found in my colleagues Robin, Srikanth, and Lara. Robin's considerable contribution to the development of Mothersegger was indispensable, adding lustre to the project. Our daily discussions and shared joy have formed the backbone of my Ph.D. journey. My heartfelt appreciation goes to my batchmates, particularly Isa, for their camaraderie throughout these years. Special thanks to all past and present members of the Department of Systems and Synthetic Microbiology. Judita and Manika, your pleasant company and stimulating conversations have greatly enriched my experience.

A big thank you to IMPRS coordinator, Dusica Rados. From my initial days in Marburg, her support has been immense, guiding me through settling in and providing key details throughout my Ph.D. journey. I'm equally thankful to all researchers in Marburg, my collaborators who introduced me to fascinating microbes. My thesis committee members have been excellent guides, and I couldn't be more grateful.

I am immensely grateful to my friends, Revathi, Midhula, Amritha, and Chinnu. You brought much joy to my time in Marburg, and having Revathi as my flatmate stands as one of my most cherished memories.

To my partner, Mirsana, whom fate brought into my life through the pursuit of this Ph.D., this acknowledgment wouldn't be complete without mentioning you. Your companionship has been my anchor, keeping me grounded while adding a sense of serenity to my life throughout these years. Our travels together have not only created memories but also brought us closer together.

My family's quiet, unwavering support throughout this journey deserves my deepest gratitude.

Lastly, this journey has been significantly shaped by the many incredible people I've met along the way. To everyone who crossed paths with me during my Ph.D., thank you for contributing to my growth and making this journey unforgettable.

Thank you all.